END BURNING TECHNOLOGY PROGRAM, TASK A - LABORATORY EFFORT. TASK B - SUBSCALE MOTOR TESTS

AEROJET SOLID PROPULSION COMPANY
SACRAMENTO, CALIFORNIA

OCTOBER 1971

KEEP UP TO DATE

Between the time you ordered this report—which is only one of the hundreds of thousands in the NTIS information collection available to you—and the time you are reading this message, several *new* reports relevant to your interests probably have entered the collection.

Subscribe to the **Weekly Government Abstracts** series that will bring you summaries of new reports *as soon as they are received by NTIS* from the originators of the research. The WGA's are an NTIS weekly newsletter service covering the most recent research findings in 26 areas of industrial, technological, and sociological interest—invaluable information for executives and professionals who must keep up to date.

The executive and professional information service provided by NTIS in the **Weekly Government Abstracts** newsletters will give you thorough and comprehensive coverage of government-conducted or sponsored research activities. And you'll get this important information within two weeks of the time it's released by originating agencies.

WGA newsletters are computer produced and electronically photocomposed to slash the time gap between the release of a report and its availability. You can learn about technical innovations immediately—and use them in the most meaningful and productive ways possible for your organization. Please request NTIS-PR-205/PCW for more information.

The weekly newsletter series will keep you current. But *learn what you have missed in the past* by ordering a computer **NTISearch** of all the research reports in your area of interest, dating as far back as 1964, if you wish. Please request NTIS-PR-186/PCN for more information.

WRITE: Managing Editor
5285 Port Royal Road
Springfield, VA 22161

Keep Up To Date With SRIM

SRIM (Selected Research in Microfiche) provides you with regular, automatic distribution of the complete texts of NTIS research reports *only* in the subject areas you select. SRIM covers almost all Government research reports by subject area and/or the originating Federal or local government agency. You may subscribe by any category or subcategory of our WGA **(Weekly Government Abstracts)** or **Government Reports Announcements and Index** categories, or to the reports issued by a particular agency such as the Department of Defense, Federal Energy Administration, or Environmental Protection Agency. Other options that will give you greater selectivity are available on request.

The cost of SRIM service is only 45¢ domestic (60¢ foreign) for each complete microfiched report. Your SRIM service begins as soon as your order is received and processed and you will receive biweekly shipments thereafter. If you wish, your service will be backdated to furnish you microfiche of reports issued earlier.

Because of contractual arrangements with several Special Technology Groups, not all NTIS reports are distributed in the SRIM program. You will receive a notice in your microfiche shipments identifying the exceptionally priced reports not available through SRIM.

A deposit account with NTIS is required before this service can be initiated. If you have specific questions concerning this service, please call (703) 451-1558, or write NTIS, attention SRIM Product Manager.

This information product distributed by

NTIS U.S. DEPARTMENT OF COMMERCE
National Technical Information Service
5285 Port Royal Road
Springfield, Virginia 22161

AD-891362

END BURNING TECHNOLOGY PROGRAM
INTERIM REPORT

TASK A - LABORATORY EFFORT
TASK B - SUBSCALE MOTOR TESTS

Report AFRPL-TR-71-138

October 1971

aerojet solid propulsion company

P. O. BOX 13400 SACRAMENTO, CALIFORNIA 95813 • A DIVISION OF AEROJET-GENERAL

Security Classification

DOCUMENT CONTROL DATA - R & D

(Security classification of title, body of abstract and indexing annotation must be entered when the overall report is classified)

1. ORIGINATING ACTIVITY *(Corporate author)*
Aerojet Solid Propulsion Company
P. O. Box 13400
Sacramento, CA 95813

2a. REPORT SECURITY CLASSIFICATION
UNCLASSIFIED

2b. GROUP

3. REPORT TITLE
End Burning Technology Program

4. DESCRIPTIVE NOTES *(Type of report and inclusive dates)*
Interim Report

5. AUTHOR(S) *(First name, middle initial, last name)*

6. REPORT DATE
October 1971

7b. NO OF REFS

8a. CONTRACT OR GRANT NO.
F04611-70-C-0044

b. PROJECT NO.

c.

d.

9a. ORIGINATOR'S REPORT NUMBER(S)
AFRPL-TR-71-138

9b. OTHER REPORT NO(S) *(Any other numbers that may be assigned this report)*
None

10. DISTRIBUTION STATEMENT
Distribution limited to U.S. Government agencies only; test and evaluation of military hardware: December 1971.

11. SUPPLEMENTARY NOTES

12. SPONSORING MILITARY ACTIVITY
Air Force Rocket Propulsion Laboratory
Solid Rocket Division
Edwards AFB, California

13. ABSTRACT

This report describes the End Burning Technology Program effort being conducted to establish solutions to the burning rate variability which contributes to nonuniform surface regression in end-burning motors. Laboratory and subscale motor test efforts are discussed with full-scale motor tests and overall program results to be presented in the final report.

PRICES SUBJECT TO CHANGE

12

DD FORM 1 NOV 65 1473

Security Classification

Report AFRPL-TR-71-138

END BURNING TECHNOLOGY PROGRAM

INTERIM REPORT

Task A - Laboratory Effort
Task B - Subscale Motor Tests

Contract F04611-70-C-0044
CDRL Item B011

October 1971

This technical report has been reviewed and is approved:

Richard E. Smith
Project Eng, Solid Rocket Division
Air Force Rocket Propulsion Laboratory

aerojet solid propulsion company
A DIVISION OF AEROJET GENERAL

FOREWORD

This is the Interim Report on Contract F04611-70-C-0044, submitted in partial fulfillment of the contract work statement. This interim report describes the results of the Task A laboratory effort and the Task B subscale effort conducted under the "End Burning Technology Program" during the period May 1970 through September 1971. A final report covering the Task C full-scale motor test and the expanded laboratory effort will be issued at the completion of the program. The work on this program was performed by the Aerojet Solid Propulsion Company under the technical direction of Mr. Richard E. Smith, representing the Air Force Rocket Propulsion Laboratory, Solid Rocket Division, Edwards AFB, California.

ABSTRACT

Migration of mobile species from the propellant into the liner and insulation was found to be the main cause of burning rate variability in the interphase which contributes to nonuniform surface regression in end-burning motors. Migration of these mobile species was significantly inhibited through the use of highly crosslinked liner/barrier systems which contained bonding fillers. Utilization of the liner/barrier system applied to highly permeable insulation materials resulted in no detectable interphase burning rate variability under the conditions tested. The propellants selected for evaluation were an HTPB/UFAP system using a liquid burning rate catalyst and a polyether-urethane (C-1/PU) propellant utilizing a solid burning rate accelerator.

Other propellant factors, such as particle orientation and propellant dilatation were shown to be insignificant in causing interphase burning rate variability. Under certain conditions of flow and vibration, a high-viscosity unplasticized HTPB/UFAP propellant formulation exhibited particle classification which caused burning rate variability in the interphase.

Statistical analysis of the burning rate data obtained from propellant grains prepared by a variety of casting techniques revealed no burning rate variability which could be attributed to the cast method used with the HTPB/UFAP and C-1/PU propellants selected for evaluation. These findings were verified in cast grains up to 16 inches in diameter.

Laboratory results were verified in end-burning motor test firings of 4- and 8.5-in. dia grains. X-ray monitoring of eight end-burning motor test firings (4 each of C-1/PU and HTPB/UFAP propellant grains) at the China Lake Naval Weapons Center showed that the burning surface regression was uniform and neutral pressure- and thrust-time traces were obtained.

A computer program has been prepared to predict the performance of end-burning motors. The program is based on the results of subscale motor test firings as well as theoretical considerations.

TABLE OF CONTENTS

FIGURE LIST

FIGURE LIST (cont)

FIGURE LIST (cont)

FIGURE LIST (cont)

APPENDIX

I. INTRODUCTION

This interim report describes the results of the Task A laboratory effort and the Task B subscale motor tests conducted as part of Contract F04611-70-C-0044, "End Burning Technology", for the Rocket Propulsion Laboratory (Edwards Air Force Base, California) by the Aerojet Solid Propulsion Company (Sacramento, California). A final report covering the Task C full-scale motor tests and the expanded laboratory effort will be issued at the completion of the program.

II. OBJECTIVES

The objectives of this program are:

1. To identify the important individual propellant, liner, and motor environment parameters contributing to irregular end-burner surface regression, especially in the propellant/liner interphase.

2. To quantitatively establish the effect contributed by each individual cause.

3. To develop in the laboratory methods permitting their elimination or control.

4. To demonstrate in subscale and full-scale motor tests that the developed solutions apply to motor conditions, i.e., that the pressure vs time performance of end-burning grains can be predicted, and that neutrality can be obtained.

III. SUMMARY OF RESULTS

A. TASK A, LABORATORY INVESTIGATION OF CAUSES OF NONUNIFORM BURNING SURFACE REGRESSION

Migration of mobile species from the propellant into the liner and insulation was found to be the principal cause of burning rate variability in the interphase which contributes to nonuniform burning surface regression in end-burning motors. The nature of the migrating specie determines the type of interphase

III.A. Task A, Laboratory Investigation of Causes of Nonuniform Burning Surface Regression (cont)

burning rate variability, i.e., migration of an inert propellant plasticizer such as IDP causes an increase in burning rate of up to 10% adjacent to the liner/insulation while migration of a liquid burning additive such as Catocene produces a decrease in the interphase burning rate (as much as 20%).

As a result of work done on this program, approaches have been defined which will permit the design of end-burning motors with acceptable neutrality of pressure and thrust. Three methods for control of interphase burning rate variability caused by migration were explored and found feasible:

1. Balancing the concentration of inert plasticizer and liquid burning rate additive in the propellant so that migration of both species produced no net change in burning rate.

2. Incorporation of liquid burning rate additive and/or plasticizer in the liner/insulation to eliminate the tendency of these species to migrate from the propellant.

3. Use of a barrier with low permeability to the migrating species between propellant and insulation.

Two barrier materials with low permeability to both plasticizer and liquid burning rate additive were tested and found to be effective in preventing interphase burning rate variability. These were an NPGA/MNA/DER-332 polymer filled with glass beads and a modification of the liner SD-886, an epoxy-polyurethane composition. The latter material, designated SD-886-1, was selected for use in the Task B and Task C motor tests. In addition to its capability to resist migration, SD-886-1 also provides excellent bonds to the HTPB and C-1 polyurethane propellants.

Deagglomeration and/or attrition of fine oxidizer particles was found to be a factor affecting the bulk burning rate of the propellant, but did not of itself affect variability of burning rate in the interphase. The amount of

III.A. Task A, Laboratory Investigation of Causes of Nonuniform Burning Surface Regression (cont)

deagglomeration was shown to be a function of the viscosity of the propellant during mixing as well as the mix time. These results indicate the importance of optimizing the mix cycle for a specific formulation to maximize burning rate and minimize batch-to-batch variability.

Under certain conditions of flow and vibration it was found that classification of the oxidizer particles in the uncured propellant can occur with resulting burning rate variability in the interphase. Of a number of formulations examined, only one (a high viscosity unplasticized HTPB propellant) showed these classification effects.

Other propellant parameters evaluated included orientation of solid particles, dilatation, and microvoid formation. Statistical analyses of the data indicated that these parameters were not significant contributors to interphase burning rate variability.

The results of the laboratory studies were confirmed in scale-up and casting parameter investigations involving casting of 4-, 8.5-, and 16-in.-dia molds. Based on statistical analyses of the burning rate profiles, a vacuum casting technique with vibration and free fall of the propellant was selected for preparation of the subscale and full scale motors.

From six basic propellant formulations evaluated in the laboratory studies, two were selected for further testing in the Task B and C motor tests. These were ANP-3391, a C-1 polyurethane propellant containing a solid burning rate additive with no UFAP; and ANB-3392, an HTPB/UFAP propellant with 1 wt% Catocene as the burning rate additive.

III. Summary of Results (cont)

B. TASK B, SUBSCALE MOTOR TESTS

A total of eleven 3KS-1000 size (4-in.-dia grain) subscale motors were tested at Aerojet to evaluate the effects of propellant and motor variables and to confirm the findings of the Task A laboratory effort. Motor design variables such as L* and nozzle entrance angle were found to have no effect on end-burner performance. Subscale motors containing both ANP-3391 and ANB-3392 provided neutral performance when the barrier liner SD-886-1 was used. With a liner which was permeable to the migrating species (SD-896) progressive pressure- and thrust-time traces were obtained.

Based on the results of the Aerojet firings, a selection was made of propellants, liner, and motor configuration for confirmation of end-burning motor neutrality in eight subscale motor tests conducted at NWC (China Lake) with X-ray motion picture coverage in addition to pressure and thrust instrumentation. Four motors were tested with each propellant formulation (ANP-3391 and ANB-3392), all motors used the SD-886-1 barrier liner. Performance of all eight motors was excellent, the neutrality of the pressure- and thrust-time traces was confirmed by the X-ray motion pictures which showed an even uniform burning surface regression.

Two 10KS-2500 size motors (8.5-in.-dia grain) were tested to evaluate the effects of further scale up in motor size. One motor was cast with each propellant formulation. The first test (with ANP-3391) resulted in a motor burnthrough due to a faulty closure seal, but the second test showed good neutrality.

Based on the results of the Task B subscale motor tests as well as on theoretical considerations, a computer program has been prepared to predict the performance end-burning motors. The program is complete but additional refinements are being made to improve prediction capability.

IV. TECHNICAL DISCUSSION

A. TASK A, LABORATORY INVESTIGATION OF CAUSES OF NONUNIFORM SURFACE REGRESSION

In the Task A laboratory investigations, the critical factors affecting the surface regression characteristics of end-burning solid propellant grains were determined, and methods were devised for control of these factors to ensure neutrality of end-burning motor pressure- and thrust-time characteristics. Laboratory scale work was performed to define the effects of propellant parameters and interactions with the liner/insulation in the interphase, and selected propellant formulations were then scaled up for investigation of effects of casting methods applicable to the Task B subscale and the Task C full-scale motors. Bond evaluations were also conducted to permit final selection of propellants and liners for use in the Tasks B and C motors. Details of this work are summarized in the following sections.

1. Propellant Parameters and Effects

The critical propellant parameters evaluated were:

a. Deagglomeration of fine oxidizer particles during mixing
b. Orientation of solid particles
c. Classification of solid particles
d. Migration of liquid components into liner/insulation
e. Dilatation

Six basic propellant formulations were investigated to assess the significance of these parameters. The six formulations were selected to permit evaluation of the effects of binder type, plasticizers, solid and liquid burning rate catalysts, oxidizer particle size, and propellant viscosity. As the critical parameters were defined, the number of propellant formulations were reduced. Two formulations were selected for testing in subscale (5- and 9-in.-dia) end-burning motors (Task B) for confirmation of the laboratory findings.

IV.A. Task A, Laboratory Investigation of Causes of Nonuniform Surface Regression (cont)

The formulations used in the laboratory studies were based on carboxy terminated polybutadiene (CTPB), hydroxy terminated polybutadiene (HTPB), and polyurethane (C-1/PU) binders. Compositions are presented in Figure 1. As shown, the C-1/PU formulation contains CuO202 as a burning rate catalyst with 7μ oxidizer as the fine portion of the oxidizer blend. All of the other formulations contain 0.5μ UFAP and, with the exception of Formulation 2, 1% Catocene as burning rate catalyst.

a. Formulation Adjustments

The six basic propellant compositions described above were adjusted to a burning rate of approximately 1.5 in./sec at 1000 psia while maintaining adequate processing and cure characteristics.

The preliminary adjustments were conducted in 1- and 10-lb laboratory propellant mixes. Burning rates were measured in a microstrand burner using 0.60 by 0.30 by 1.3-in. strands. Previous tests with a well characterized propellant (ANB-3066, used in Minuteman) showed that the microstrand burning rates (MSBR) agreed well with solid strand rates (SSBR) determined in the standard Crawford bomb (Figure 2). The microstrands were prepared for testing by microforming from a small piece of cured propellant to the correct thickness and width but slightly longer than the finished length of 1.3-in. The strands were then individually restricted with a rapid-cure epoxy adhesive and cut to exact final length. The tests were conducted in a closed bomb at an average pressure of approximately 1000 psig. Highly reproducible results were obtained as indicated by data in Figure 3 for ten firings of an HTPB/UFAP propellant (ANB-3392) which indicates a standard error of only 0.8%.

The processing characteristics of the propellants were assessed with a Rotovisko viscometer. Viscosity buildup at infinite shear stress and viscosity as a function of applied shear stress were determined.

IV.A. Task A, Laboratory Investigation of Causes of Nonuniform Surface Regression (cont)

A summary of the results of this tailoring effort is shown below. The target burning rate was achieved with four of the six formulations; processing considerations limited the burning rate of the CTPB formulation to approximately 1.1 in./sec at 1000 psia. For the highly plasticized HTPB formulation (4% IDP) more than 28% UFAP would be required to meet the 1.5 in./sec burning rates.

Number	Binder Type	Oxidizer Blend				Wt % Catocene	Wt % IDP	MSBR, in./sec at 1000 psi
		Unground	SSMP	MA	UFAP			
1	C-1/PU	30	-	70	-	-(2)	4	1.44
2	HTPB	-	-	58	42	0	3	1.57
3	HTPB	-	72	-	28	1	0	1.88
4a	CTPB	-	65	-	35	1	5	1.10
4b	HTPB	-	72	-	28	1	2	1.54
4c	HTPB	-	72	-	28	1	4	1.13

(1) Each formulation contains 72 wt% oxidizer and 14 wt% spherical aluminum.
(2) Contains 2 wt% Cu0202.

A summary of the formulation adjustment effort for each propellant is presented below.

(1) C-1 Polyurethane Propellant

The C-1 polyurethane propellant (C-1/PU, No. 1 in Figure 1) utilizing the solid burning rate additive, copper chromite (Cu0202), is a modification of the propellant developed on the HART/ZAP motor programs. The burning rate, 1.44 in./sec at 1000 psi, was achieved in an 88 wt% total solids formulation containing 72 wt% oxidizer (70/30 MA/unground blend), 14 wt% spheroidal aluminum (~60μ), and 2 wt% of Cu0202. The binder (IDP plasticized) is composed of B-2000 (polyether prepolymer), TP-4040 (polyether crosslinker), C-1 (oxidizer bonding agent) and HDI curing agent. Minor adjustments in the crosslinker level were made to achieve the desired mechanical properties. This formulation was designated ANP-3391.

IV.A. Task A, Laboratory Investigation of Causes of Nonuniform Surface Regression (cont)

The processing characteristics of ANP-3391 were very good as indicated by data in Figure 4 which compares the viscosity buildup of this propellant to that of the other five basic formulations. After 4 hours from curing agent addition, the viscosity of ANP-3391 was approximately 30,000 poises.

(2) HTPB Propellants

(a) No Burning Rate Additive

A series of HTPB formulations with no Catocene burning rate additive was mixed to evaluate the effect of IDP plasticizer level and MA/UFAP oxidizer ratio on the burning rate. The propellants all contained 86 wt% total solids (72% oxidizer and 14 wt% H-60 spheriodal aluminum), and the binder was composed of R-45 HTPB cured with TDI. Based on the results of these tests a formulation containing 3 wt% IDP plasticizer and an oxidizer blend ratio of 58/42 MA/UFAP was selected for further evaluation. This formulation is typical of high burning rate propellants with no burning rate additive. The burning rate of this formulation was 1.57 in./sec and the viscosity while initially low, increased rapidly. At 3 hours from curing agent addition the viscosity was approximately 45,000 poises, but increased to >200,000 poises after 4 hours. The oxidizer blend of 58/42 MA/UFAP yielded a burning rate of 1.57 in./sec at the 3% IDP plasticizer level. This formulation (No. 2. in Figure 1) was chosen for further evaluation since it met the burning rate requirement and exhibited satisfactory as-cast processability.

(b) Unplasticized Propellant

An unplasticized HTPB propellant containing 1% Catocene (Formulation 3, Figure 1) had the highest burning rate of the series, 1.88 in./sec at 1000 psi. This propellant contains 86 wt% total solids composed of 14 wt% spherical aluminum and 72 wt% oxidizer (72/28 blend of SSMP and UFAP).

IV.A. Task A, Laboratory Investigation of Causes of Nonuniform Surface Regression (cont)

Because of the cure catalysis attributable to the Catocene burning rate additive and the rapid cure reaction associated with an unplasticized binder, isophorone diisocyanate (IPDI) rather than TDI was used as the curing agent to improve the potlife and processing characteristics. However, even with IPDI this nonplasticized formulation (Batch 10GP-1549) showed a rapid viscosity buildup; greater than 60,000 poise at 4 hours from curing agent addition (Figure 4).

(c) Propellants Containing Both Plasticizer and Catocene

HTPB propellant systems containing both IDP and Catocene are represented by Formulation 4b and 4c in Figure 1. Propellants containing 2 and 4 wt% IDP which provide burning rates of 1.54 and 1.13 in./sec at 1000 psi, respectively, were formulated using the same binder system described above (R-45 HTPB cured with IPDI). The oxidizer blend used was 72/28 SSMP and UFAP.

The processing characteristics of both propellants were excellent (Figure 4); viscosities four hours from curing agent addition were less than 20,000 poises. The burning rate of Formulation 4c was below the desired 1.5 in./sec at 1000 psi. This low rate probably resulted from a combination of the higher IDP content and the very low viscosity which was found to inhibit deagglomeration of the UFAP. Formulation 4b was designated ANB-3392.

(3) CTPB Propellants

Propellant 4a (Figure 1) was prepared using a CTPB binder. To improve processability, 5 wt% IDP was used. Total solids level was 86 wt% (14 wt% spheroidal aluminum), and the oxidizer blend was 65/35 SSMP/UFAP. The polymer was HC-434 CTPB and the curing agents a BISA/MAPO combination. The propellant mix thickened noticeably after curing agent addition, probably due to

IV.A. Task A, Laboratory Investigation of Causes of Nonuniform Surface Regression (cont)

the interaction of the BISA and the high surface area UFAP particles. Further vacuum mixing produced some reduction in viscosity but processing characteristics were marginal at this solids content. The burning rate of the CTPB/BISA/MAPO propellant was 1.10 in./sec at 1000 psi.

b. Studies of Propellant Effects

(1) Particle Deagglomeration

Ground oxidizer in general and UFAP in particular tends to form soft agglomerates during storage. Generally these agglomerates are broken up during the relatively high shear propellant mixing, and for propellants containing large amounts of fine-ground oxidizer (MA or UFAP), the propellant burning rate was found to increase with increasing propellant mix time.

Although propellant burning rate is a good indirect measurement of the extent of deagglomeration of the UFAP, a corroborative method was developed involving a direct determination of particle size distribution of the oxidizer in the propellant mix. In this procedure a sample of the uncured propellant is extracted with chlorobenzene to separate the (insoluble) oxidizer and aluminum from the (soluble) binder, plasticizer, and burning rate additive. The solids mixture is thoroughly dispensed in the chlorobenzene in a sonic agitator and then allowed to stand undisturbed for a specified length of time (0.5 hr). The supernatant liquid containing the UFAP dispersion is decanted off from the coarser oxidizer and aluminum particles which have settled out. Standard MSA particle size measurements can then be made on both fractions of propellant solids. This technique has proven to be a valuable tool in assessing the effects of oxidizer deagglomeration and classification. The reproducibility of the test is good as indicated by the results of duplicate measurements from a single batch of propellant (Figure 5).

IV.A. Task A, Laboratory Investigation of Causes of Nonuniform Surface Regression (cont)

(a) C-1/PU Propellant

The C-1/PU propellant ANP-3391 (1 in Figure 1) utilizes large amounts of MA ground oxidizer rather than UFAP to attain the desired burning rate. The effect of extended mixing on this propellant is shown in Figure 6. When the extended mix occurred before the HDI curing agent was added and the mixture is viscous, an increase in burning rate was observed with increased mix time. When the mix time was extended after HDI addition (low mix viscosity), there was no change in burning rate. These results are indicative of the strong effect that propellant viscosity has on particle deagglomeration and/or attrition.

(b) HTPB Propellants

The effects of mix time on the propellant burning rate and the particle size of UFAP extracted from the four HTPB formulations are tabulated below:

					Burning Rate at 1000 psig/UFAP Particle Size (μ) 50% pt MSA Extended Mix Time:		
SSMP	MA	UFAP	Catocene	IDP	0.5 hr	1.5 hr	2.0 hr
-	58	42	0	3	1.48/3.4(1)	1.51/3.1(1)	1.51/2.9(1)
72	-	28	1	0	1.81/0.67	1.88/0.62	1.97/0.58
72	-	28	1	2	1.55/0.69	1.59/0.64	1.64/0.51
72	-	28	1	4	1.13/0.84	1.13/0.66	1.10/0.56

Avg particle size of neat UFAP was 0.56μ

(1) Mixture of UFAP and MA

The UFAP was extracted from the remainder of the propellant solids by the techniques described above, and the particle size (50% pt) was determined in the MSA particle size analyzer.

IV.A. Task A, Laboratory Investigation of Causes of Nonuniform Surface Regression (cont)

For the propellant containing no Catocene burning rate additive there was a small increase in burning rate (between 0.5 and 1.5 hr mix time) and a small decrease in average particle size as the mix cycle was increased. The particle size measurements on this propellant were less conclusive because most of the MA ground oxidizer was present along with the UFAP in the decanted supernatant liquid and the average measured particle sizes are comparatively large.

The higher viscosity unplasticized propellant (with 1 wt% Catocene) showed significant increases in burning rate and significant decreases in UFAP particle size with extended mixing. Furthermore, MSA particle size analyses on the coarse fraction of extracted solids (SSMP plus aluminum) indicated that some attrition of the SSMP fraction had occurred (Figure 7). Similar increases in burning rate and decreases in particle size were observed with the propellant containing 2 wt% IDP.

For the formulation with 4 wt% IDP there was no apparent increase in burning rate with extended mix time although a reduction in measured UFAP particle size did occur.

(c) CTPB Propellant

The CTPB propellant (4a in Figure 1) showed no effect of extended mix time on burning rate:

Extend Mix Time, hr	MSBR at 1000 psia, in./sec
0.5	1.08
1.5	1.11
2	1.08

Interaction of the CTPB polymer with the high surface area UFAP may have interfered with the particle size measurements of the UFAP extracted from the propellant so that no meaningful MSA data were obtained. Because of the difficulties with processing and cure of this propellant, no further work was done with CTPB formulations in the Task A effort.

IV.A. Task A, Laboratory Investigation of Causes of Nonuniform Surface Regression (cont)

(2) Migration

While deagglomeration of the UFAP was found to be a significant factor affecting the bulk or average propellant burning rate, migration of liquid burning rate additive (Catocene) and/or plasticizer into the liner/insulation was shown to be the major cause of burning rate variability in the interphase. In evaluating the effects of migration of these mobile species, propellant was cast against the insulation or liner and cured. Variations in propellant burning rate as a function of distance from the insulation or liner interface were then determined using the microstrand burning rate technique described above.

In Figure 8 are shown burning rate profiles for HTPB/UFAP propellants containing 1 wt% Catocene and IDP levels of 0, 2 and 4 wt% cast against a 30-mil thick layer of SD-878-2, a liner which readily absorbs IDP and Catocene. As would be expected, the migration of IDP and Catocene have opposite effects on the burning rate. Migration of the former tends to increase the rate while migration of the latter lowers the rate. As shown in Figure 8 the effects were balanced out with a propellant containing 1 wt% Catocene and 4 wt% IDP.

The opposite effect on burning rate is observed (Figure 9) for ANP-3391 (C-1/PU) propellant cast against Rocketdyne's R-151 insulation. Here the main migrating species is IDP plasticizer (a solid burning rate catalyst is used), and the result is an increase in burning rate in the propellant interphase.

These results indicate that migration of the mobile species can have a large influence on nonuniform burning front regression in end-burning motors. Methods for control of migration and/or elimination of these interphase burning rate gradients are discussed in Section IV., A., 3. of this report.

IV.A. Task A, Laboratory Investigation of Causes of Nonuniform Surface Regression (cont)

(3) Particle Orientation

The irregular shaped solid particles (oxidizer, aluminum) in solid propellants become oriented with respect to their long axis in the direction of propellant flow during the casting operation. The extent of orientation and the degree to which the propellant properties are affected is dependent on the aspect ratio (L/D) of the particles. In some propellant systems, changes of 10 to 15% in burning rate (anisotropy) ascribable to particle orientation have been observed. In the work described below, the propellants were cast against a totally impermeable barrier (aluminum foil) to preclude migration of the mobile ingredients. Thus any changes in burning rate would be caused by orientation effects.

Orientation studies with the HTPB/UFAP propellant, ANB-3392 (4b in Figure 1), revealed that alignment of the coarse oxidizer particles does in fact occur. However, no significant anisotropic characteristics in either burning rate or mechanical properties were noted. The particles were oriented by pressure casting the propellant into a tube 24 inches long by 1.5-in.-dia. After cure, burning rates (MSBR) and microtensile properties were measured in both horizontal (H) and vertical (V) directions at the top, middle and bottom of the tube. Photomicrographs revealed significant orientation of the coarse oxidizer. However, as shown below, no directional differences were found in either burning rate or mechanical properties.

	Bottom			Middle			Top		
Tube Position	V	H	% Diff	V	H	% Diff	V	H	% Diff
MSBR at psi, in./sec	1.51	1.48	-2.0	1.49	1.48	-0.7	1.43	1.43	0.0
Modulus, psi	1308	1256	-4.1	1267	1204	-5.2	1297	1337	+3.1

V = Vertical
H = Horizontal

This lack of anisotropic occurrence is likely due to the fact that the burning rate is controlled by the UFAP, and the UFAP particles, because of a low aspect ratio, do not orient sufficiently to cause anisotropic burning rate behavior.

IV.A. Task A, Laboratory Investigation of Causes of Nonuniform Surface Regression (cont)

Tests were also conducted with the C-1/PU propellant (ANB-3391) with the following results:

	Bottom			Middle			Top		
Tube Position	V	H	% Diff	V	H	% Diff	V	H	% Diff
MSBR at 1000 psi, in./sec	1.54	1.49	-3.4	1.51	1.49	-1.3	1.52	1.45	-4.8
Modulus, psi	2355	2175	-8.3	2576	2305	-11.7	2430	2562	+5.4

V = Vertical
H = Horizontal

These data indicate that this non-UFAP-containing formulation may show a small degree of flow-induced anisotropy. However, additional evidence that neither of these formulations exhibit significant anisotropic behavior was obtained in the casting studies on large scale (up to 16-in.-dia) grains described in Section IV., A., 2. of this report.

(4) Particle Classification

It is conceivable that in propellants containing mixtures of very coarse and very fine particles, conditions of vibration and flow adjacent to an interface could exist which would result in classification of the particles, e.g., the UFAP particles could filter through the spaces between the coarser particles and concentrate next to the interface. A priori, it was believed that vibration would facilitate classification. Since flow orientation of the particle was shown to have no effect on the properties of these propellants, tests were conducted to determine if flow classification could cause burning rate variability in the interphase. To evaluate conditions conducive to particle classification, propellant was cast so that it flowed down on inclined plane and collected in a reservoir:

IV.A. Task A, Laboratory Investigation of Causes of Nonuniform Surface Regression (cont)

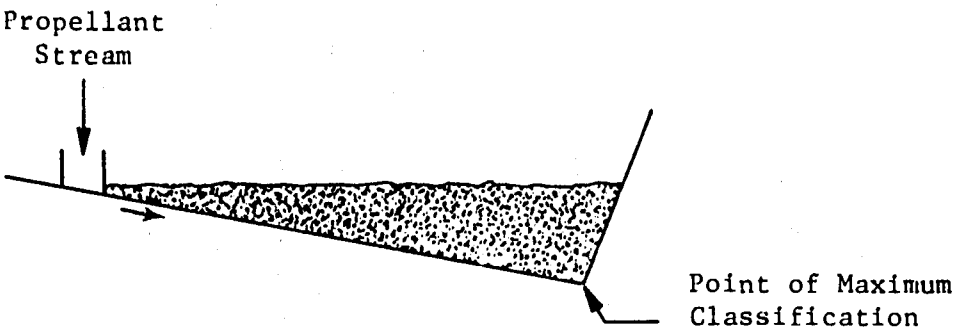

Castings similar to the above were made with and without vibration using the C-1/PU and the HTPB/UFAP propellants. The mold was lined with an impermeable barrier to prevent migration. Microstrand burning rate data on specimens taken at the bottom corner of the reservoir and in the bulk of the propellant showed the following results:

	Change in MSBR Between Bottom Corner and Bulk of Propellant	
Propellant	Vibration	No Vibration
C-1/PU	0%	0%
HTPB/1% Catocene/0% IDP	+4.1%	+0.4%
HTPB/0% Catocene/3% IDP	-	0%
HTPB/1% Catocene/2% IDP	0%	-

Only the unplasticized HTPB/UFAP (no Catocene) propellant showed a significant difference in burning rate. It also appears that vibration plays a significant role in particle classification as evidenced by a ten-fold increase in burning rate variability compared to the sample cast without vibration. The burning rate profiles for this propellant and the 2% IDP plasticized propellant are shown in Figures 10 and 11 respectively.

IV.A. Task A, Laboratory Investigation of Causes of Nonuniform Surface Regression (cont)

To confirm this apparent difference, these two propellants were again prepared and cast in a similar fashion into aluminum-foil lined molds. To facilitate removal of the solid particles for direct measurement of particle size, no curing agent was used in the batches. The propellant was sampled at the point of impingement and at distances from the bottom corner ranging from 0.1 to 0.6 in.

No change was observed in the UFAP particle size distribution at the various samping positions (Figures 12 and 13). There was, however, a difference in the coarse particle distribution for the two propellants as shown in Figures 14 and 15. In Figure 14 the distribution curves for the coarse fraction of the particles show no trend with respect to sampling position in the IDP-plasticized propellant. However, for the unplasticized formulations (Figure 15) the sample taken nearest the interface shows a higher concentration of fines than do the other positions which are all grouped within a relatively narrow band. These particle size analyses of the coarse fraction of solids confirm the interphase burning rate behavior of the two propellant systems and indicate that particle classification may be a factor affecting interphase burning rate variability of the unplasticized HTPB/UFAP formulation.

(5) Dilatation Effects

Dilatation, or the formation of vacuoles adjacent to oxidizer particles, can occur in propellant under certain levels of stress and strain. Continued growth of the vacuoles can lead to the release of the entire polymer matrix from the oxidizer surface (dewetting) with an appreciable effect on the burning rate. To determine if dilatations would be a factor in interphase burning rate variability, ANP-3391 (C-1/PU) and ANB-3392 (HTPB/UFAP) propellants were prepared with and without oxidizer bonding agents. The dilatation strain level was determined for each modification. Microstrands of each formulation were then prestrained to this dilatation strain level, encapsulated with a rigid epoxy resin, and fired in the microstrand burner. The burning rates of the propellants

IV.A. Task A, Laboratory Investigation of Causes of Nonuniform Surface Regression (cont)

at the dilatation strain level are shown in Figure 16. No effect of strain on the burning rate was noted except where the oxidizer bonding agent was not included in the formulation. The presence of the oxidizer bonding agent limits the formation of vacuoles or tears to the binder matrix during dilatation. Without the bonding agent the weak binder-oxidizer bond fails and vacuole formation adjacent to the oxidizer surface results in an increase in burning rate.

Based on these data it is concluded that if the strain level in a motor approaches the dilatation strain of the propellant, reinforcement of the binder-oxidizer bond (bonding agent) may be necessary to prevent burning rate variability.

2. Scale-Up and Casting Studies

The results of the laboratory work described above indicate that the major contributor to interphase burning rate variability is migration of mobile species. To confirm this conclusion, two of the propellants (ANP-3391 and ANB-3392) were scaled-up in batch size and cast into subscale (4- and 9-in.-dia) and full-scale (16-in.-dia) molds for evaluation of effects of scale-up and casting technique on interphase burning rate. All molds were aluminum-foil lined to prevent migration.

A 60-lb batch of each formulation, ANB-3392 and ANP-3391 was cast into 4.5- to 5-in.-dia molds by a variety of casting techniques. These were:

Cast Method	Casting Head	Vibration
Vacuum, free-fall	2 in. dia orifice	No
Vacuum, free-fall	2 in. dia orifice	Yes
Bayonet	2 in. dia orifice	No
Bayonet	4 in. dia multi-orifice	No
Vacuum, free-fall	4 in. dia multi-orifice	No

IV.A. Task A, Laboratory Investigation of Causes of Nonuniform Surface Regression (cont)

After propellant cure, microstrand burning rates were measured normal to the grain surface in the areas shown in Figure 17. These data are shown in Figure 18 for ANB-3392 and in Figure 19 for ANP-3391.

To provide an improved basis of comparison of the burning rate data obtained from the different casting methods, the data were normalized by dividing the individual burning rates by the average burning rate obtained over the sampling surface. These data are presented in Figure 20 for ANB-3392 and Figure 21 for ANP-3391 where the ratio of each data point to the mean value is shown for each sampling position in all the casting methods examined. As indicated by the data, no consistent pattern of burning rate variability across the grain attributable to a particular casting method was observed. However, an analsis of variance was performed on the pooled data shown in Figures 20 and 21 which revealed that although there was no statistically significant difference in the ANP-3391 data, there was a difference in the ANB-3392 data. This difference could not be correlated with the casting methods used, and it was postulated that it was the result of small temperature fluctuations in the microstrand burner during testing of the strands. The temperature sensitivity of burning rate of ANB-3392 is much higher than ANP-3391 (Section IV., A., 4., b.) which could explain why no differences could be detected with this latter formulation.

To substantiate this hypothesis, the data for ANB-3392 were corrected for temperature effects based on control strand firings routinely conducted prior to and during each series of tests. This analysis was performed on data obtained from the top and bottom of a grain prepared by bayonet casting through a 4-in.-dia multiorifice head (no vibration) and another grain which was vacuum cast through a 2-in.-dia orifice with vibration. The uncorrected data (Figure 22) showed a significant difference in the variance analysis, while the data corrected for temperature effects (Figure 23) did not. Based on these results, improved temperature control equipment was installed on the microstrand burner.

IV.A. Task A, Laboratory Investigation of Causes of Nonuniform Surface Regression (cont)

These statistical analyses verify the earlier observations that there is no appreciable variability in the burning rate profiles in grains of these particular propellants that can be influenced by the casting method used.

Based on an analysis of these test results, a vacuum casting with vibration technique was tentatively selected for processing the subscale and full-scale motors. To confirm that this method would not introduce within-grain variability in burning rate for these motors, 4-, 8.5-, and 16-in.-dia grains were cast from 30-gal batches of ANB-3392 through a 2-in.-dia orifice. Microstrand burning rates were measured normal to the surfaces across the diameters of the grains. The burning rate profiles (Figures 24, 25, and 26) showed no effect which could be attributed to propellant or casting parameters.

Analysis of the regression lines through the data points showed no significant differences from the mean values.

3. Liner Interphase Parameters

The results of the laboratory investigations of propellant formulation effects and the scale-up and casting technique studies provide strong evidence that migration of the liquid burning rate additive (Catocene) and/or plasticizer into the liner/insulation is the chief cause of burning rate variability in the propellant interphase. It then becomes necessary to define methods for preventing migration or compensating for its effects while maintaining good bonds between propellant and motor insulation.

a. Balancing Concentration of Mobile Species

The liner SD-878-2 has been used successfully at Aerojet with a number of HTPB formulations; ANB-3392 bonds to this liner with a strength exceeding the cohesive strength of the propellant. However, the tendency of this

IV.A. Task A, Laboratory Investigation of Causes of Nonuniform Surface Regression (cont)

liner to absorb Catocene and plasticizer from the propellant with corresponding changes in interphase burning rate (see Section IV., A., 1., b., (2)) is an unacceptable characteristic.

One method of minimizing or eliminating migration into this liner is to incorporate the Catocene or plasticizer into the liner itself prior to casting with propellant. This approach was demonstrated with ANB-3392 propellant cast against SD-878-2 liner containing Catocene in amounts equivalent to 1/4, 1/2, or equal to that in the propellant binder. Microstrand burning rates measured across the interphase (Figure 27) show this method to be effective in minimizing burning rate gradients due to migration of Catocene.

Although this test was conducted with the liner only (on aluminum foil) it would be expected that the principle could be extended to include addition of plasticizer or Catocene to both liner and insulation in a motor bonding system.

b. Barrier Coats

The tendency of the mobile species in the propellant to migrate is a direct function of the permeability of the liner and insulation to the migrating materials. This permeability is related to the polymer structure and cross link density and varies widely among different liners and insulations as indicated by data on absorption of IDP and Catocene (Figure 28). Two of the least permeable materials are the SD-886-1 liner and an epoxy material composed of NPGA/MNA/DER-332 with glass beads as a filler.

The low permeability of these materials suggests that they could be used as barrier coats on the insulation to inhibit migration of plasticizer or burning rate additive. To evaluate the advantages of such a barrier, 30 mil coats of each material were applied to R-151 insulation and cast with ANB-3392 propellant. As shown by data in Figure 29, both materials effectively

IV.A. Task A, Laboratory Investigation of Causes of Nonuniform Surface Regression (cont)

eliminated burning rate decrease in the interphase. The burning rate increased in the interphase with ANP-3391 (C-1/PU) was likewise eliminated (Figure 30) by use of a 30 mil barrier coat of SD-886-1.

The R-151 used in the above tests was 0.10 in. thick. Barrier evaluation tests were also performed with thicker (3/8 in.) sections of R-151. Burning rate profiles of the R-151/ANP-3391 system are presented in Figure 31 for the interphases composed of R-151 (3/8 in. thick) with 0, 15, and 50 mils SD-886-1. Analysis showed no significant difference between the mean value of the burning rates and the regression line for either thickness of SD-886-1 (Figure 31). The data for the interphase containing the uncoated R-151 insulation show the effect of migration in that the burning rates are above the $+3\alpha$ limits of the R-151/SD-886-1 system for a distance of 0 to $\sim$250 mils from the interface.

Similar tests were performed with ANB-3392 propellant (Figure 32). The R-151 was coated with 15, 30 and 50 mils SD-886-1. The regression line determined from the combined data shows a slope significantly different from the mean (Figure 32). Regression analyses run on the individual interphase burning rate profiles show that the slope is significantly different from the mean only where the 50 mil thick coating of SD-886-1 is used. It is believed that this discrepancy is due to temperature variation during strand firing, since it is unlikely that a thicker coat of SD-886-1 would promote burning rate variability. Further confirmation of this supposition is found in the fact that the burning rates show a slight increase near the interface rather than a decrease (which would occur if migration of Catocene had taken place).

Since the permeability of the barrier and its capability to inhibit migration could depend on the physical and chemical properties of the cured binder, a series of tests was conducted to evaluate the effects of SD-886-1 liner processing variables on migration of plasticizer from ANP-3391 propellant. The processing variables examined were liner thickness (30 and 50 mils), cure temperature

IV.A. Task A, Laboratory Investigation of Causes of Nonuniform Surface Regression (cont)

(135 to 180°F), and cure time (6 to 24 hours). Microstrand burning rates were measured across the interphase of molds containing SD-886-1 liner prepared under the above conditions and cast with ANP-3391 propellant. The data (Figure 33) show no significant effect on interphase burning rate in spite of this wide variation in liner processing conditions.

Although these barriers effectively inhibit migration of plasticizer and Catocene under the conditions tested, this solution may not be completely satisfactory in preventing burning rate variability because the barriers do not have a zero permeability but rather possess low permeability. Thus changes in burning rate may occur during long term storage, particularly at elevated temperatures. Since migration of these materials is governed by diffusion equations (such as Fick's law), the magnitude of the change in burning rate with a given barrier will depend on temperature, time, and concentration of the migrating species.

To gain a preliminary assessment of the effects of storage at elevated temperature on the effectiveness of the SD-886-1 liner barrier, interphase burning rates were measured in ANB-3392 propellant cast against R-151 insulation with and without the barrier. The measurements were made after storage of the specimen for 38 days at 80°F and after storage for 17 days at 80°F followed by 21 days at 135°F. The data (Figure 34) indicate that migration does increase in the sample without the barrier as a result of the elevated temperature. However, the interphase burning rates of the samples with the barrier show no variability, indicating that the barrier is still effective under these conditions. There appears to be an upward shift in the burning rate of the propellant as a result of 135°F storage; this effect was confirmed subsequently in other storage tests described in Section IV., A., 4., b., (3) of this report.

Based on the above data, it is concluded that the use of a low permeability barrier to inhibit migration is a sound approach, but additional work is being conducted in an expanded laboratory effort to better define the effects of storage conditions, barrier composition, and chemical nature of the mobile species on migration through these low permeability barriers.

IV.A. Task A, Laboratory Investigation of Causes of Nonuniform Surface Regression (cont)

c. Liner-Propellant Bond

In addition to minimizing migration of mobile species, a barrier coat must also be capable of providing a good bond strength to the propellant. Both the SD-886-1 and the epoxy barriers (A-35 washcoat used with the latter) do bond well to the HTPB/UFAP propellant ANB-3392 propellant as shown by standard DPT screening tests shown below:

	Bond Tensile Strength, psi			
	-65°F	77°F	150°F	
R-151/EpoxyBarrier*/A-35	518	156	110	
R-151/SD-886-1	673	199	128	
			139	(after 48 hr at 150°F)

* NPGA/MNA/DER-332/Glass beads

The bond tensile strength of the C-1/PU propellant, ANP-3391, to SD-886-1 was also quite high:

	Tensile Strength, psi		
Insulation/Liner	-65°F	77°F	150°F
R-151/SD-886-1	618	245	145

These results suggest that good bonds are obtainable with either type of propellant to SD-886-1 liner. However, additional tests were conducted using poker chip specimens to better define the bond strength as a function of temperature and to compare the bondability of SD-886-1 liner to that of the NPGA/MNA/DER barrier originally evaluated by Rocketdyne. The specimens were constructed as follows: metal/Chemlok-305 adhesive/ANB-3392 propellant/liner (barrier) R-151 insulation/Epon-901 adhesive/metal. A-35 washcoat was used on the DER-332/MNA/NPGA barrier material. The propellant thickness was 0.3 in. by 3.5-in.-dia and cut back 0.5 in. along the periphery at the liner/propellant interface, so that

IV.A. Task A, Laboratory Investigation of Causes of Nonuniform Surface Regression (cont)

the effective diameter of the liner/propellant bond interface was 2.5 in. The specimens were tested at a crosshead speed of 0.02 in./min at temperatures of -70, -45, 77, and 140°F. Even though the stress was concentrated in the reduced propellant/liner bond area, the failures all occurred at the propellant/Chemlok-305 glue line. Thus, the true strengths of propellant/liner systems tested are greater than the measured values (Figure 35). The values for both bonding systems appear to be essentially identical.

Preliminary tests indicate satisfactory bond storage stability for both barrier systems. DPT specimens composed of ANB-3392 bonded to either barrier show no appreciable change in bond strength over a nine week storage period at 77°F (Figure 36).

Because of the superior bond strength of both propellant systems to SD-886-1 and its effectiveness in minimizing burning rate variability in the interphase, it was selected for use in lining the test motors to be fired in the Task B Subscale Motor Test effort.

d. Microvoids

One possible cause of uneven burning surface regression in end-burning motors was postulated to be microvoids entrapped by an uneven liner surface during grain casting. To evaluate this possibility, the HTPB/UFAP propellant ANB-3392 was cast against clear plastic in sheet and cylindrical form. Even with a very uneven surface (caused by lettering impressions in the plastic), no voids could be observed in a microscopic examination (250X) of the interface. From the results of these tests it was concluded that microvoids are probably not a contributing factor to the uneven burning surface regression.

IV.A. Task A, Laboratory Investigation of Causes of Nonuniform Surface Regression (cont)

4. Propellant Selection for Task B

a. Basis for Selection

Two propellant systems were selected for scale-up and testing in subscale motors in Task B. These were the C-1/PU system (1 in Figure 1) designated ANP-3391 and the HTPB/UFAP formulation containing 2 wt% IDP (4b in Figure 1) which was coded ANB-3392. An important consideration in eliminating Formulations 2 (HTPB/UFAP, no Catocene), 3 (HTPB/UFAP, no IDP) and 4a (CTPB/UFAP) was the rapid viscosity buildup associated with these propellants (refer to Figure 4). Formulation 4c (HTPB/UFAP, 4 wt% IDP) was extremely fluid but too low in burning rate. The low burning rate as well as the low viscosity of this formulation is a direct result of the high IDP content. Increasing the IDP content of the HTPB/UFAP propellants from 0 to 4 wt% has a marked effect on the burning rate as shown in Figure 37.

ANP-3391 was selected because, in addition to its excellent processing characteristics, it has a solid burning rate accelerator, Cu0202. Also, since there is no UFAP in this formulation, a broader base of formulation characteristics could be examined.

b. Properties of Selected Propellants

(1) Processing Properties

Both propellants have excellent processing characteristics as determined by viscosity measurements for periods up to six hours after curing agent addition, thus providing ample time to cast the full-scale motors. ANP-3391 (C-1/PU) was the more fluid of the propellants with viscosities of ~2000 to 13,000 poises (110°F) at 2.5 and 6 hours, respectively, after curing

IV.A. Task A, Laboratory Investigation of Causes of Nonuniform Surface Regression (cont)

agent addition (Figure 38). ANB-3392 (HTPB/UFAP) possessed a somewhat higher initial viscosity, ~10,000 poises, which increased to 20,000 to 24,000 at 6 hours after curing agent addition.

The effect of applied shear stress on viscosity for these propellants (Figure 39 for ANP-3391 and Figure 40 for ANB-3392) indicate that ANP-3391 was essentially Newtonian in flow behavior up to six hours after curing agent addition. ANB-3392 exhibited near-Newtonian flow behavior for up to four hours from curing agent addition with slight pseudoplasticity at six hours. These excellent flow characteristics virtually assure that sound end-burning grains can be cast.

(2) Mechanical Properties

The analysis of the mechanical properties ANP-3391 and ANB-3392 are presented in Appendix A.

(3) Burning Rates

The solid strand burning rates (Crawford bomb) of ANP-3391 and ANB-3392 measured over the temperature range of -65 to +150°F (shown in Figures 41 and 42 respectively) indicated that temperature sensitivities of the propellants were 0.09°F for ANP-3391 and 0.26%/°F for ANB-3392. This 0.26% value is considerably higher than anticipated; motor firing to define the correct value are planned.

The excellent reproducibility of the burning rates as well as viscosity characteristics of ANB-3392 prepared in batch mixes ranging from 1- to 350-lb is illustrated by data shown in Figure 43. This highly desirable reproducibility of both burning rate and processability was obtained even though four different grinds of UFAP were used.

IV.A. Task A, Laboratory Investigation of Causes of Nonuniform Surface Regression (cont)

Fine adjustments to the burning rate of this propellant can be easily accomplished through small changes in the Catocene level. Data available (Figure 44) indicate that burning rates of approximately 0.5 to 3.2 in./sec at 1000 psia can be achieved by varying the Catocene content from zero to 5 wt%.

To evaluate the effects of elevated temperature aging on the burning rates of these propellants, bulk specimens of ANP-3391 and ANB-3392 were stored at 135°F for periods of 0, 3 and 6 weeks and solid strands were fired over a pressure range of 800 to 3000 psig. As shown by the data (Figure 45) ANP-3391 exhibited essentially no change in burning rate during these storage periods. ANB-3392, however, did show a small increase in burning rate (average of 4.4%) during storage with all the change occurring during the first three weeks at 135°F (Figure 46). The increased burning rate did not change the pressure exponent, Figure 47).

The insensitivity of the burning rate of ANP-3391 under accelerated aging conditions is in agreement with previous experience with C-1/PU propellant utilizing the solid burning rate catalyst, CuO202. ANB-3392 uses a liquid burning rate accelerator, Catocene, which apparently undergoes a chemical or activity change in propellant stored at elevated temperatures.

B. TASK B, SUBSCALE MOTOR TESTS

The objectives of the Task B subscale motor tests were (1) to confirm the causes of uneven burning surface regression established in the Task A laboratory effort, (2) demonstrate methods of burning control and performance prediction, (3) determine effects of motor and nozzle design parameters, and (4) provide data basis for work to be conducted in Task C.

IV.B. Task B, Subscale Motor Tests (cont)

Nineteen 3KS-1000 size motor tests were conducted as part of the Task B effort. Eleven of these motors were tested at Aerojet and eight at NWC. The specific objectives of each of these motor tests are summarized below:

Test Number	Tested At		Propellant ANB-
1	Aerojet		3392
2	Aerojet	Evaluate effects of nozzle entrance angle and motor L*	3392
3	Aerojet		3392
4	Aerojet		3392
5	Aerojet	Confirm L* effect with C-1/PU	3391
6	Aerojet	Confirm effect of low L*	3392
7	Aerojet	Test at +140°F	3392
8	Aerojet	Stress relieved bonding system	3391
9	Aerojet		3392
10	Aerojet	Evaluate effect of migration	3391
11	Aerojet	Stop-fire	3392
12	NWC		3392
13	NWC	Evaluate flame front regression with	3392
14	NWC	X-ray motion pictures	3392
15	NWC		3392
16	NWC		3391
17	NWC	Evaluate flame front regression with	3391
18	NWC	X-ray motion pictures	3391
19	NWC		3391

A tabulation of the results of these subscale motor tests is given in Figure 48, and a detailed description of the igniter and motor designs and the results of the individual tests are presented in the following paragraphs. Also presented is an interior ballistics analysis of end-burning grain performance as related to the experimental findings under this task.

IV.B. Task B, Subscale Motor Tests (cont)

1. Igniter Design

a. Arc-Image Ignitability Tests

Arc-image furnace ignitability tests were conducted on ANB-3392 and ANP-3391 propellants. The objectives of the tests were to determine the threshold ignition energy requirement (TIER) and the low-pressure ignition limit, P*, of the fresh cut surfaces of each propellant. This information was needed to design igniter systems for the motors.

The threshold ignition energy requirement is defined as the radiant energy required to ignite the propellant with a 0.50 probability as determined by observation of consecutive fire and no-fire tests, which have the narrowest possible range of exposure times allowed by the ignition characteristics of the propellants. From 10 to 20 tests are conducted per flux-pressure condition to determine the ignition energy requirement. The low-pressure ignition limit, P*, is defined as the pressure below which sustained ignition and combustion does not occur. This is done at a constant, arbitrarily chosen exposure time of 300 milliseconds, which was selected because it exceeds the action time of most igniters by a wide margin and yet is short enough to preclude total ablation of the sample in the event of a no-fire test. The ignitability measurements were conducted at a flux level ($\dot{Q}$) of 80 cal/cm^2-sec and pressure levels of 1, 2, and 3 atmospheres in nitrogen gas.

The ignitability data are presented in Figures 49 and 50. The threshold ignition energy requirement (TIER), is the product of the flux and exposure time at a given pressure because the radiant energy pulse-time profile is essentially a square wave. Data in Figure 49 show that the propellants vary only slightly in TIER at one atmosphere and are nearly equal at two and three atmospheres. In Figure 50 it is seen that the ignitability (exposure time) of each propellant is a strong function of pressure. The pressure asymptote is estimated to be at five atmospheres. The P* values are not unusually low for fast burning propellants;

IV.B. Task B, Subscale Motor Tests (cont)

however, TIER data for both propellants (1.3 and 1.4 cal/cm^2 at 2 atm) place them in an extremely ignitable category compared with other polybutadiene and polyurethane propellants, such as ANB-3066 and ANP-2932, both of which have TIER values of 4.0 to 5.0 cal/cm^2 above two atmospheres.

b. Igniter Selection

Based on the motor size, grain design, and arc-image testing the igniter selected was a pencil-type consisting of a paper tube filled with an 11-gm charge of $BKNO_3$ pellets.

2. 3KS-1000 Size Motor Design

Standard ASPC 3KS-1000 motor chambers and hardware were modified for the subscale end-burning motor tests. The chambers were made from 5-in. dia steel pipe and were hydrotested at 2500 psi. The head end and nozzle were assembled to the chamber with a single set of tie bolts. Motor free-volume was adjusted for L* evaluation by varying the head end potting thickness. The chambers were modified to accept two Taber pressure transducers, a Kistler high-frequency pressure transducer and a Hy-Cal Asymptotic calorimeter. Uniformity of flame front regression was to be determined by thermocouples placed in the propellant grain.

The nozzles were designed for optimum expansion with either a 45- or 20-degree entrance (with respect to centerline) and a 15-degree conical exit. Silver-infiltrated tungsten throats were fitted into ATJ graphite inserts to preclude significant erosion.

Provisions were made for installation of thermocouples in the grain located in staggered axial and radial positions to allow for a semi-quantitative assessment of the shape of the burning surface. It was planned to install the thermocouples either prior to casting or by drilling and potting the junctions into the cured grain.

IV.B. Task B, Subscale Motor Tests (cont)

3. Results of 3KS-1000 Size Motor Tests

a. Motor 1

The first subscale test motor fired was to have been part of a series of four to evaluate the effects of L* and nozzle entrance angle with ANB-3392 propellant.

The performance of this 13KS-1000 subscale motor was progressive, starting at 1400 psia and increasing to 3150 psia at 1.18 sec, when the aft chamber seal failed. The nominal pressure was to have been 1900 psia for 5.5 sec.

It was concluded that the progressive increase in pressure was caused by a progressive failure of the bond between the SD-830 potting compound and the propellant. The burnthrough occurred near the location of a Vibradamp ring seal that apparently failed. The design of the subsequent motors was altered in that the grains were fully released, restricted, and cartridge loaded into an insulated chamber.

b. Motor 2

Motor 2 used ANB-3392 HTPB propellant with an L* of 630 in. and a nozzle entrance angle of 45 degrees. Pressure and thrust-time histories are given in Figure 51. The ignition transient was smooth and uniform. Burning of the motor was neutral until 4.918 sec, when the center thermocouple was exposed. The thermocouples located at 1.0-in. radius and the liner/interface (at the same axial station as the center thermocouple) were exposed at 4.980 and 5.058 sec, respectively, indicating thermocouple restriction failures and adding to the pressure rise, which peaked at 2405 psia at 5.403 sec, when web burnout started. The motor thrust trace followed the pressure profile and indicated an essentially constant throat area.

IV.B. Task B, Subscale Motor Tests (cont)

c. Motor 3

Motor 3 was the same configuration as Motor 2, except that the nozzle entrance angle was 20 degrees with respect to the centerline. Performance was also similar to Motor 2, as shown in Figure 52. The effect of nozzle entrance angle was apparently insignificant. A slight pressure rise started at about 4.0 sec and leveled off at 4.6 sec. The center, 1.0 in. radius and liner interface grain thermocouples were exposed at 5.085, 5.170, and 5.184 sec, respectively, again causing a sharp pressure rise. The maximum pressure of 3550 psia occurred at 5.323 sec, when the nozzle insert ejected.

Based on the results of these first two tests, installation of thermocouples by potting into the cured grain was discontinued.

d. Motor 4

The fourth motor used the 45-degree nozzle with the smaller L* of 264 in.. No thermocouples were installed in the grain. The initial performance, including the ignition transient, was similar to Motors 2 and 3. The difference in performance as result the L* change was apparently insignificant. The remainder of the ballistic performance was exceptionally neutral, with a sharp tailoff as shown by the pressure and thrust traces (Figure 53).

e. Motor 5

The ANP-3391 C-1 polyurethane formulation was used for the first time in Motor 5. The grain was bonded to a Micarta sleeve. Grain thermocouples were placed in the uncured propellant to assure adequate restriction of the insulated wires.

The performance of this motor (Figure 54) indicates a significant degree of progressivity in the first second of burning. After an indication of "rounding over" to neutral burning at 1.0 to 1.2 sec, additional

IV.B. Task B, Subscale Motor Tests (cont)

progressivity was experienced causing a maximum chamber pressure of 2380 psia at 2.5 sec. The remainder of the trace is regressive, except for the period of 4.02 to 4.20 sec. At 3.885 and 3.995 sec, the grain thermocouples at the liner interface and at 1.0 in. radium was exposed without incident. At 4.020 sec the center thermocouple at the same station was exposed, causing a 180 psi pressure increase.

The non-neutral performance of this motor was attributed to a bond stress-induced failure causing burn front acceleration, with the effect of a progressive restriction failure in the period up to 2.0 sec. The regressivity of the last portion of the trace would be the effect of the burn front returning to a more normal shape, or nearly flat. The failure at the center thermocouple demonstrates this progressive-regressive behavicr.

f. Motor 6

Motor 6 was fired to confirm the performance of Motor 4, using the small L* of 264 in. with ANB-3392 propellant. As can be seen in Figure 55, the ballistic trace is slightly progressive up to about 1.5 sec and is neutral-to-regressive for the remainder of the firing. There is an unexplained momentary dip at 1.8 to 1.9 sec. However, the overall curve shape can be considered to be neutral, being within $\pm$ 2% of average after 0.5 sec.

g. Motor 7

Motor 7 was test fired to evaluate ballistic performance of the ANB-3392 propellant at 140°F. The grain was stress-relieved by casting the propellant into a Gen-Gard 4030 insulation sleeve lined with SD-886-1. The motor L* was 600 in..

IV.B. Tssk B, Subscale Motor Tests (cont)

Performance of this motor was not neutral, as shown in Figure 56, snd the opersting pressure wss significantly higher thsn expected. The appsrent π_K derived from the sverage burning rste was determined to be 0.67%/°F, compared with a value of 0.33%/°F for solid strands over the 80 to 140°F range, or 0.26%/°F over the range of -65 to +140°F.

The abnormal performance of this motor can be partially attributed to surface area varistions occurring at small voids within the propellant grain. Figure 56 also shows s qualitative comparison of void exposure within the pressure-time characteristic, indicating that st least the small perturbations and the progressive trend relate to burning surface variation. The true temperature sensitivity of the ANB-3392 propellant burning rate cannot be accurately assessed on the basis of this test.

h. Motor 8

The eighth 3KS-1000 motor fired using a stress relieved grsin of ANP-3391 propellant. Motor parameters were similar to Motor 5.

As seen in Figure 57, the ballistic curves are neutral, with the exception of s slow ignition transient. The ignition phase, as well as the distinct change in pressure level at 1.4 sec, are not immediately explainable. Otherwise, the performance is neutral with a sharp tailoff, indicating uniform flame front regression. The burning rate in 3KS-1000 motors for ANP-3391 propellsnt is slightly higher than the ANB-3392 propellant burning rate obtained in previous firings st 80°F, i.e., 2.05 vs 1.94 in./sec at 2000 psia.

i. Motor 9

3KS-1000 Motor 9 was test fired to demonstrate ballistic performance of the HTPB formulation ANB-3392 with a plasticizer permeable liner (SD-878-2). Migration of both plasticizer and burning rate catalyst into the EPR

IV.B. Task B, Subscale Motor Tests (cont)

insulation results in a lower burning rate adjacent to the liner, since the loss of the burning catalyst overrides the loss of plasticizer. This behavior has been demonstrated with microstrand samples. The effect on motor performance is to cause initial burning progressivity as partial surface doming develops, followed by neutral burning as the amount of doming stabilizes, at approximately the level of pressure produced without migration.

As seen in Figure 58, the test results do not fully substantiate the expected behavior. Between 1.0 and 4.5 sec, the chamber pressure is higher than expected, as scaled from Motor 4 using the larger throat diameter (0.479 vs 0.419-in.^{2}) with no migration effects. Some of this non-neutrality can be attributed to throat area variation, also shown in Figure 58, but back-calculations of surface area and a high average burning rate (about 7%) suggest that the unusual performance might have resulted from grain defects. The pressure increases at 1.0 and 3.7 sec correspond to axial locations of groups of small voids observed in X-ray examinations, although the void surface area appears insufficient to cause the magnitude of pressure increase. The effective grain diameter (also plotted in Figure 58) indicates variations up to 0.12 in. in dia, which is considerably more than the observed maximum variations (from radiographs) of up to 0.03 to 0.04 in. The expected initial progressivity occurred before 1.0 sec and the neutral pressure level after 4.5 sec is close to that expected. Thermocouples implanted in the grain 0.5 in. from the forward end at three radial locations indicated doming of approximately 0.10 in.

j. Motor 10

The tenth 3KS-1000 motor was test fired to demonstrate ballistic performance of the C-1/PU formulation ANP-3391 with a plasticizer-permeable liner (SD-896). With this propellant a solid burning rate additive is used, so that plasticizer migration into the EPR insulation results in increased burning rate at the liner interface. The effect of this on end-burner performance is to develop a coning of the burn front and corresponding progressive pressure

IV.B. Task B, Subscale Motor Tests (cont)

and thrust characteristics. Figure 59 shows that this behavior was well-demonstrated in this firing with full-duration progressivity indicated. Thermocouples in the grain measured a cone height of 0.52 in. at web burnout.

The initial operating pressure was predicted to be 913 psia on the basis of solid strand burning rate, measured throat area and C_w. An increase of 2% in pressure was estimated for the effect of the higher peripheral burning rate, resulting in a pressure of 931 psia, which is only slightly higher than the actual pressure of 910 psia. This 2% increase in pressure was based on the microstrand burning rates and profile across the interface of a section of the propellant removed from the aft end of the grain.

The maximum pressure was calculated in a similar manner based on a surface area derived from the thermocouple exposure times. The increase in surface area was about 8%. The calculated pressure, including an estimate of burning rate gradient was 1135 psia, slightly lower than the measured value of 1245 psia. This difference is probably related to inaccuracy in completely describing the developed surface area.

k. Motor 11

Motor 11 was planned as a stop-fire so that the quenched burning surface could be observed. The motor was similar to those tested at NWC using ANB-3392 propellant. The chamber was modified in the aft end to provide access for a high-pressure water quench. The nozzle insert was retained in the housing by a ring held in place by eight explosive bolts. The bolts were to be fired at an intermediate burning duration, followed by actuation of the quench at low pressure.

The motor ignited normally and operated at the expected pressure level shown in Figure 60. At 3.24 sec the throat insert was ejected by firing the explosive bolts. Chamber pressure dropped correspondingly, but burning

IV.B. Task B, Subscale Motor Teats (cont)

continued at a very low preaaure. The quench actuation waa inadvertently delayed until 11.91 sec. The quench caused a subatantial increaae in preaaure until 13.06 aec when motor operation was terminated by ejection and destruction of the grain cartridge

At the time the nozzle insert waa ejected, the grain cartridge, restrained by the nozzle housing, was apparently moved aft by the large pressure differential during depreaaurization. This reaction was necessarily accompanied by buckling of the aft end of the cartridge phenolic sleeve, thereby displacing the location of the holes in the sleeve needed to provide acceas for the quench water to spray on the grain face. Then, when the quench was actuated, the water pressure was applied outaide the grain cartridge, causing the grain ejection.

1. NWC Tests

Based on an analysis of the results of the subscale motor testa conducted at Aerojet, a motor design configuration was selected for a series of teats at NWC to provide final continuation of the solutions to the problem of non-uniform burn front regression in subscale motors. Eight 3KS-1000 size motors were tested; four with ANP-3391 and four with ANB-3392. Motor parametera were the aame for all eight tests: L* = 600 in., nozzle entrance angle of 45 degrees, and a throat area of 0.138-sq in. The barrier liner SD-886-1 was used in all motors.

All motors were X-rayed during firing (motion pictures) as well as being instrumented for pressure and thrust. Figures 61 through 68 show the pressure and thrust plots for the ANP-3391 grains. Review of the X-ray films has shown that the burn front progression was essentially uniform in all casea.

In assessing the performance of the ANP-3391 grains, the thrust curves (Figures 62, 64, 66, and 68) are indicative of the neutrality achieved. The initial progressivity up to 1.0 sec is similar to that noted in motors fired at Aerojet. The overall trend appears to be very slightly progressive, with the

IV.B. Task B, Subscale Motor Tests (cont)

exception of grain No. 6 of Batch 71-33, where the progressivity is slightly pronounced. There is no known variation in this particular grain that would result in this behavior. It is possible that the thickness of the liner was inadequate to prevent plasticizer migration, but there is no specific evidence to support this conclusion.

The pressure curves do not necessarily display the same degree of neutrality as the thrust curves. This deviation is attributable to nozzle throat area changes, primarily because of aluminum oxide deposition and removal, sometimes abruptly, such as shown in Figures 67 and 68, resulting in ringing of the thrust stand and oscillation of the thrust traces.

Figures 69 through 76 show the pressure and thrust plots for the ANB-3392 grains. Performance of the ANB-3392 grains was more uniform. Figures 70, 72, 74 and 76, show that the thrust traces are neutral, with grains 5, 7, and 8 showing a slight saddle shape and grain 6 showing slight overall progressivity. As mentioned previously, the variations in the corresponding pressure-time curves are attributable to throat area changes (Figure 69).

4. Results of 10KS-2500 Size Motor Tests

Based on the highly successful performance of the 3KS-1000 size (4.5-in.-dia grain) subscale motors at NWC, the same barrier liner and generally the same motor parameters were selected for scale-up to the 10KS-2500 size (8.5-in.-dia grain) motors.

One 10KS-2500 size motor was prepared with each propellant formulation, ANP-3391 and ANB-3392. The motors contained 39-in.-long by 8.5-in.-dia grains that were cast in 0.080-in.-thick sleeves of Rocketdyne R-151 EPR insulation lined with the SD-886-1 liner. The grains were bonded to the case only at the forward end. The motor L* was 200 in., smaller than the 3KS-1000 motors but similar to that expected in the full-scale motor, and the nozzle was sized to operate at about 1300 psia.

IV.B. Taak B, Subscale Motor Teats (cont)

As ahown in Figure 77, the firat motor (with ANP-3391) ignited and operated normally until about 2.0 sec, when the preasure traces started to behave erratically. P_{c1} apparently was plugged with aluminum oxide and failed to register accurately again. P_{c2} became intermittently plugged until the period of 4.6 to 6.05 sec. The motor thrust trace showed relatively normal but progressive behavior until 6.05 aec, when the nozzle-to-case seal failed, causing a progreasively larger hole in the pressure vessel (at the gap in the snapring and near the P_{c2} preaaure line), the resultant performance decrease, and 2 to 3 minutea of low-pressure burning. There are some abrupt changea in thrust level at several points, but these cannot be correlated with pressure and may be associated with a test atand or load cell anomaly.

The loss of chamber preasure data was attributed to aluminum oxide plugging of the pressure pickup. Posttest evidence of plugged pressure porta substantiates this conclusion. The pressure taps were located in the nozzle insulation outside the graphite insert, as there was no practical way of tapping the caae wall.

The cause of the seal failure was not readily evident. The nozzle ia attached to the chamber with a snapring, the installation of which requires the use of a compression ring between the nozzle and chamber insulation. The usual precautions were taken in inspection of the mating steel components and O-ring seal. A silicone rubber sealant was used at the insulation interfaces and the internal surfaces were ins ected using a mirror after motor assembly. On postfire inspection the 0.30 in. of IBC-111 case insulation was charred to the steel over a wide area, but this is attributable to the excessive burn time. The silicone rubber compression ring was largely intact and bonded to the nozzle, except where the leak occurred, which would be the expected condition in this situation. It was concluded that either the compression ring provided inadequate thermal protection, or the seal was initially defective.

IV.B. Task B, Subscale Motor Tests (cont)

Because of the difficulties with the pressure port plugging and nozzle sealing in the standard 10KS-2500 hardware, the second grain (ANB-3392) was removed from the 10KS-2500 chamber and reinstalled in a heavyweight workhorse chamber of slightly larger diameter, but about 12-in. shorter. This action allowed pressure measurement through the case wall, greater case insulation thickness, a more positive flange-joint seal, and a more elaborate insulation joint interface. IBC-111 insulation was cast around the grain to supplement the existing insulation.

The motor was successfully test fired showing a slightly progressive thrust-time characteristic, as shown in Figure 78. The more neutral pressure curve is the result of throat erosion. The silver-infiltrated-tungsten was severely scalloped on the entrance contour, with the pattern extending past the initial throat plane. This behavior was apparently caused by momentary deposition of unburned aluminum exaggerating the local heat transfer rate.

The initial operating pressure was very close to the predicted 1300 psia. The subsequent non-neutrality of the thrust is not readily explained on the basis of what is known about the grain. X-rays of the grain previously showed scattered small voids, but there is no evidence of significant area variations either from voids or from non-uniformities in diameter.

5. Interior Ballistics Analysis

Establishing the capability to predict the performance characteristics of end-burning motors is an important objective of the program. An analysis of the interior ballistics of end-burning motors based on theoretical considerations as well as the results of the laboratory and subscale motor tests is the first step in achieving this capability. Based on this analysis, a computer program describing the ballistic performance has been prepared and checked out, although refinements to the program are still in process.

IV.B. Task B, Subscale Motor Tests (cont)

Analysis of the interior ballistics of the end burner is divided into seven sub-sections dealing with specific problem sreas:

1. Ballistic anslysis
2. Ignition analysis
3. Nozzle erosion/deposition
4. Heat losses
5. Aluminum combustion
6. Ablation
7. Burning rate gradient

The ballistic snalysis is basically a composite of the transient mass and energy balances thst considers mass addition from the igniter, propellant and insulation (items 2, 6, 7 sbove), and energy losses as result of hest losses snd incomplete burning of aluminum (items 4 and 5). The effect of these on the pressure depends on the nozzle flow area (item 3). In the snslysis, combustion effects are assumed to occur that are shown below:

Factor	Mass Balance	Energy Bslsnce
Ignition	Adds flow. Initiates flow from propellant.	Energy gsin
Nozzle size	Influences pressure. Deposition of condensed oxide and thermal expsnsion is followed by shearing of molten oxide and eventual erosion of nozzle.	Influences L* snd aluminum combustion
Heat losses	Initial flux to insulation to provide ablation. Radiation dominates gap. Radiation and forced convection dominates insulation loss. Forced convection dominates nozzle losses.	Energy loss
Ablation	Mass addition - dominated by radiation heat flux and convective flow.	Losses decreased by energy return with insulation addition
Burning rate gradient	Affects burning area as well as burning rate.	-
Aluminum combustion	Removal of oxides affects I_s.	Energy loss affects L*. C* and I_s also affected.

IV.B. Task B, Subscale Motor Tests (cont)

Many interesting facts are shown during the analyses. First, the bag igniter tends to lose some 30% of its initial charge through the nozzle. Ignition does not appear to be affected, however, because of the high ignitability of the propellant.

In calculating the heat losses, the Bartz method was first used to calculate the convective heat losses as well as to estimate the boundary layer thickness. This classic method, however, was found to be too costly to utilize and several simplifications were introduced to reduce computer run time. Preliminary results indicated that the boundary layer thickness, θ, in the nozzle appears to grow such that the actual nozzle diameter is affected by several percent. When the burning rate is lower than for the case used in this program, boundary layer buildup appears as a real problem because of the relatively small nozzle. Generally, θ grows with chamber length. With center-perforated grains the A_t also increases with increasing chamber length and therefore will change proportionately to θ. However, in an end burner θ can grow as the burning surface recedes, whereas A_t remains constant, depending on the chamber diameter, hence the problem of an increasing θ is unique to the end-burner.

Next, the presence of a gap around the grain (resulting from stress relieving systems) can provide a significant contribution to L* and depends on the actual dimensions allowed by the tolerance. Although this effect might contribute significantly to a delay in the chamber fill time, it does not appear capable of explaining the very slow ignition periods noted.

Calculations regarding the sloughing off of condensed aluminum oxide in the nozzle were completed using the Vidya program. The calculations indicate that the rate of nozzle area change is the right magnitude to account for the changes empirically found.

IV.B. Task B, Subscale Motor Tests (cont)

Thermodynamic calculations of mixtures of ablative and propellant gases have shown that the higher I_{sp} of the HTPB propellant is effectively reduced by addition of ablation products. Also, the calculations showed that the thermodynamic properties are sufficiently pressure and temperature sensitive that detailed statements regarding these properties in the computer description were needed.

6. Ballistic Analysis

After the computer program description was completed the program was checked out. Plots prepared from calculations showing predicted performance effects are presented in Figures 79 through 82. A baseline performance curve was calculated so that the separate effects of various factors could be compared. This baseline case assumed no heat losses or ablation, all aluminum burned at the surface, no changes in throat area, and constant surface area. The baseline calculations were for the two L* values tested, 630 and 370 in. (Figures 79 and 80). The baseline cases naturally predict pressure rise times proportional to L*. When heat losses are included a shift in time of about 5 millisec is introduced and the operating pressure is decreased by about 35 psi, or 2% during ignition, and about double this over the entire firing cycle. However, the actual performance is significantly different from this simple baseline, although the final pressures are essentially correct.

Experimentally it was found that the effect of changing L* is quite small. Considering the various possibilities that could account for this it is concluded that heat losses, ablation, changes in throat area or slow ignition could not account for the observed insensitivity to L*. Further, the calculated baseline rise rate itself is too high by a factor of two. Therefore, it is apparent that the aluminum combustion is the most likely candidate for the reduced ignition rise rates observed in the 3KS-1000 size motor firings.

IV.B. Task B, Subscale Motor Tests (cont)

A preliminary estimate of the effect of aluminum combustion with and without heat losses is given in Figures 81 and 82 for the two values of L* (370 and 630, respectively). In Figure 81 the experimental case represented by 3KS-1000 size motor firings 4 and 6 (see Figures 53 and 55) are also given for comparison. The motor firing data show a slower ignition rise rate up to about 0.125 sec and then a secondary pressure rise phase up to about 1 sec and then equilibrium. Using aluminum burning and heat losses this secondary pressure rise phase is well simulated. However, the predicted ignition phase still shows a pressurization rate faster than actual. To explain this difference, the other factors affecting performance will be evaluated, but it is believed that the slow pressurization rate might have to be explained by hypothesizing a slow burning rate during ignition.

V. GLOSSARY OF TERMS

Prepolymers

B-2000	Poly(1,2-butylene)glycol
CTPB (HC-434)	Carboxy terminated polybutadiene, Thiokol Chemical Corporation
CTPB (Telagen)	Carboxy terminated polybutadiene, General Tire and Rubber Company
HTPB (R-45)	Free-radical initiated hydroxy-terminated polybutadiene, Sinclair Oil Company
NPGA	Neopentyl glycol azelate
PBAN	Terpolymer of polybutadiene, acrylic acid and acrylonitrile, American Synthetic Rubber Co.

Crosslinker

TP-4040	Polypropylene oxide adduct of trimethylolpropane
MMA	Methyl nadic anhydride

Curing Agents

HDI	Hexamethylene diisocyanate
IPDI	Isophorone diisocyanate
TDI	Tolylene diisocyanate
BISA	Butylene imine adduct of sebacic acid
MAPO	Tris(2-methyl aziridinyl)phosphine oxide
DER-332	Diepoxide of bis-phenol-A

Bonding Agent

C-1	2,3-Dihydroxypropyl-bis-(2-cyanoethyl)amine
FC-157	Aerojet proprietary item

V. Glossary of Terms (cont)

Burning Rate Catalysts

Cu0202	Copper chromite, Harshaw Chemical Company
Catocene	Nonvolatile liquid ferrocene derivative, Arapahoe Chemicals, Inc.

Insulation

Gen-Gard V-4030	EPR material, General Tire and Rubber Co.
R-151	EPR material, Rocketdyne Division of North American Rockwell
IBC-III	Castable PBAN-epoxy insulation material

Ammonium Perchlorate Oxidizer

RRD Ung	Rounded rotary-dried unground, Average particle size = 180 microns (μ)
SSMP	Slow-speed Mikropulverizer ground, 130μ
MA	Mikro Atomizer ground, ∿7μ
UFAP	Ultra Fine Ammonium Perchlorate, ∿0.5μ

Plasticizer

IDP	Isodecyl pelargonate

Other

A-35	Washcoat composed of trichloroethylene ferric acetylacetonate and TDI
erf	Error function
H-60 Aluminum	Spherical aluminum powder, ∿60μ particle diameter
MSA	Mine Safety Appliance Co.
MSBR	Microstrand burning rate
SSBR	Solid strand burning rate
Twitche-1 Base 8240	Sodium salts of sulfonated hydrocarbons extended with paraffin oils

V. Glossary of Terms (cont)

Symbols

μ	Micron
c*	Characteristic exhaust velocity
DPT	Double Plate Tensile
I_s	Impulse
I_{sp}	Specific impulse
K	Port to throat ratio
L*	Ratio of motor free volume to nozzle throat area

Mechanical Property Symbols

a_T	Shift factor
$\dot{\varepsilon}a_T$	Reduced strain rate
ε_b	% Elongation (at break)
ε_m	% Elongation at nominal maximum stress
E_o	Initial modulus, psi
σ_m	Nominal maximum stress
t_m	Time to nominal maximum stress

	Binder	Catalyst	IDP Plasticizer Concentration, wt, %	Oxidizer Blend	Parameters Examined					
					Deagglomeration	Orientation	Classification	Migration	Dilatation	Micro Voids
1.	C-1/PU	2% CuO202	4	Coarse/ 7μ	x	x		x	x	x
2.	HTPB	-	3	7μ 0.5μ	x			x		
3.	HTPB	1% Catocene	0	Coarse/ 0.5μ	x		x	x		
4a.	CTPB	1% Catocene	5	Coarse/ 0.5μ	x					
4b.	HTPB	1% Catocene	2	Coarse/ 0.5μ	x	x	x	x	x	x
4c.	HTPB	1% Catocene	4	Coarse/ 0.5μ	x			x		

Note: All formulations contained 72 wt% ammonium perchlorate and 14 wt% aluminum

Figure 1

Basic Propellant Formulations Used in the Task A Laboratory Investigations

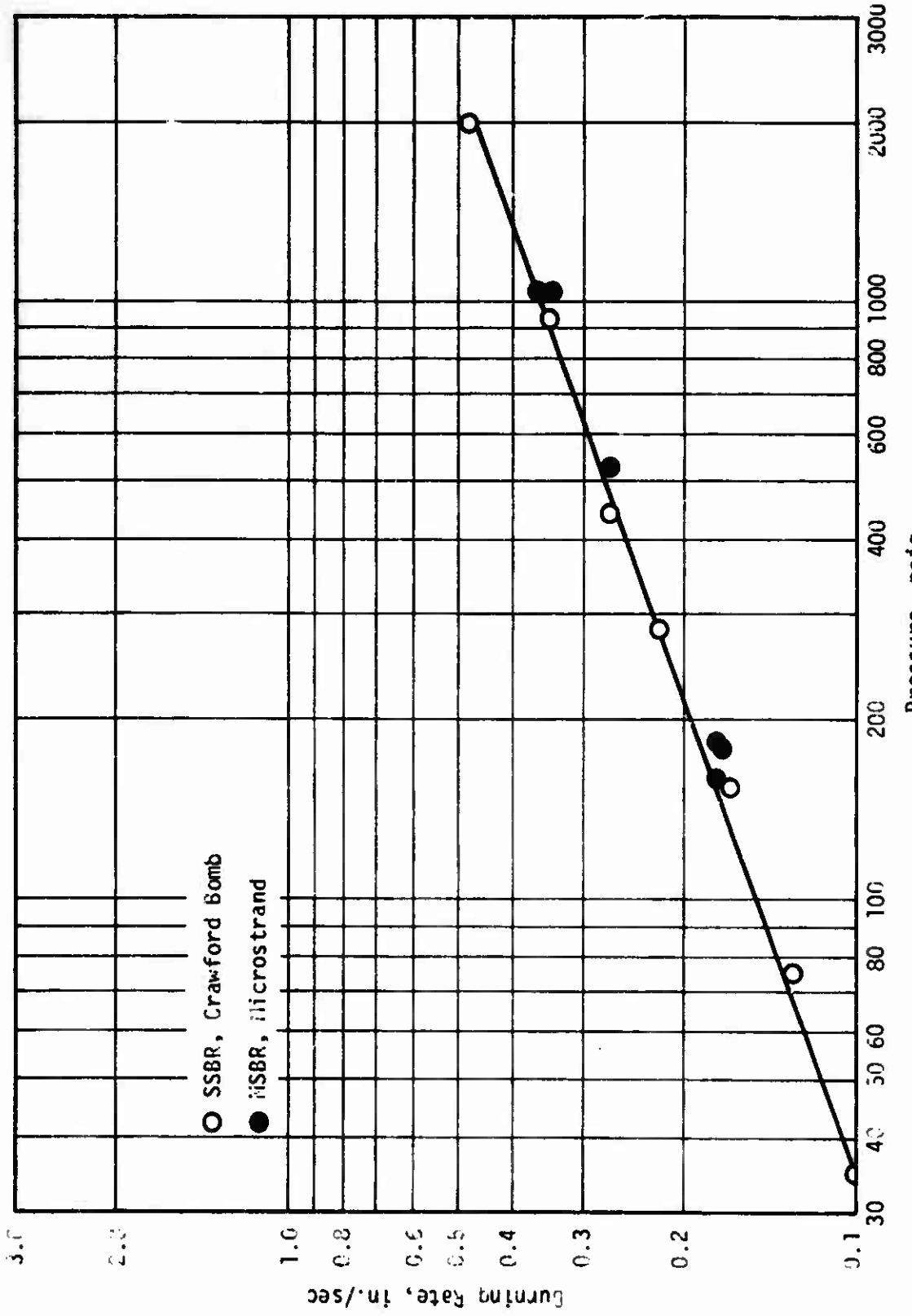

Crawford Bomb and Microstrand Burning Rates of ANB-3066 Propellant

50

Figure 2

Number	ΔP psig	Average Pressure, psig	Burning Rate at 1000 psig, in./sec
1	220	1010	1.54
2	230	1010	1.54
3	240	1010	1.52
4	230	1010	1.55
5	280	1030	1.53
6	240	1010	1.53
7	240	1000	1.56
8	220	990	1.53
9	220	1000	1.55
10	240	1000	1.55
			$\bar{X}$ = 1.540
			σ = 0.0125
			V = 0.8%

Strand Dimensions: 0.6- by 0.3- by 1.3-in.

Reproducibility of Microstrand Burning Rate Determination, ANB-3392 Propellant (Batch 70-141)

51

Figure 3

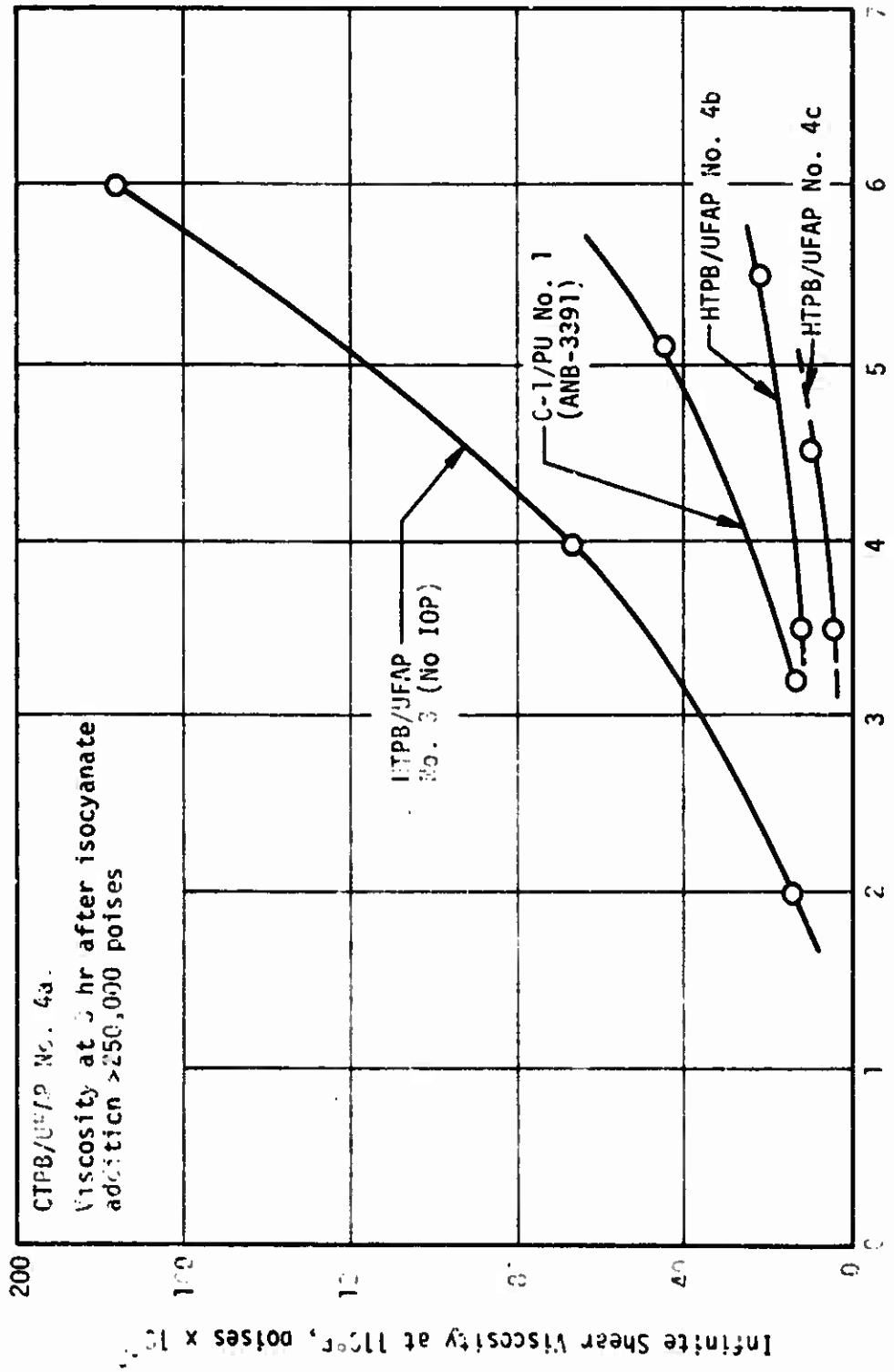

Viscosity Buildup of Basic Propellant Formulations

52

Figure 4

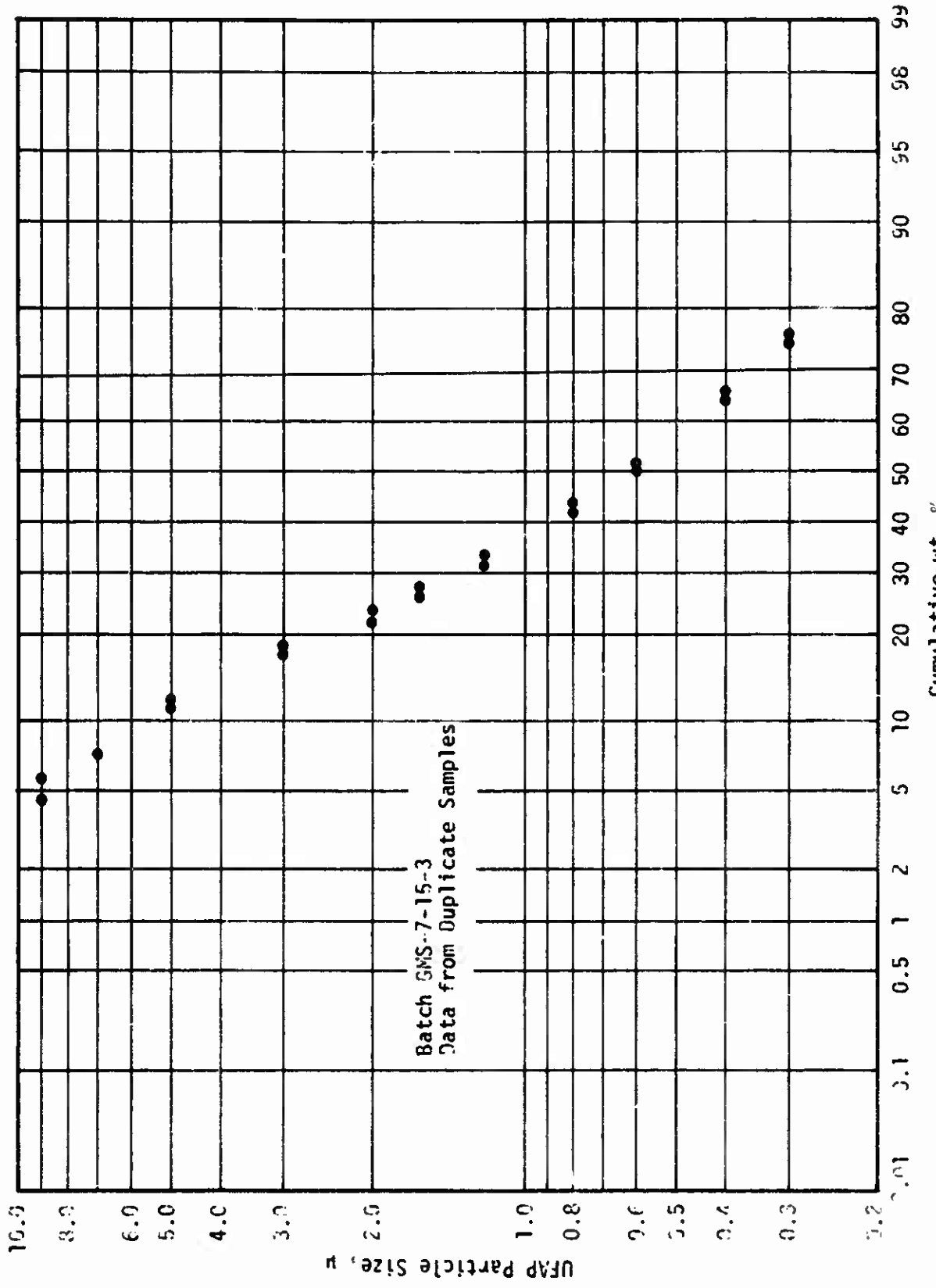

Reproducibility of MSA Analysis of UFAP Taken From Propellant

Figure 5

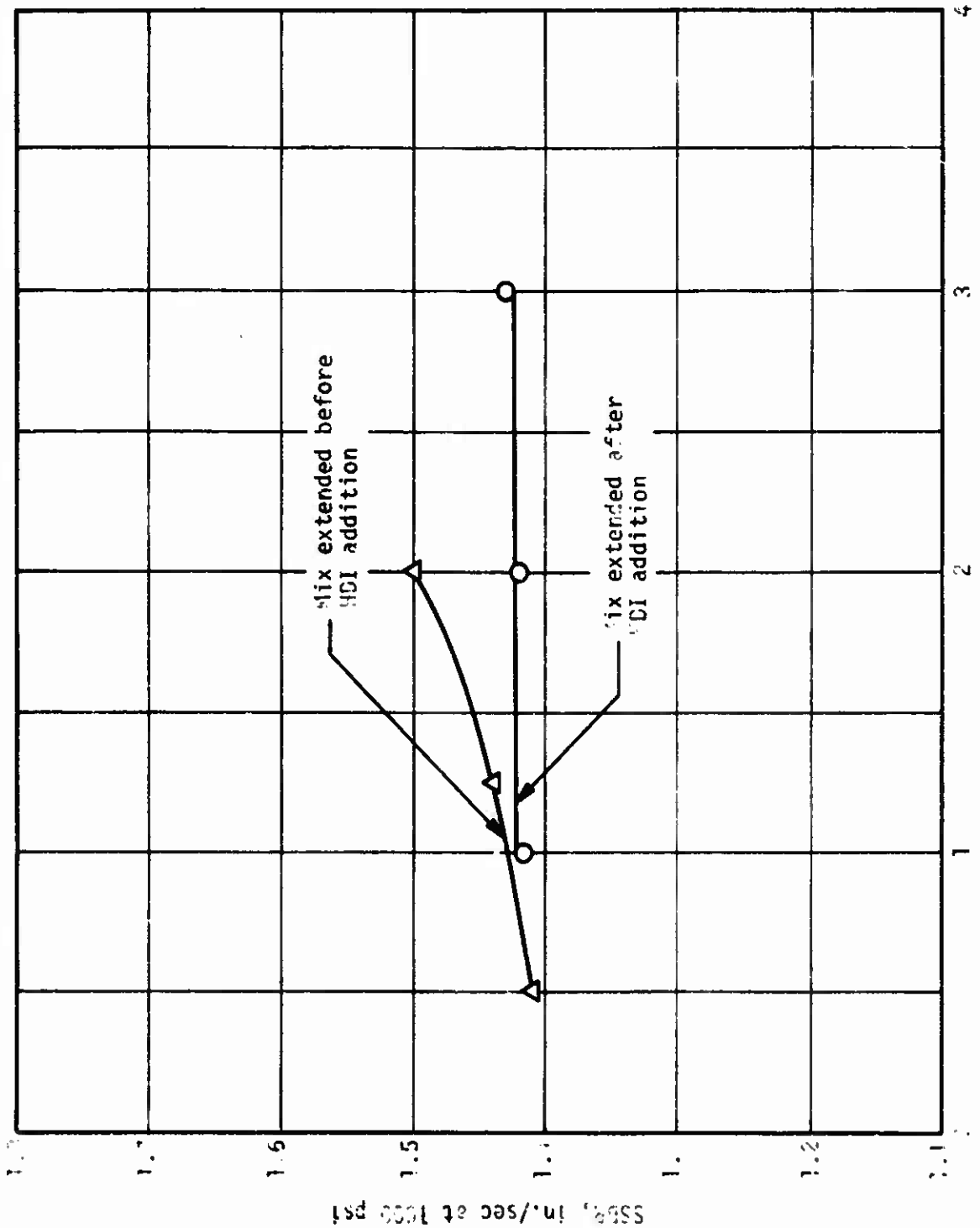

Effect of Mix Time on Burning Rate, C-1/PU Propellant

Figure 6

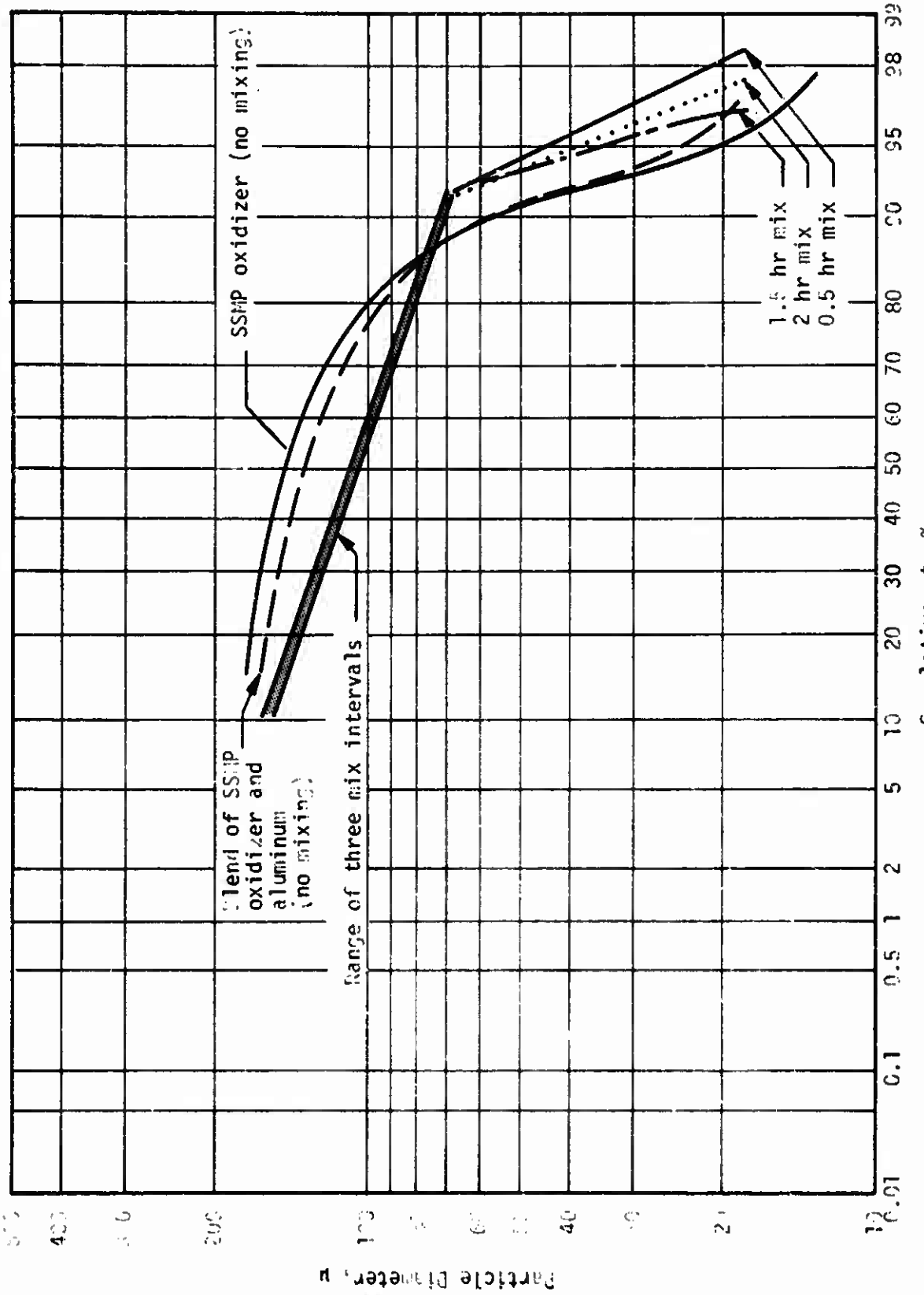

Effect of Mix Time on Coarse Oxidizer (SSMP) Particle Size in Nonplasticized HTPB Propellant Containing 1 wt% Catocene

55

Figure 7

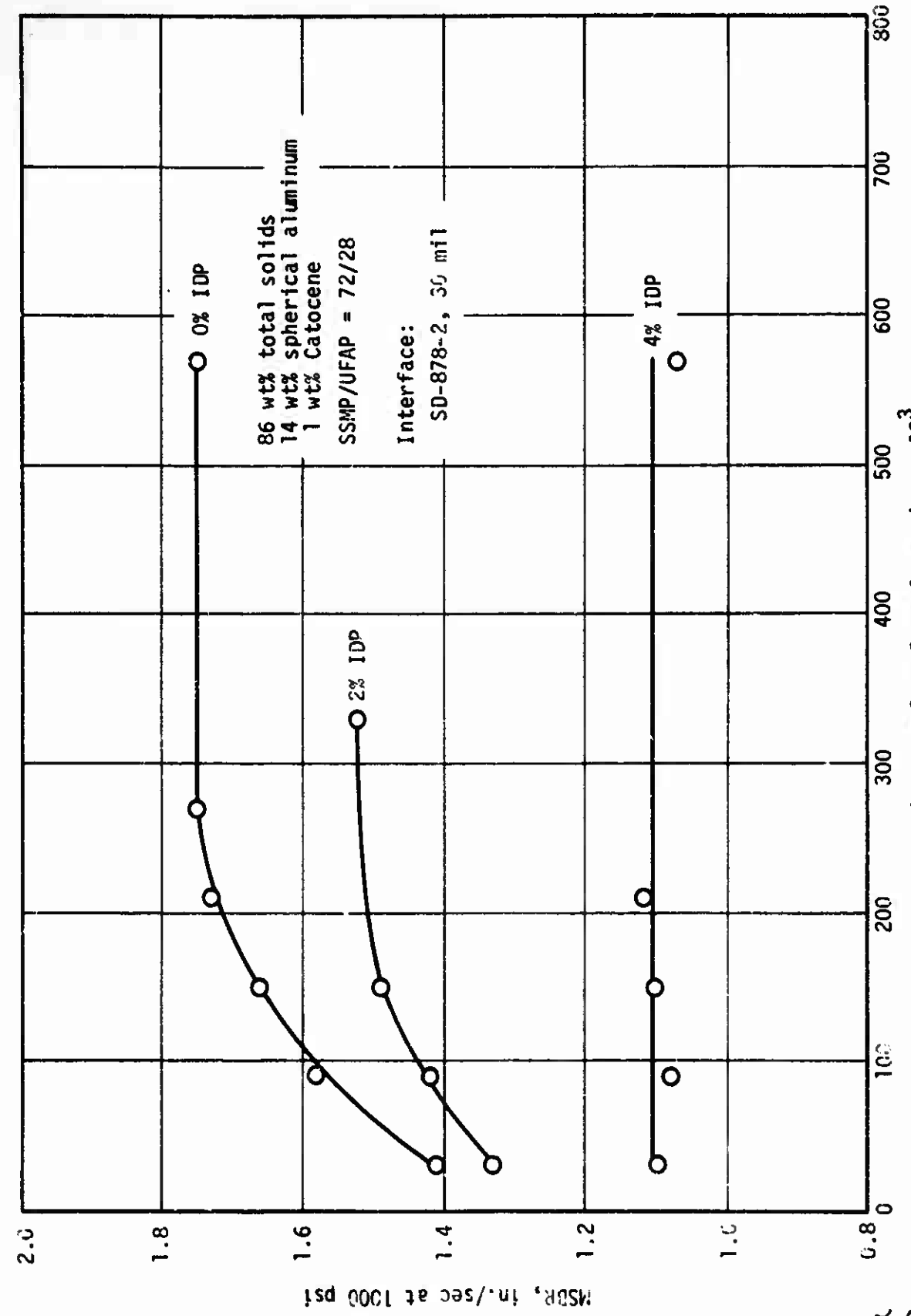

Effect of IDP Concentration on Burning Rates of HTPB/UFAP Propellant Interphase

Figure 8

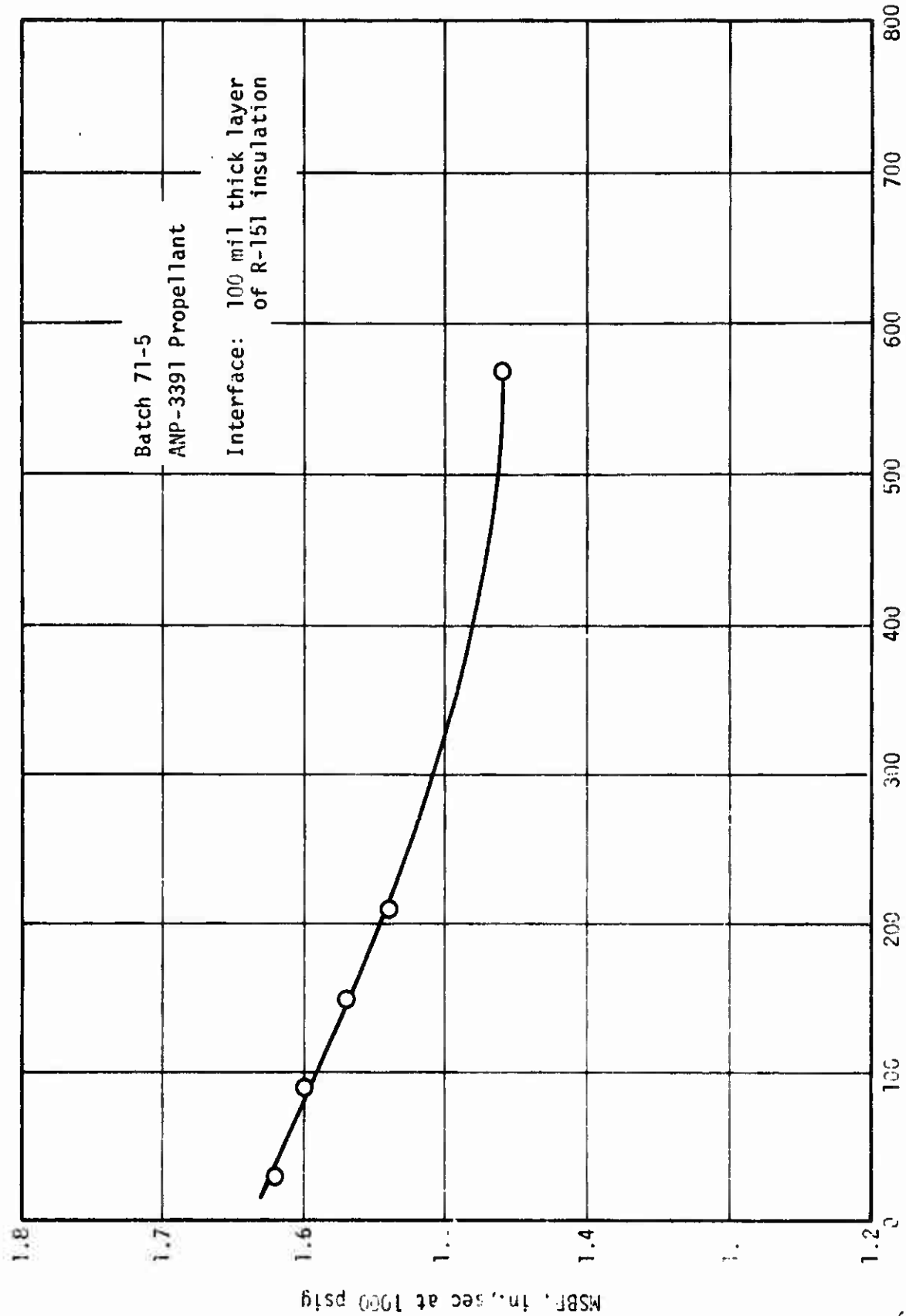

Effect of IDP Migration on Interphase Burning Rates of ANP-3391

Figure 9

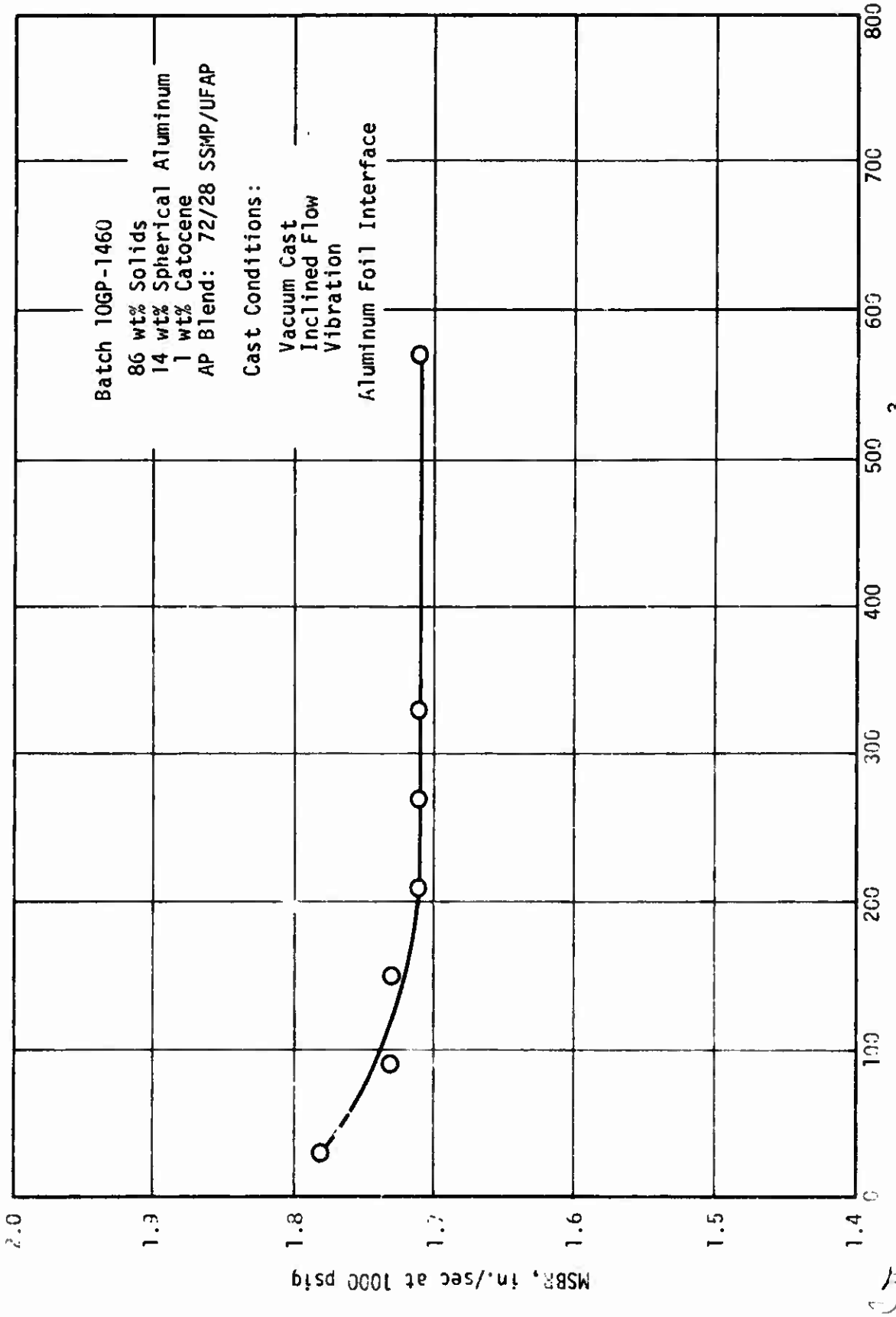

Burning Rates of Unplasticized HTPB Propellant as a Function of Interphase Distance (Cast Under Conditions Conducive to Particle Classification)

58

Figure 10

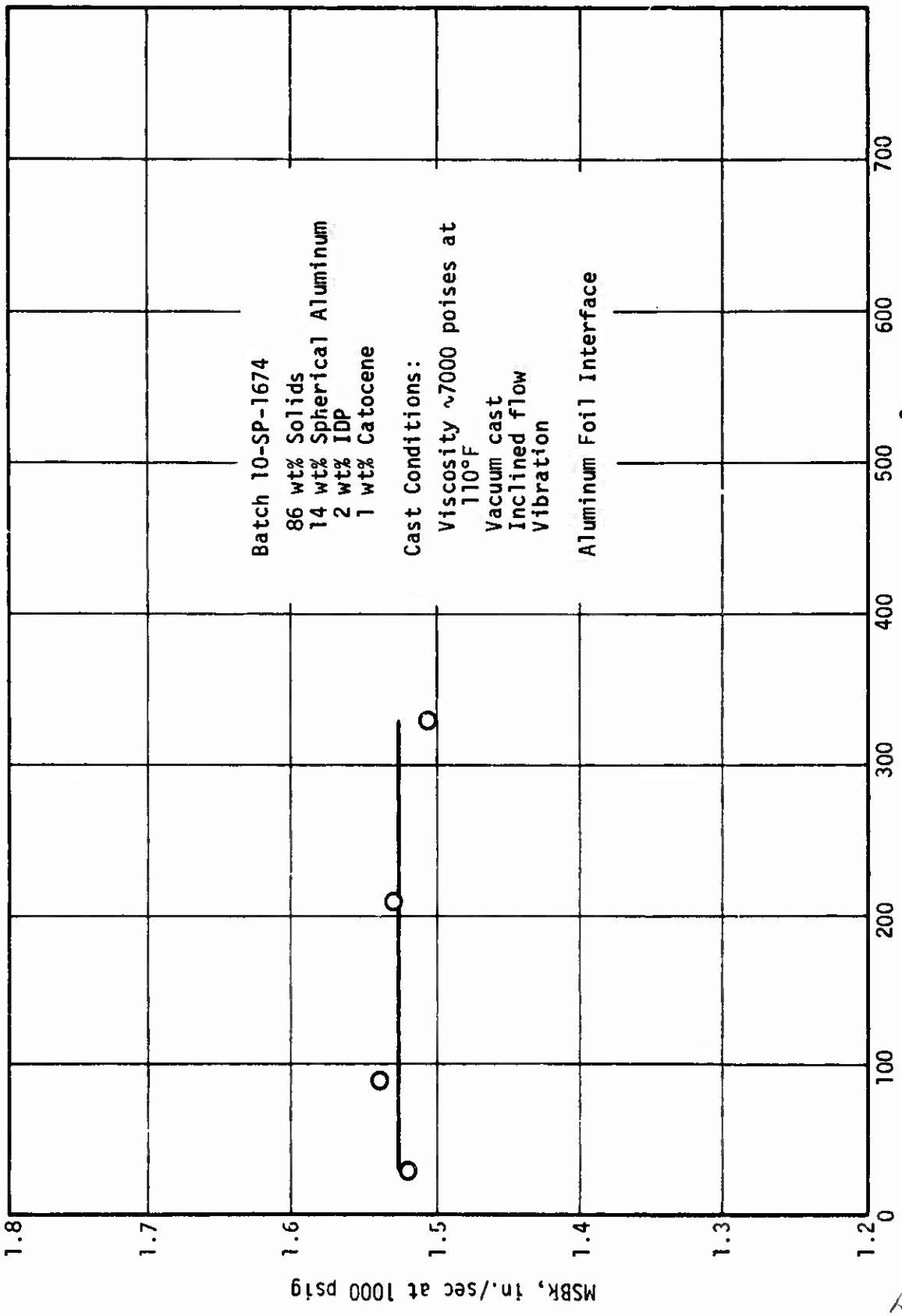

Burning Rates of IDP-Plasticized HTPB Propellant as a Function of Interphase Distance
(Cast Under Conditions Conducive to Particle Classification)

Figure 11

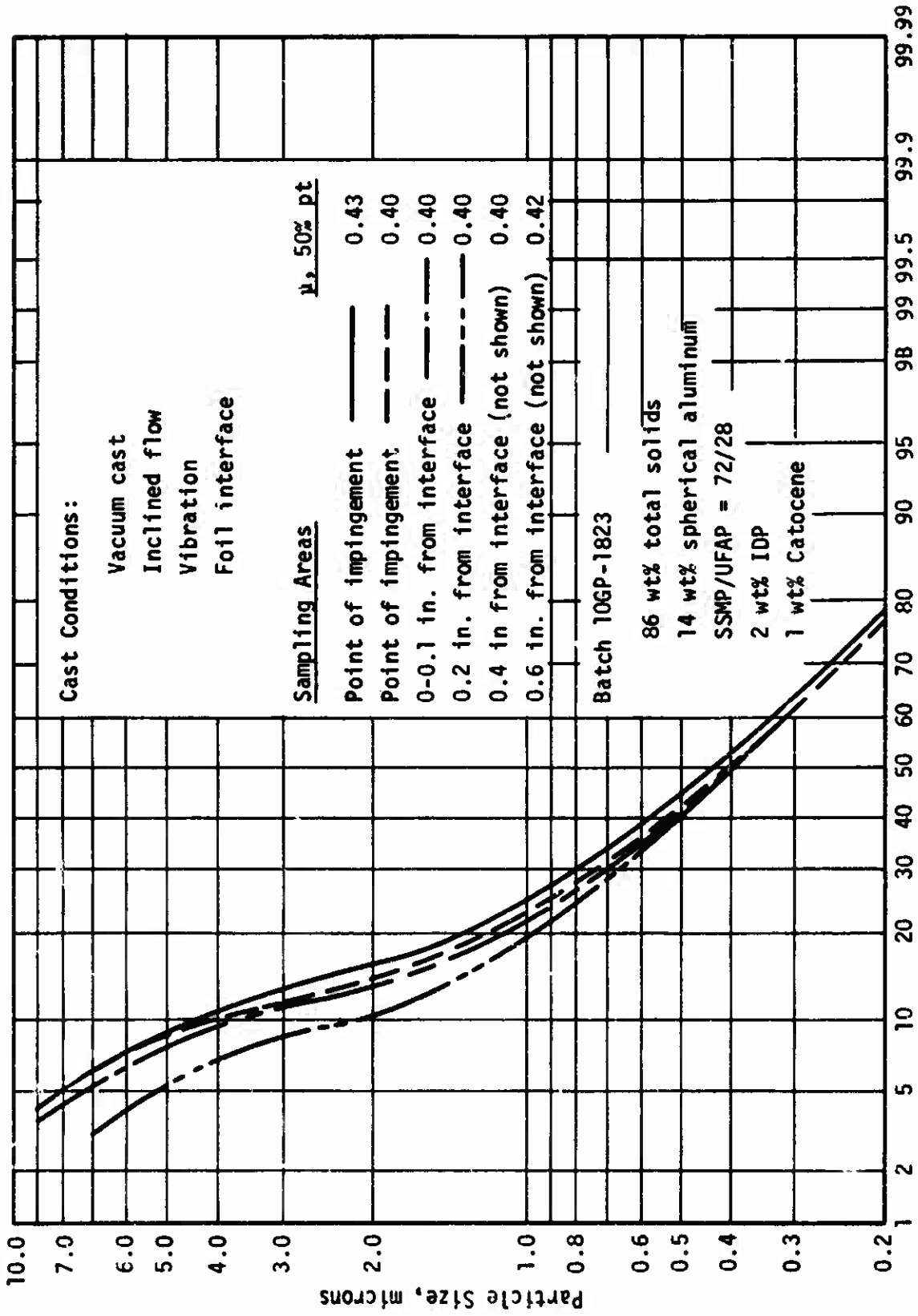

MSA Particle Size Measurement of UFAP Portion of Oxidizer Blend of IDP-Plasticized HTPB/UFAP Propellant

60

Figure 12

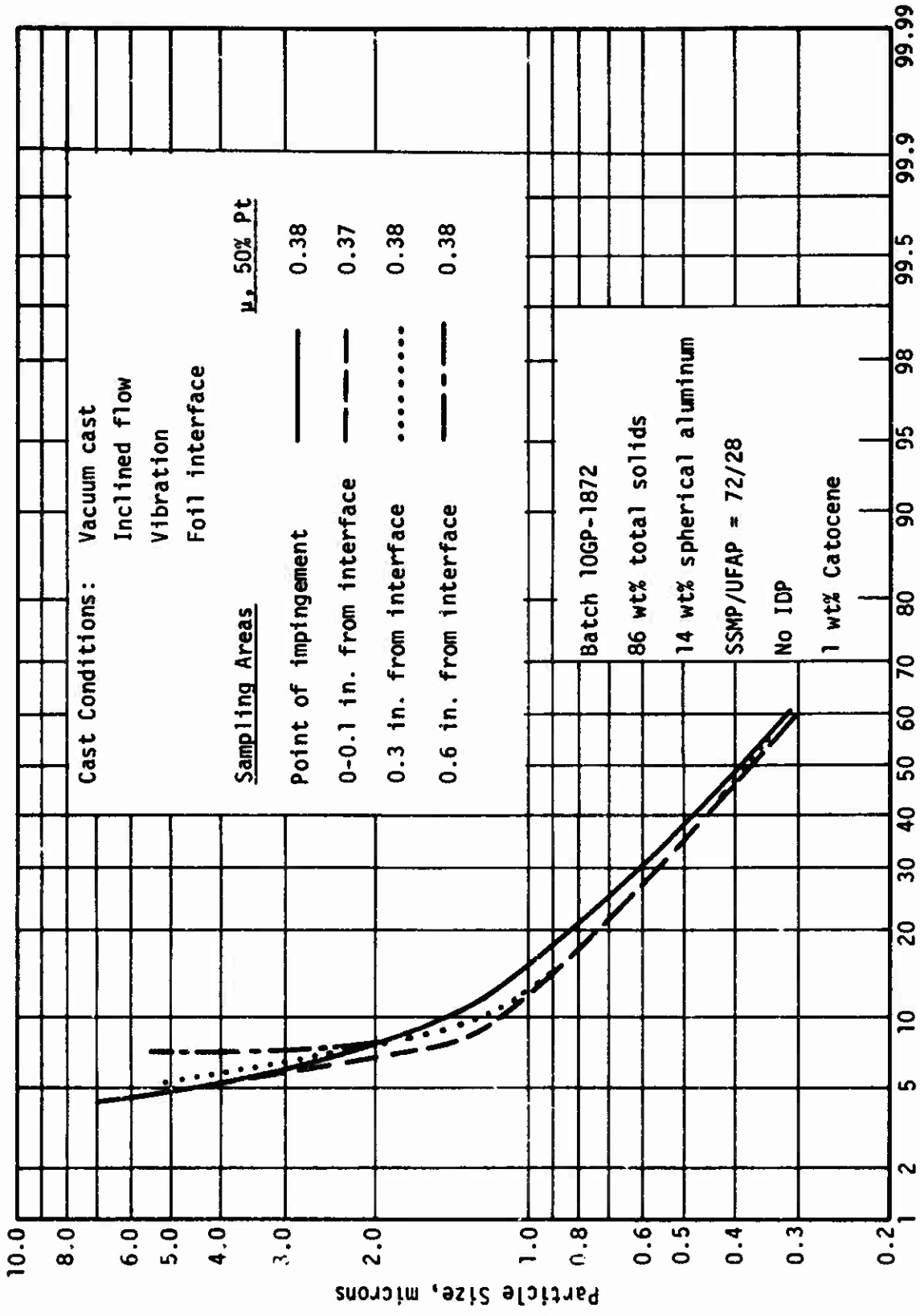

MSA Particle Size of UFAP Portion of Oxidizer Blend of Nonplasticized HTPB/UFAP Propellant

Figure 13

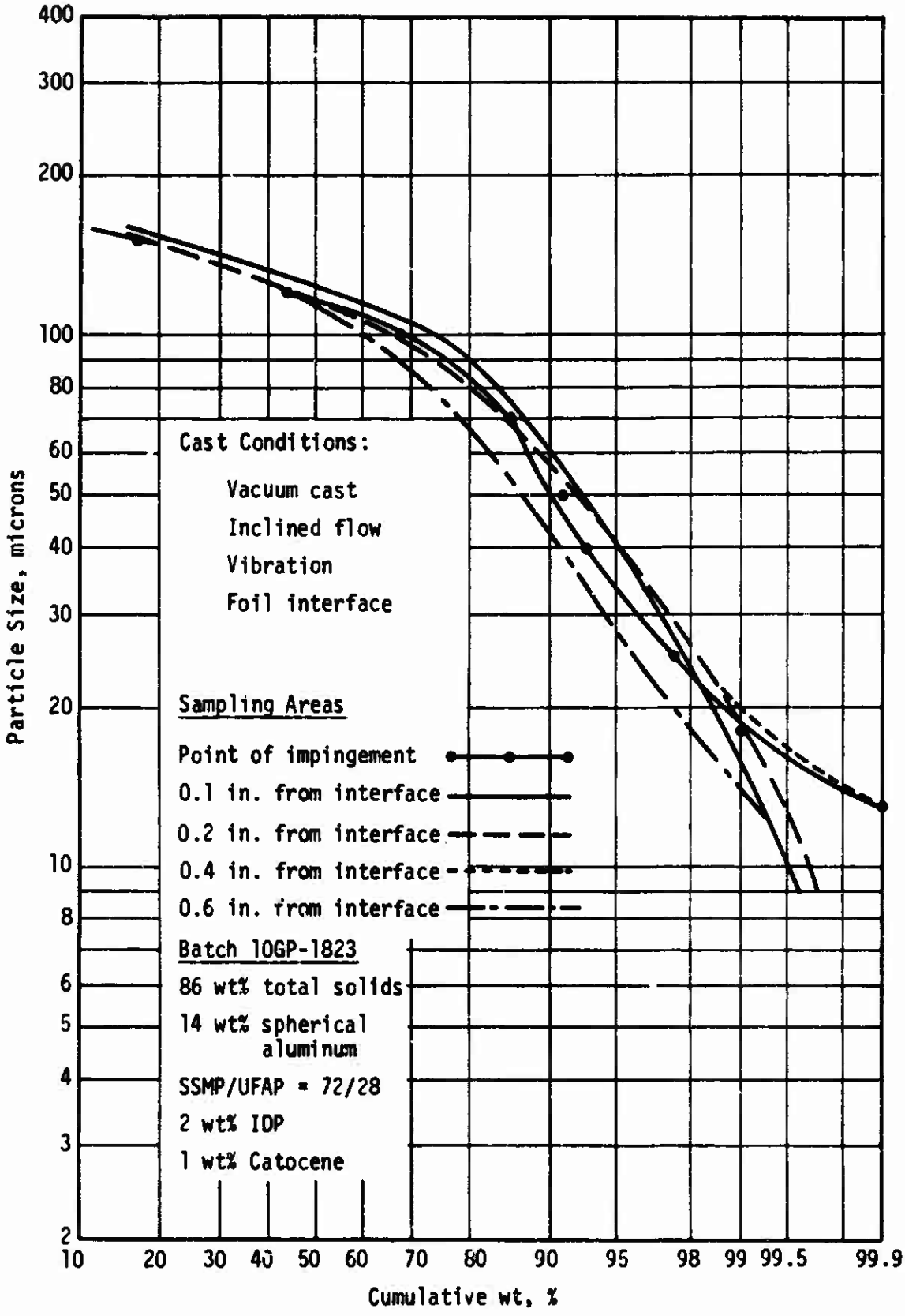

MSA Particle Size Measurement of Coarse Fraction of Solids in IDP-Plasticized HTPB/UFAP Propellant

62

Figure 14

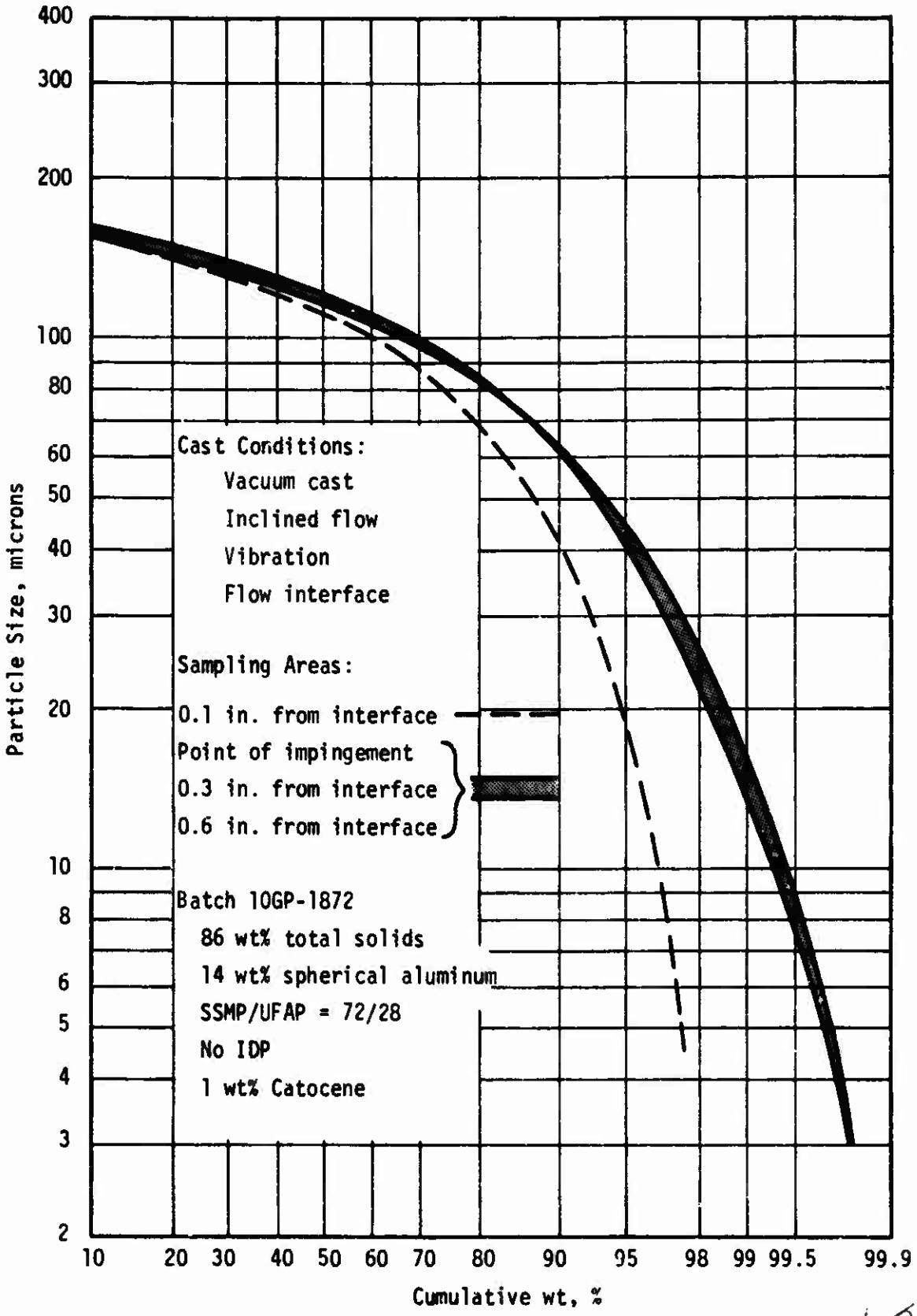

MSA Particle Size Measurement of Coarse Fraction of Solids in Nonplasticized HTPB/UFAP Propellant

Figure 15

Propellant	Bonding Agent	Direction of Strain	Dilatation Strain Level, %	Burning Rate at 1000 psig in./sec	
				0% Strain	Dilatation Strain
HTPB/UFAP	FC-157	|| to burning direction	13.2	1.46	1.45
HTPB/UFAP	None	||	12.2	1.58	1.65
HTPB/UFAP	FC-157	⊥	13.2	1.41	1.42
PU	C-1	||	8.6	1.50	1.47
PU	None	||	10.5	1.46	1.62

Figure 16

Effect of Dilatation on Burning Rate

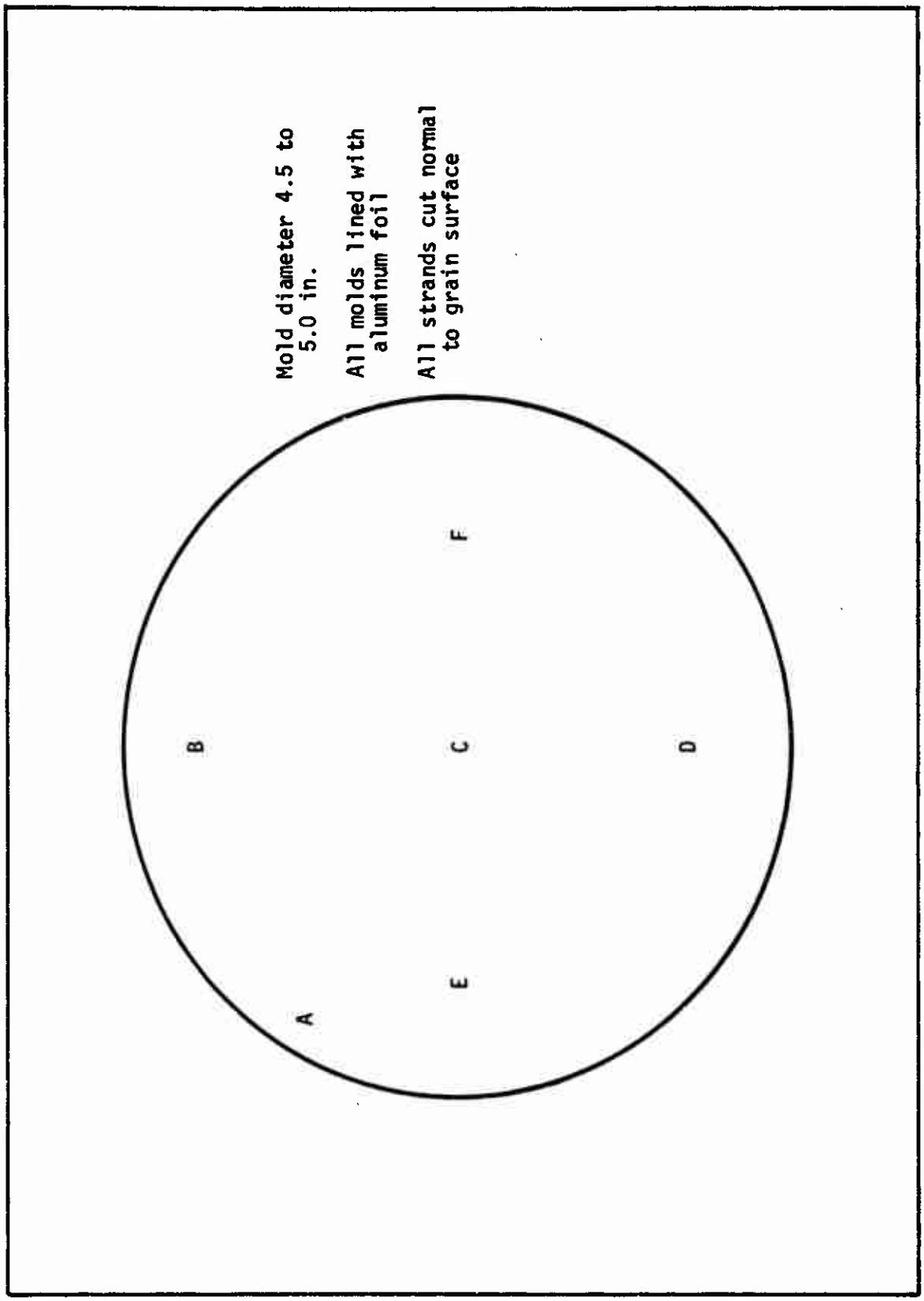

Microstrand Burning Rate Sampling Position on Grain Surface

Figure 17

Mold	Casting Method	In Mold	Average MS8R, in./sec at 1000 psi at Sampling Position — Cross Section Position* A	B	C	D	E	F
Micarta Sleeve 4.5-in. ID	Free-fall, vacuum cast through 2-in. dia orifice - no vibration	Top	1.44	-	1.41	-	-	-
		Middle	1.45	1.44	1.45	1.49	1.45	1.50
		Bottom	1.47	1.42	1.40	1.46	1.46	1.45
0.5-gallon 5.0-in. ID	Free-fall, vacuum cast through 2.0-in. dia orifice, vibration	Top	1.48	1.47	1.48	1.45	1.48	1.48
		Bottom	1.50	1.49	1.44	1.49	1.48	1.47
0.5-gallon 5.0-in. ID	Multi-orifice 4.0-in. dia bayonet cast, no vibration	Top	1.47	1.46	1.48	1.47	1.46	1.50
		Bottom	1.50	1.45	1.48	1.48	1.50	1.52
0.5-gallon 5.0-in. ID	Multi-orifice 4.0-in. dia casting head vacuum cast, no vibration	not tested						
0.5-gallon 5.0 in. ID	2.0-in. dia orifice, bayonet cast, no vibration	not tested						

* Refer to Figure 17 for description of test position.

Effect of Casting Method on ANB-3392 Propellant Burning Rate Uniformity

Figure 18

Mold	Casting Method	Average MSBR, in./sec at 1000 psi at Sampling Position						
			Cross Section Position*					
		In Mold	A	B	C	O	E	F
Micarta Sleeve 4.5-in. IO	Free-fall, vacuum cast through 2.0-in. dia orifice, no vibration	Middle	1.60	1.55	1.57	1.52	1.57	1.57
0.5-gallon 5.0-in. IO	Free-fall, vacuum cast through 2.0 in. dia orifice, vibration	Middle	1.59	1.58	1.59	1.59	-	-
0.5-gallon 5.0-in. IO	Multi-orifice 4.0-in. dia bayonet cast, no vibration	Middle	1.56	1.56	1.56	1.59	-	-
0.5-gallon 5.0-in. IO	Multi-orifice 4.0-in. dia casting head, vacuum cast, no vibration	Middle	1.60	1.56	1.58	1.62	-	-

* Refer to Figure 17 for sampling positions.

Figure 19

Effect of Casting Method on ANP-3391 Propellant Burning Rate Uniformity

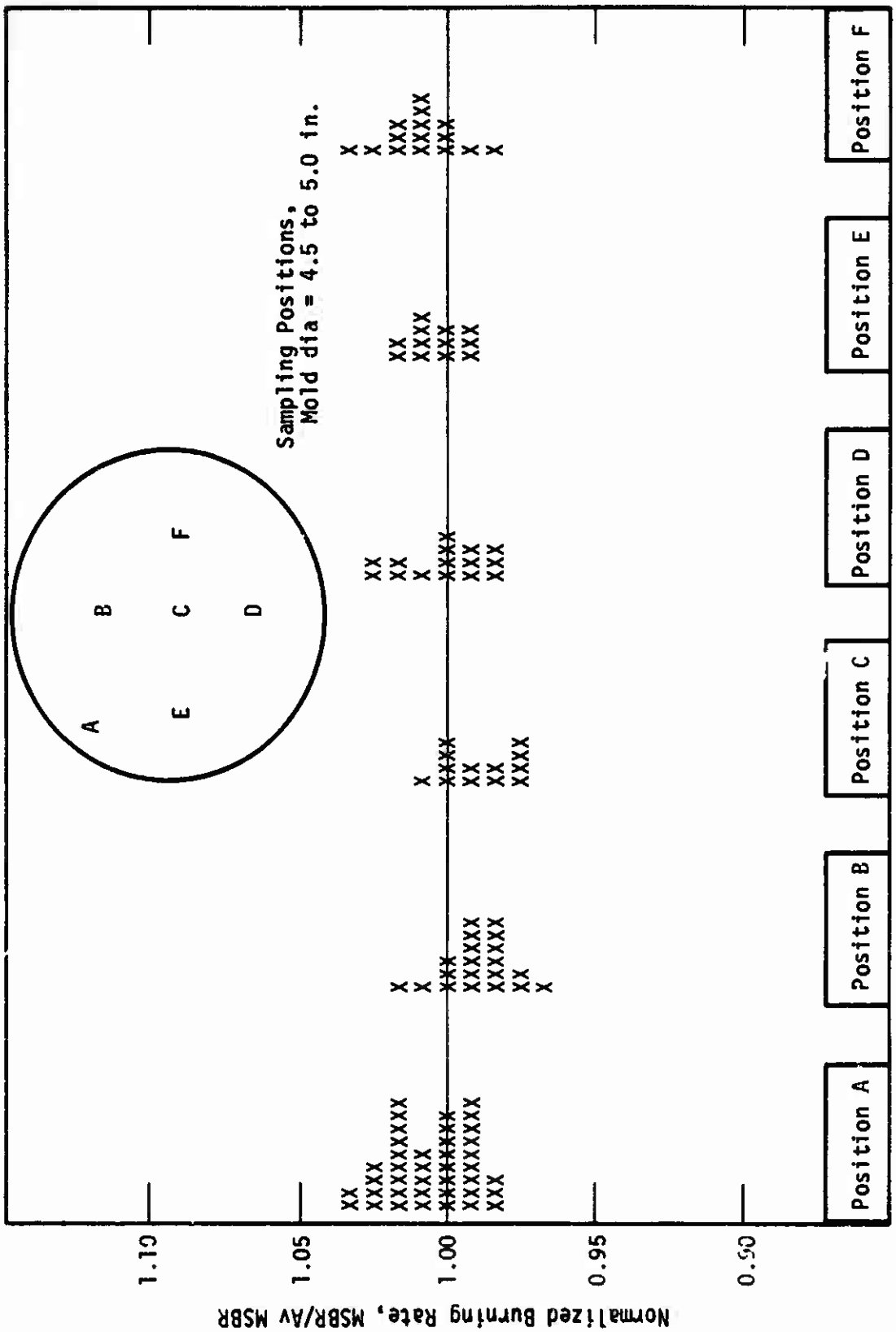

Effect of Sampling Position on Burning Rate of ANB-3392 Propellant

Figure 20

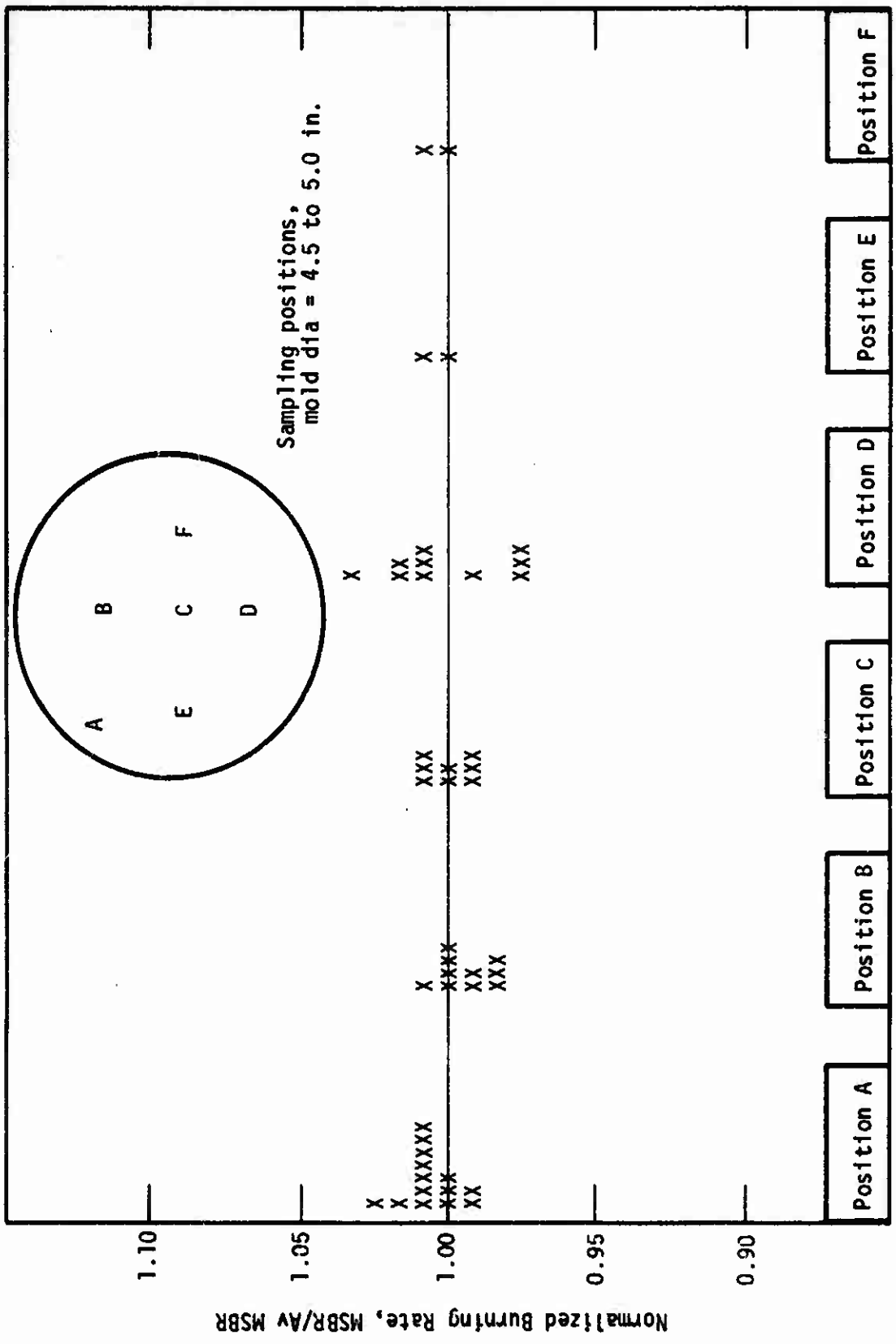

Effect of Sampling Position on Burning Rate of ANP-3391 Propellant

Figure 21

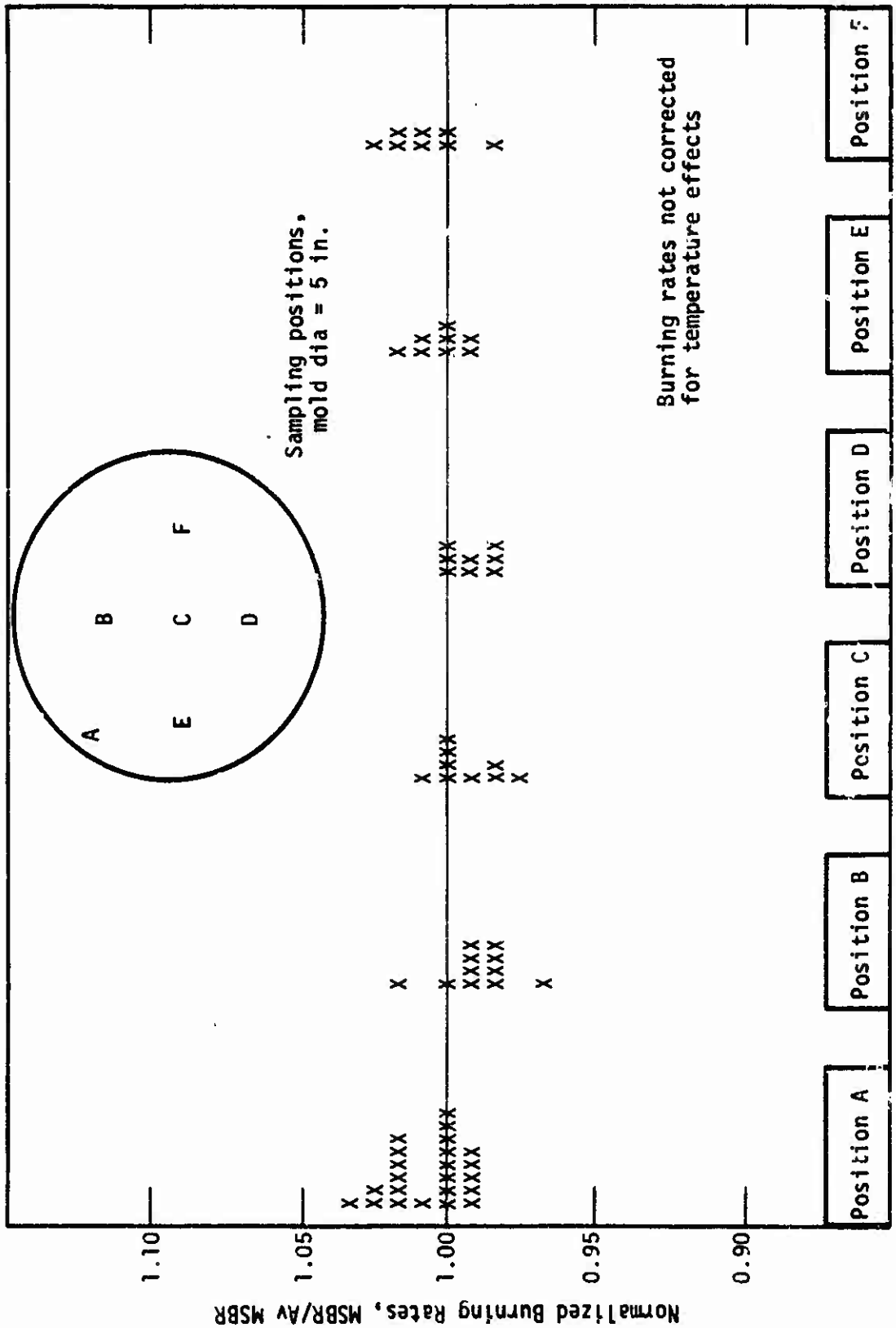

Effect of Sampling Position on Burning Rate of ANB-3392 Propellant (I)

Figure 22

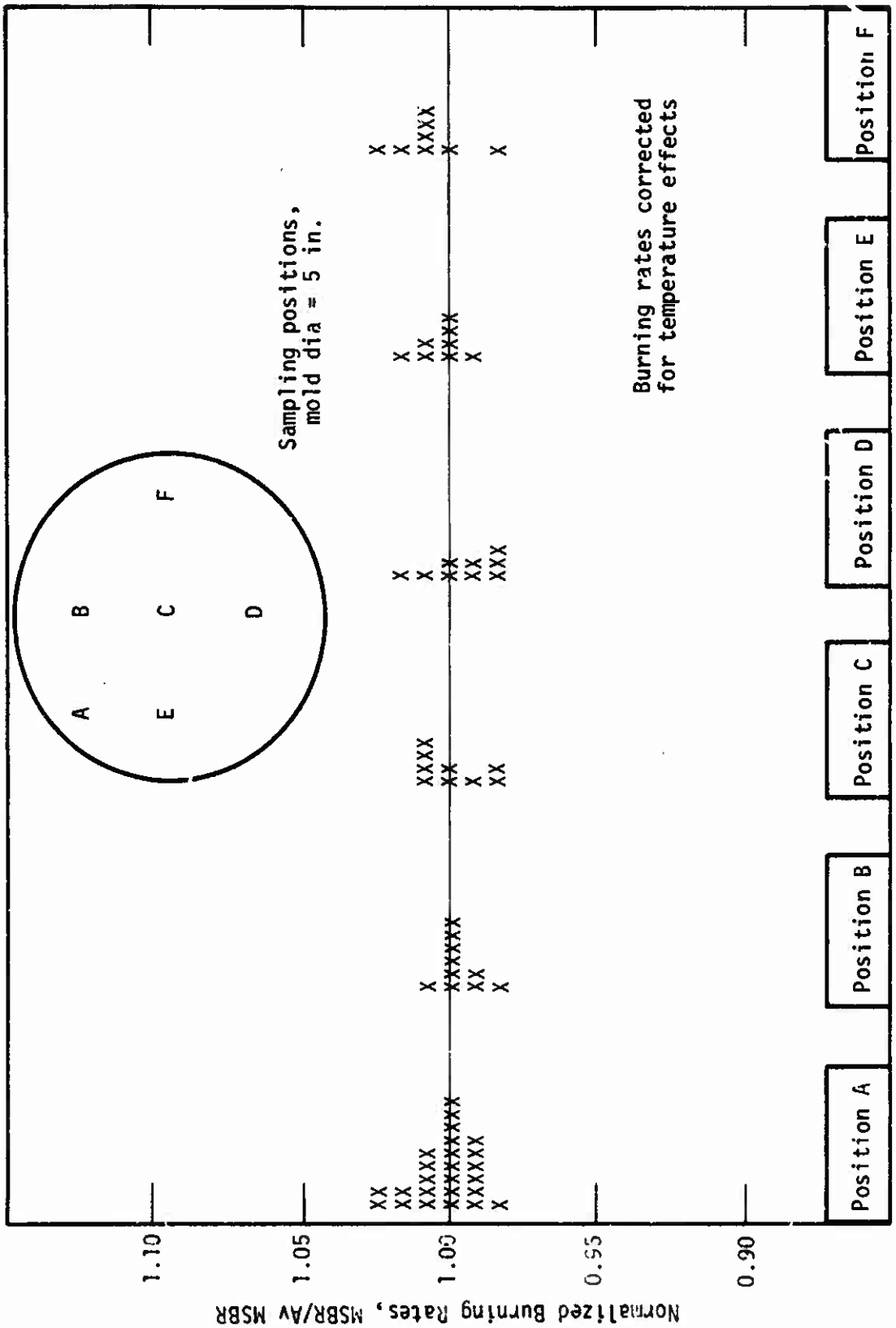

Effect of Sampling Position on Burning Rate of ANP-3392 Propellant (II)

Figure 23

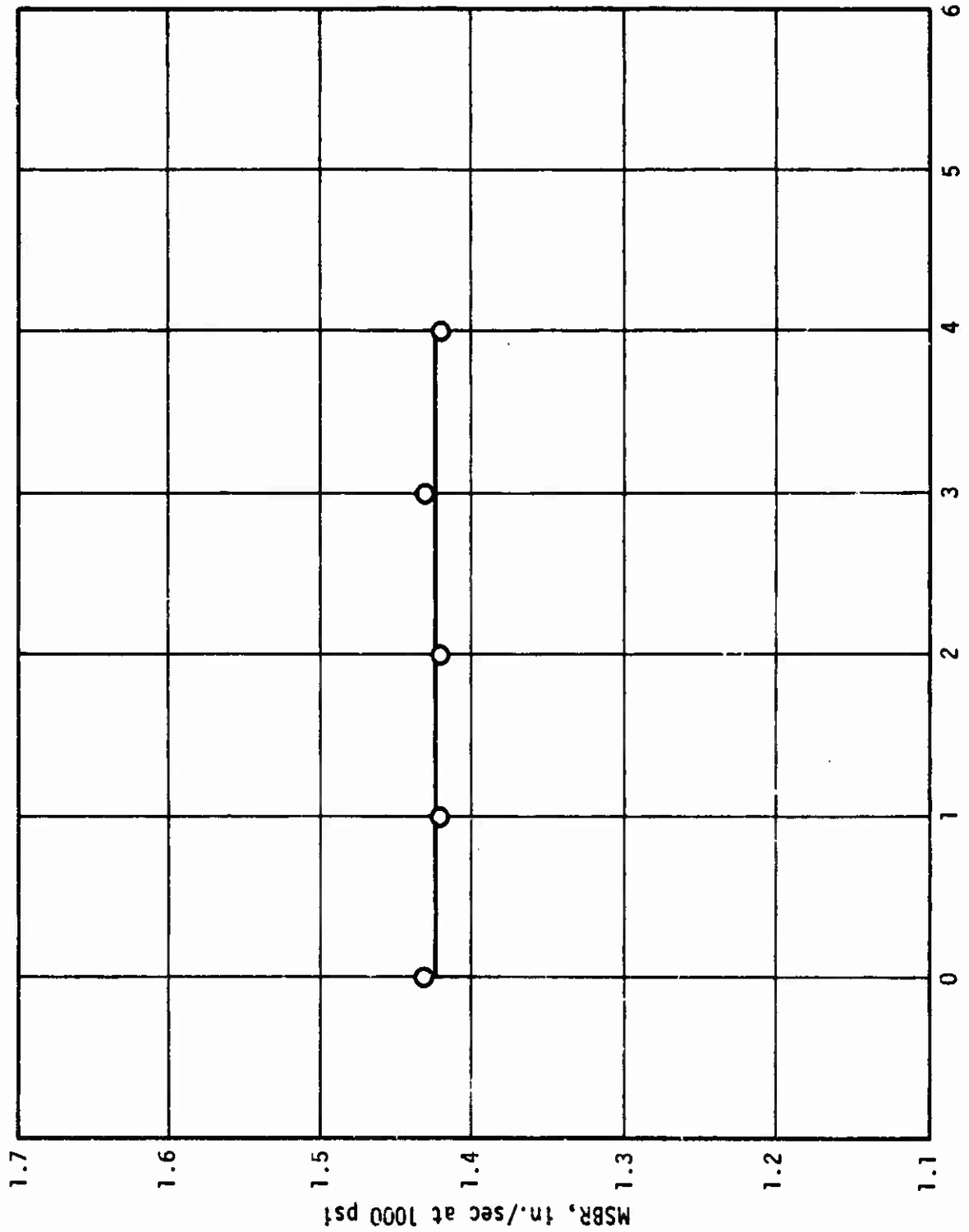

Burning Rate Profile of ANB-3392 Across 4.0-in. Dia Grain

Figure 24

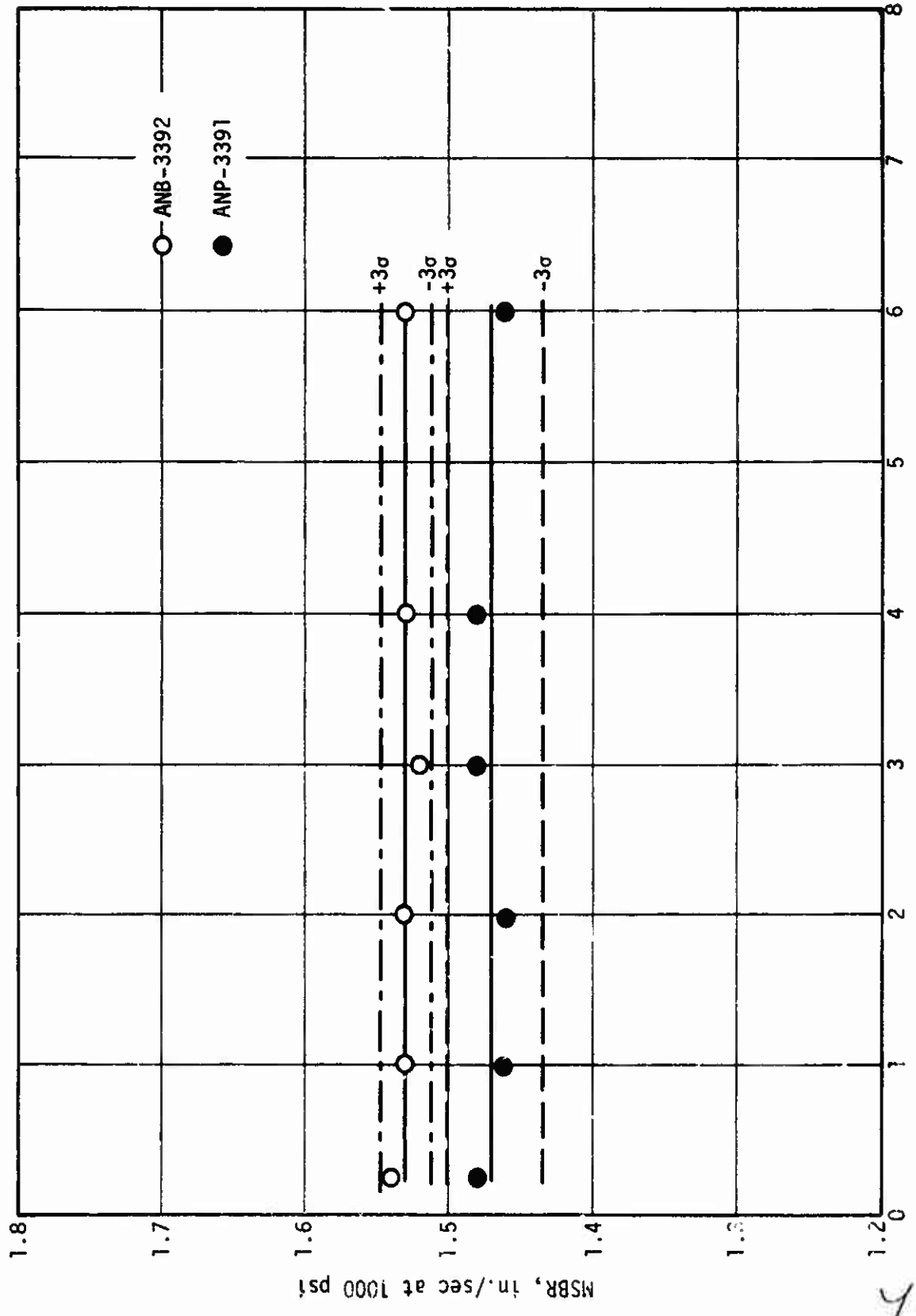

Burning Rate Profile Across 8.0-in. Dia Propellant Grains

Figure 25

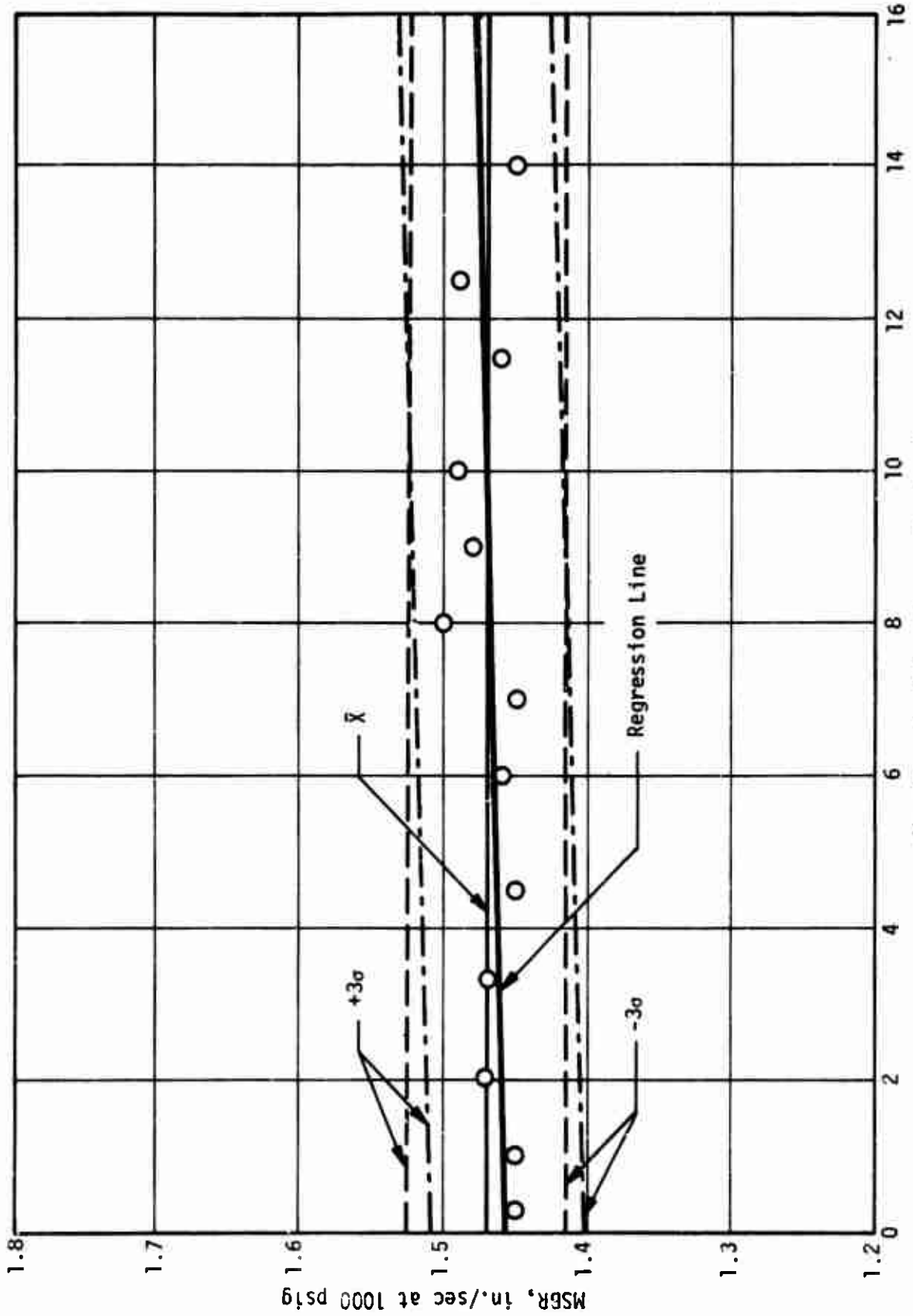

Burning Rate Profile Across 16.0-in. Dia Grain of ANP-3392 Propellant

Figure 26

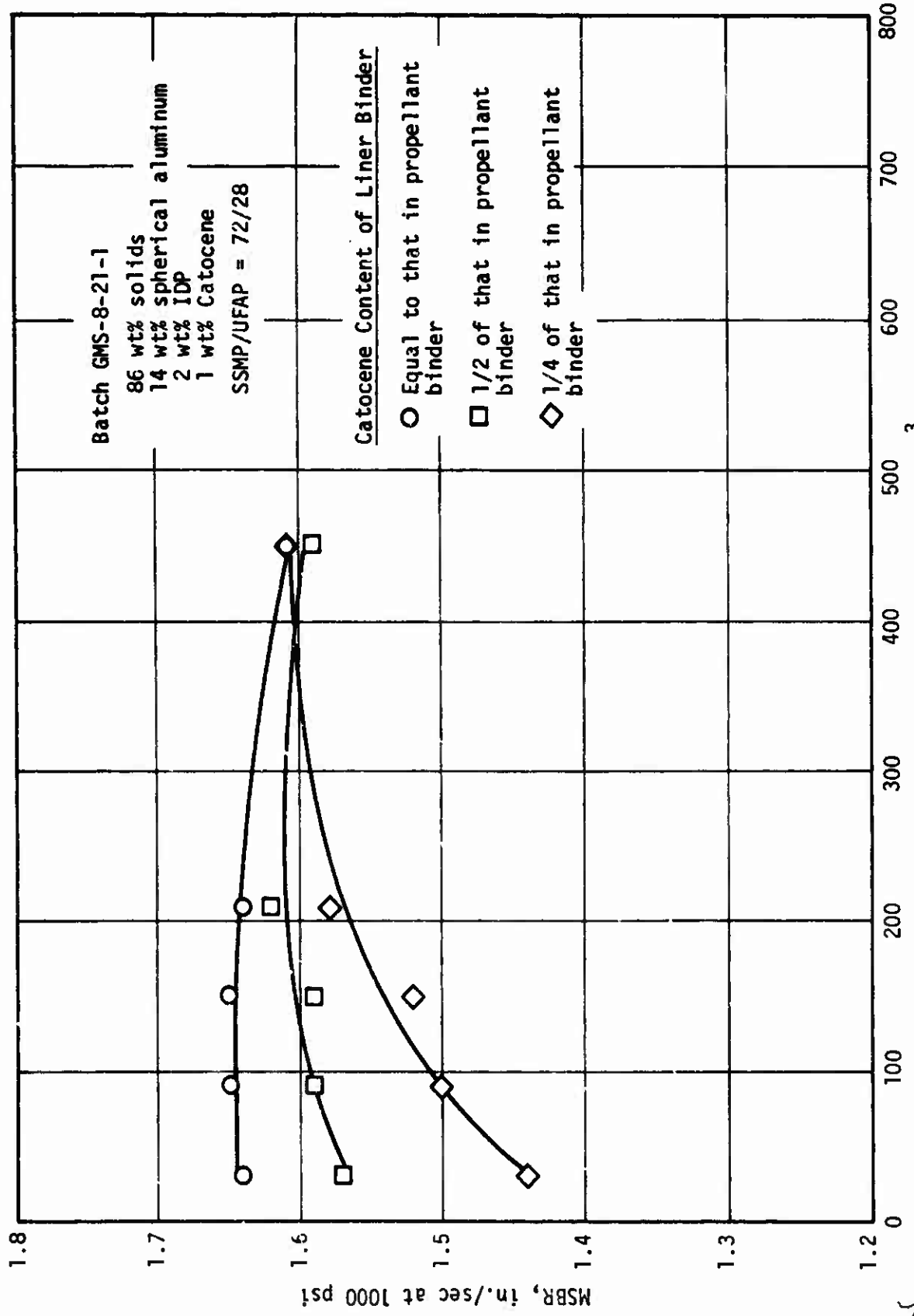

Effect of Catocene Content of SD-878-2 Liner on Burning Rate of HTPB Propellant

Figure 27

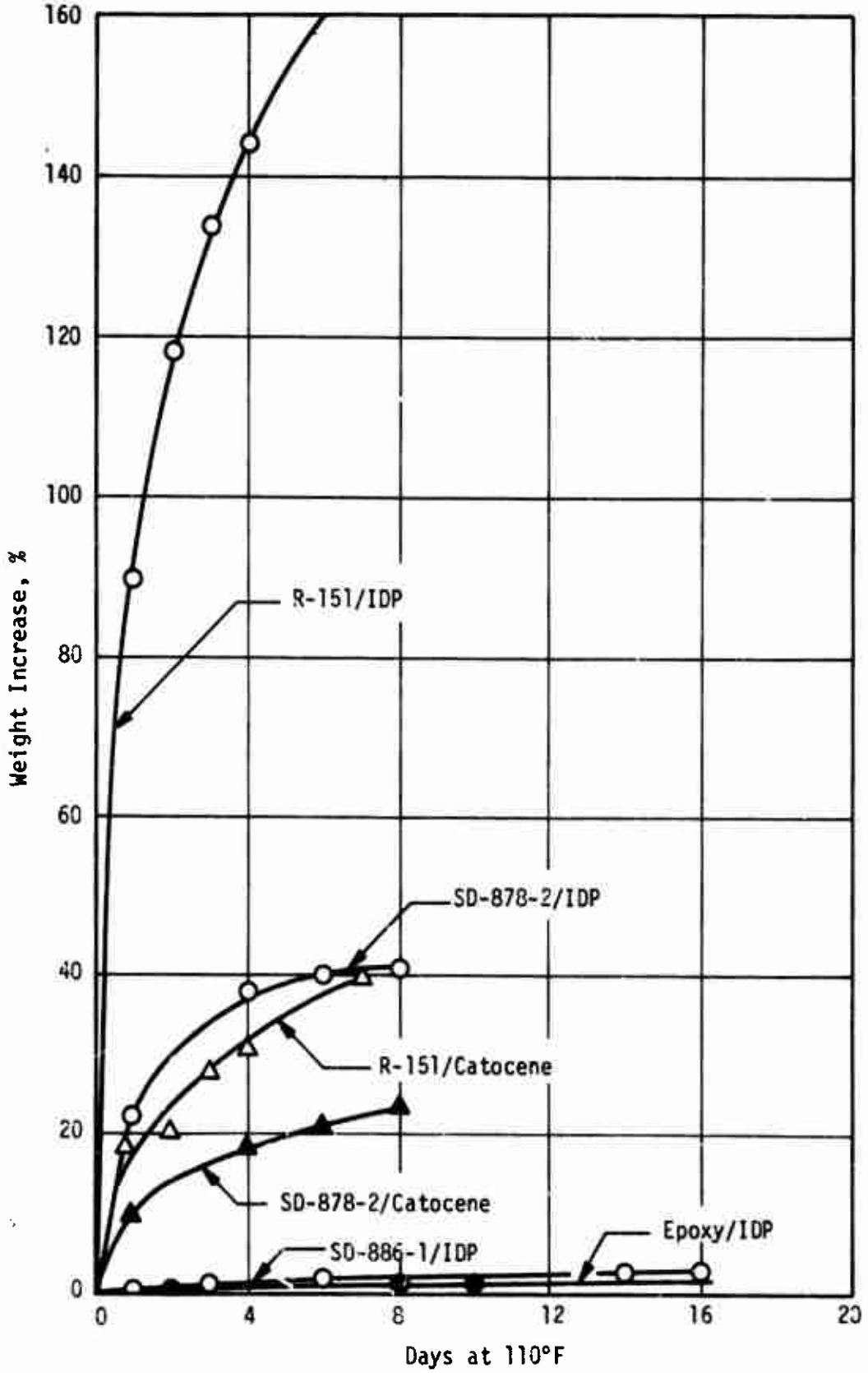

Absorption of IDP and Catocene by Liners and Insulation

Figure 28

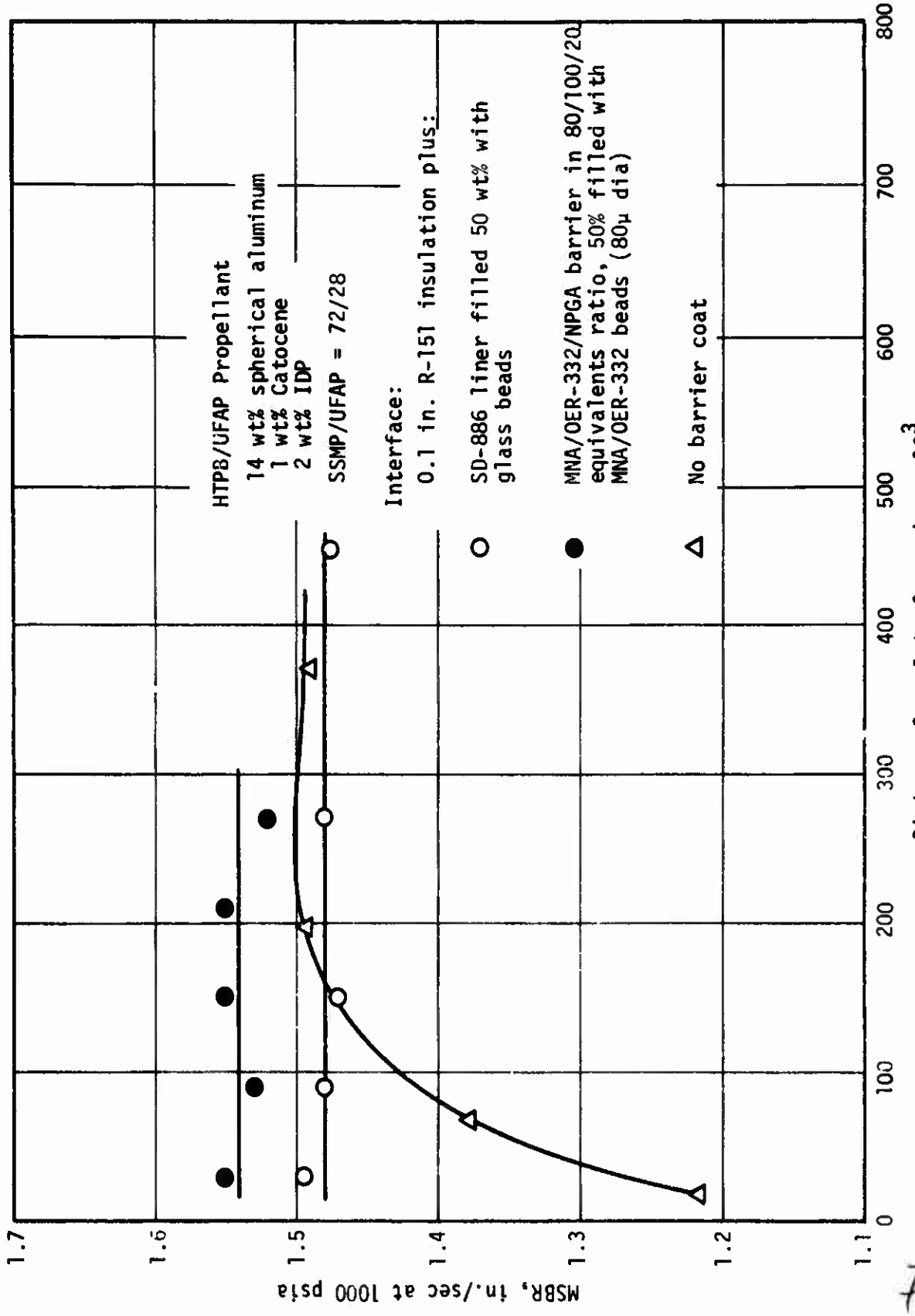

Effect of Barrier Coat on Interphase Burning Rate

77

Figure 29

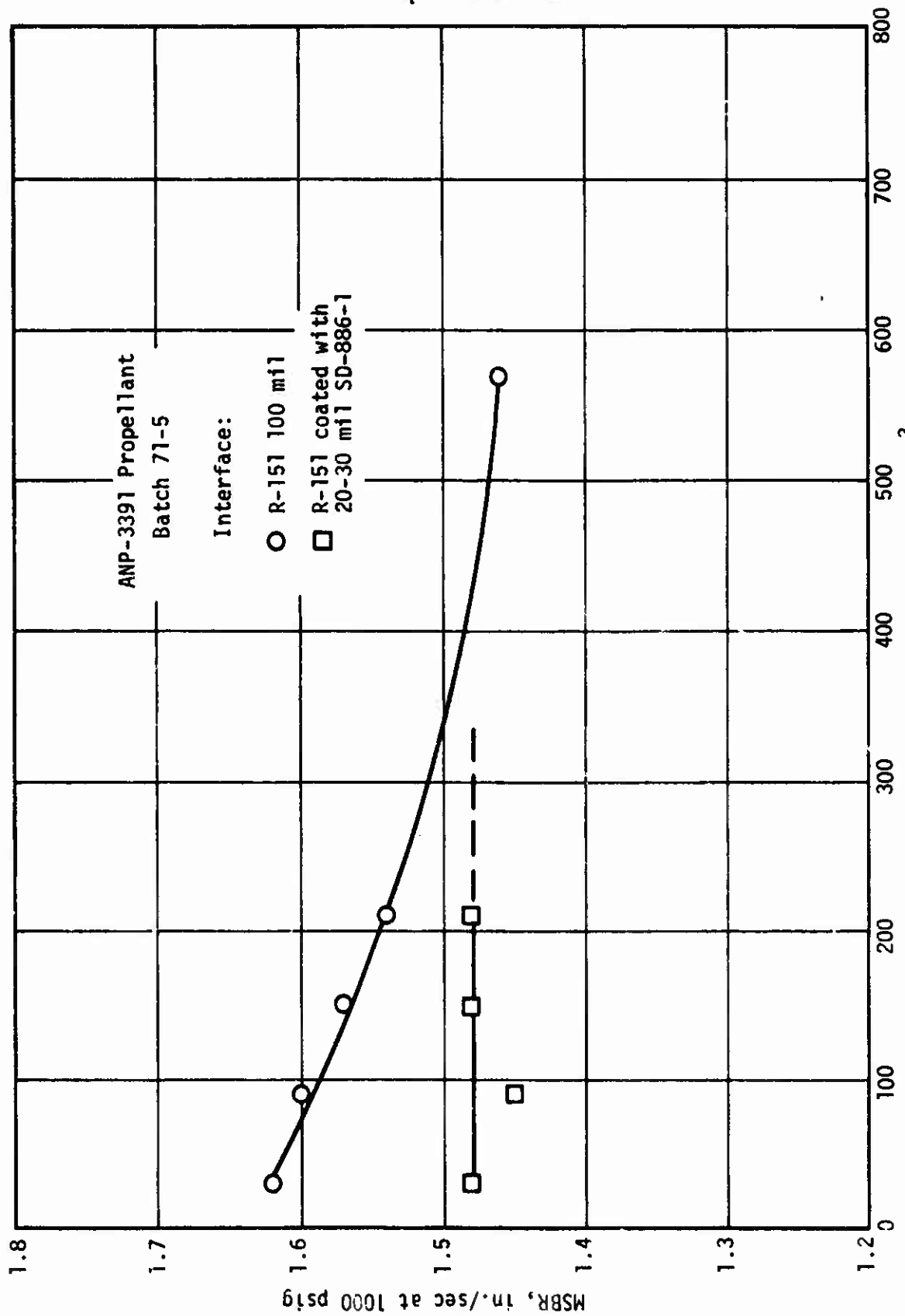

Burning Rate Profiles of R-151 and R-151/SD-886-1 Propellant Interphases

Figure 30

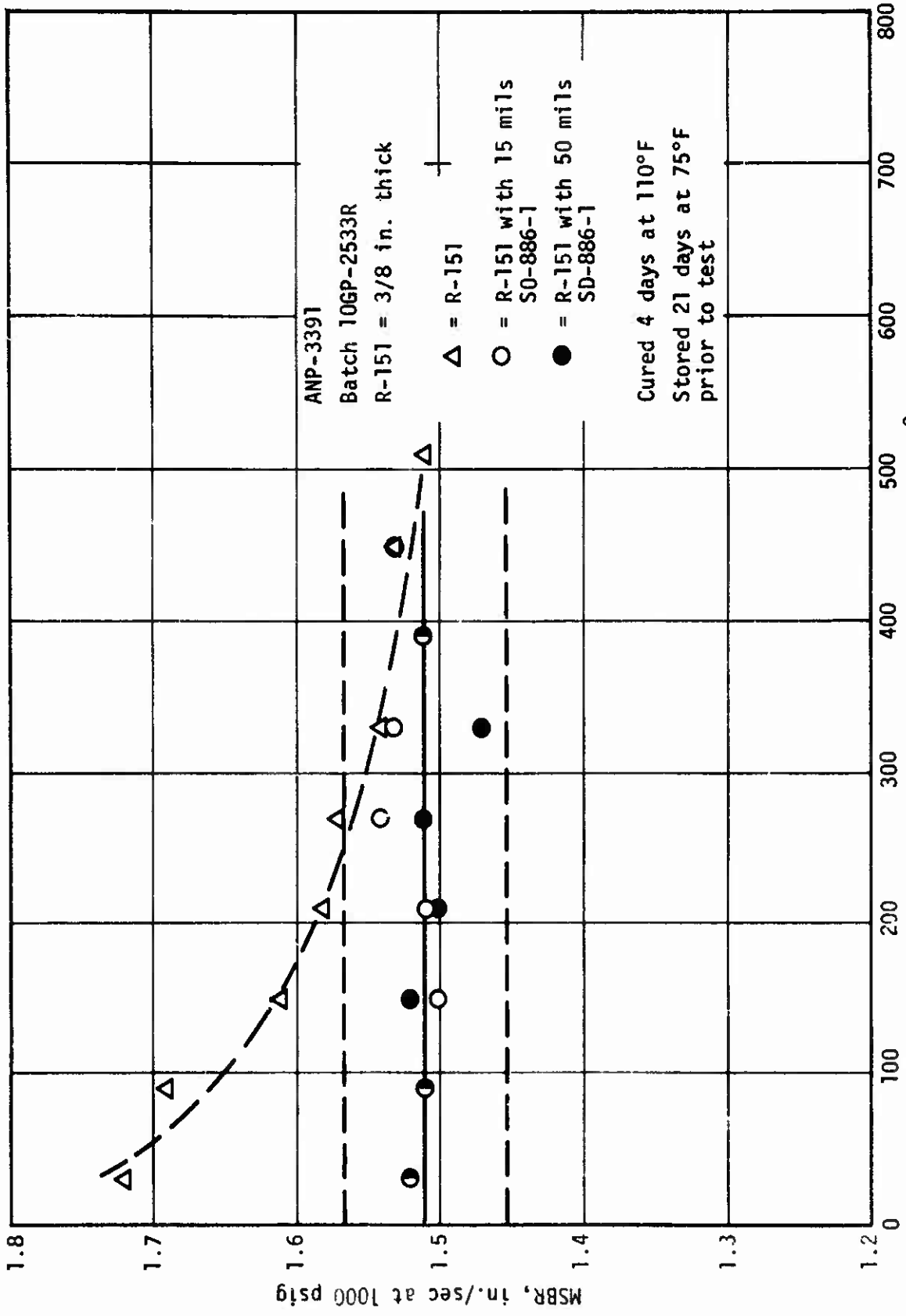

Burning Rate Profiles of R-151/ANP-3391 and R-151/SD-886-1/ANP-3391 Interphases

Figure 31

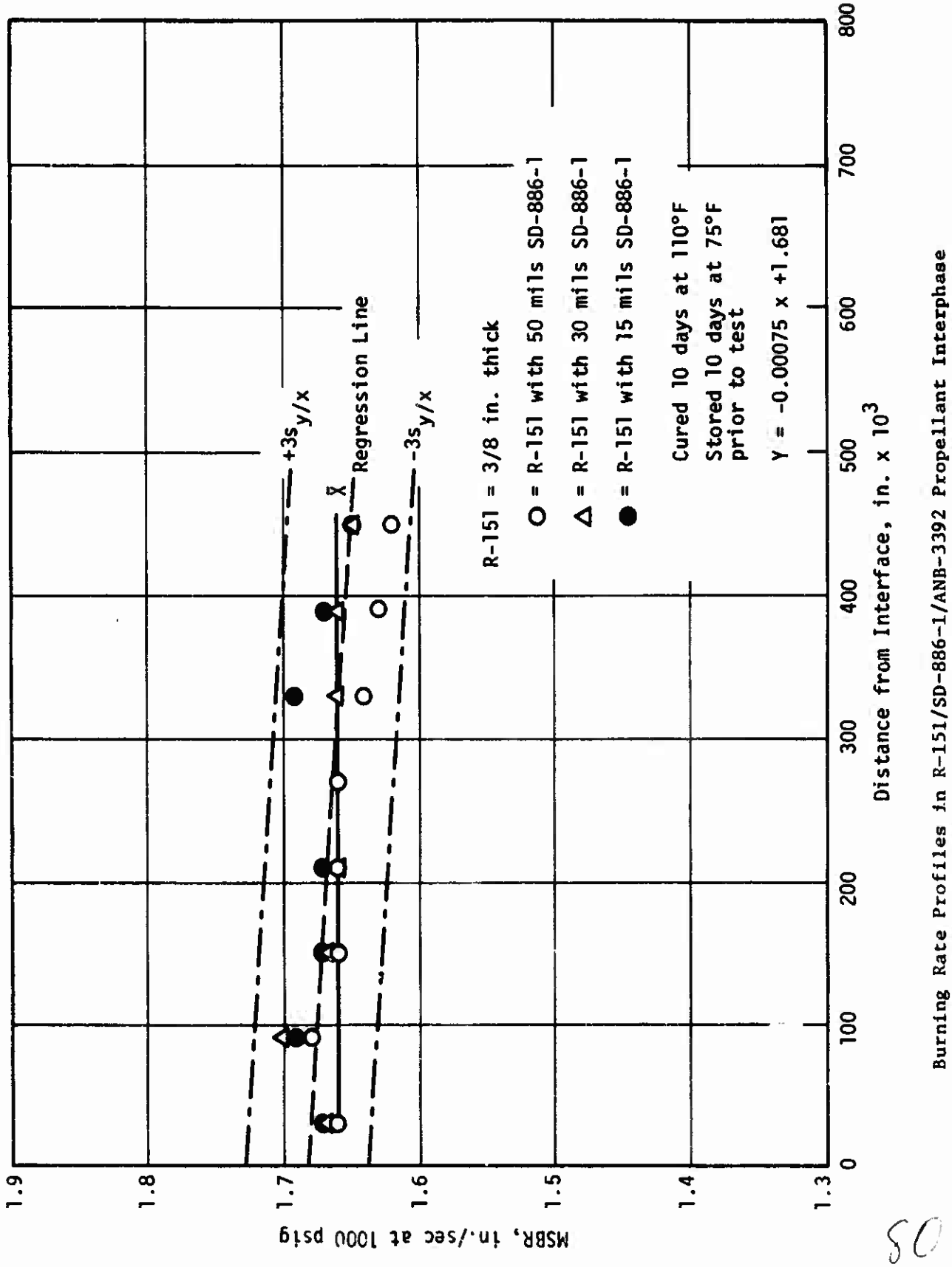

Burning Rate Profiles in R-151/SD-886-1/ANB-3392 Propellant Interphase

Figure 32

SD-886-1 Processing			Microstrand Burning Rate, in./sec at 1000 psi			
Cure		Thickness, mils	Distance from Liner, mils			
Temperature, °F	Time, hr		0 to 60	60 to 120	120 to 180	>240
135	6	30	1.42	1.42	1.42	1.40
	16	30	1.41	1.41	-	1.41
	24	30	1.43	1.45	-	-
	6	50	1.44	1.46	-	1.42
150	6	30	1.42	1.44	1.40	1.42
	16	30	1.48	1.42	-	-
	24	30	1.41	1.40	-	-
180	6	30	1.43	1.44	-	1.45
	16	30	1.41	1.43	-	-
	24	30	1.40	1.49	1.42	-
	24	50	1.41	1.42	-	-
150 (no rubber)	16	30	1.42	1.42	-	-

NOTE: SD-886-1 was used to coat dried and abraded 100 mil R-151 rubber; A-35 washcoat was applied to the SD-886-1.

ANB-3391 propellant - 10-lb batch 10GP-2534.

Figure 33

Effect of SD-886-1 Process Variations on Burning Rate Profile of ANB-3391 Propellant

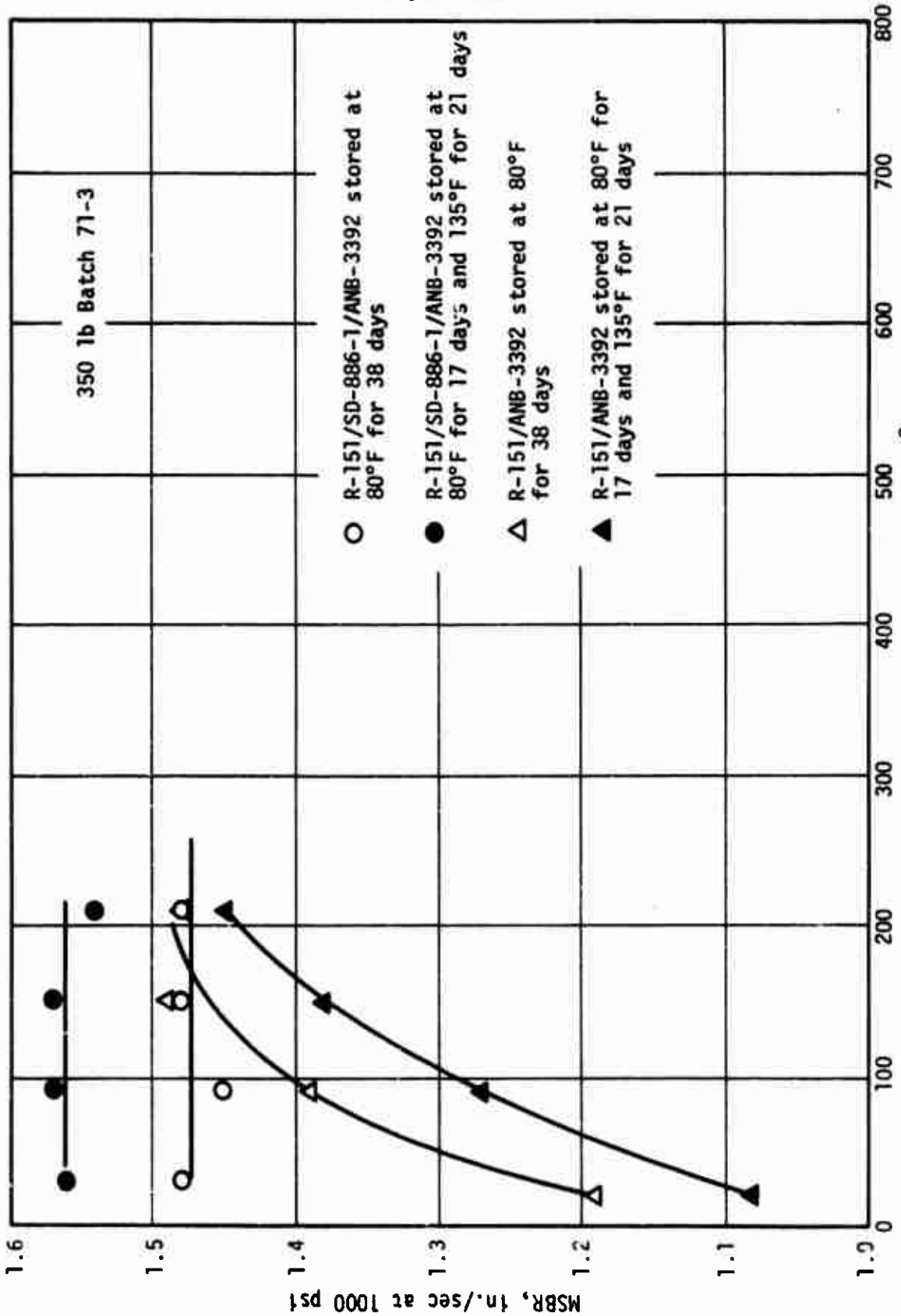

Effect of Storage Temperature on Interphase Burning Rate of ANB-3392

Figure 34

Crosshead Rate = 0.02 in./min

Liner	Test Temperature, °F	Tensile Strength, psi** (based on reduced cross-section)
DER/MNA Barrier/A-35*	-70	654
SD-886-1		676
DER/MNA Barrier/A-35	-45	338
SD-886-1		401
DER/MNA Barrier/A-35	+77	98
SD-886-1		119
DER/MNA Barrier/A-35	+140	96
SD-886-1		99

NOTE: All specimens composed of metal/R-151/liner/propellant/Chemlok adhesive/metal. The propellant was 0.3-in. thick and recessed 0.5 in. circumferentially at liner bond to give a 2.5 in. reduced diameter.

* Composed of DER-332, MNA, NPGA, filled 50 wt% with glass beads and 10 wt% with carbon black, A-35 washcoat was used on these specimens.
** All failures occurred in the propellant to Chemlok-305 adhesive glue line.

Figure 35 Bond Strength of ANB-3392 Propellant Determined in 3.5-in. Poker Chip Specimens

Liner	Wk at 75°F	Tensile Strength at 77°F, psi
R-151/SD-886-1	0	189
	3	202
	6	196
	9	219
R-151/DER-332/MNA/NPGA Barrier	0	192
	3	218
	6	215
	9	223
		All breaks were CP

Effect of Ambient Storage on Bond Strength of Liners to ANB-3392

Figure 36

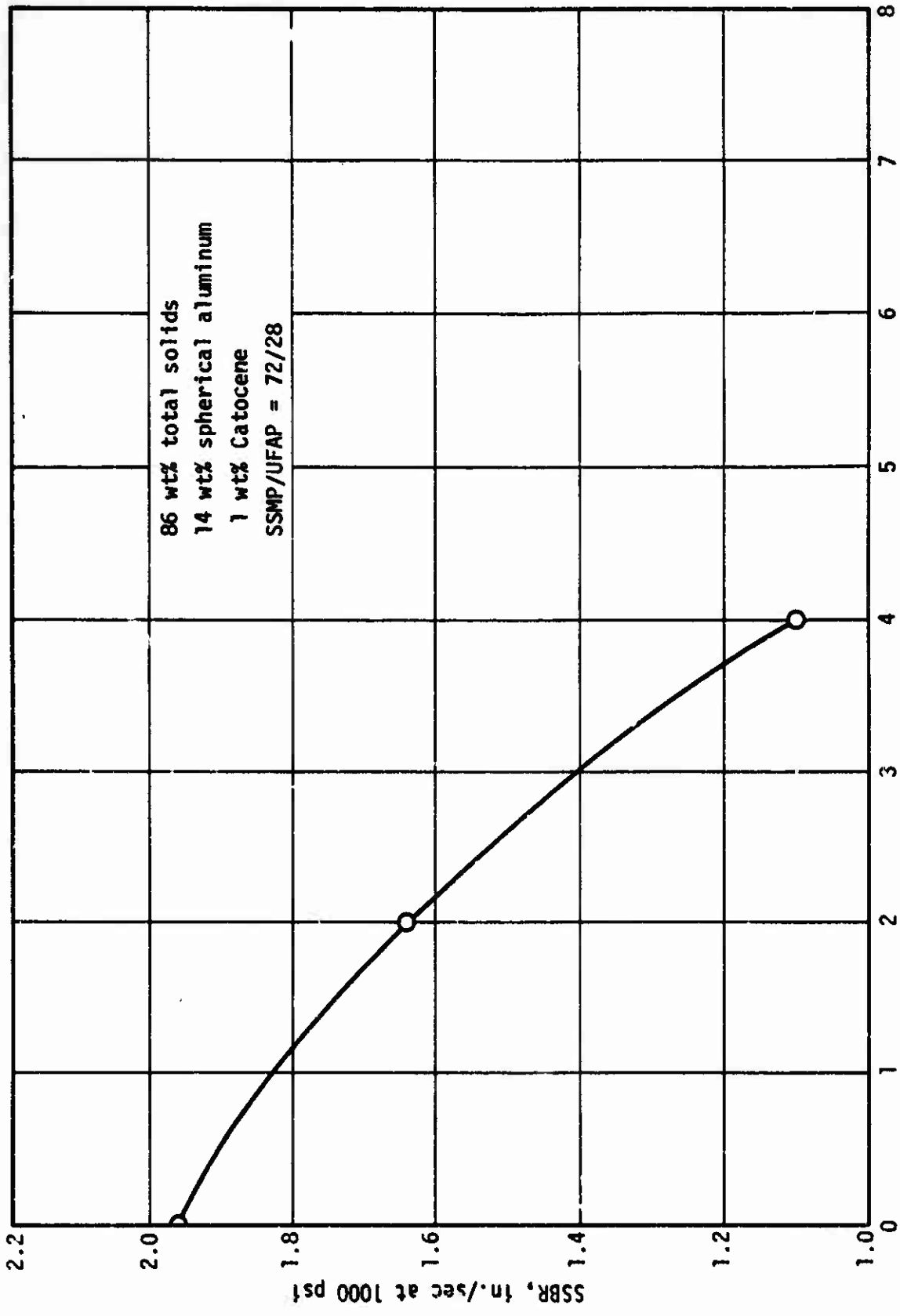

Effect of IDP Level on Burning Rate of HTPB Propellants Containing UFAP

Figure 37

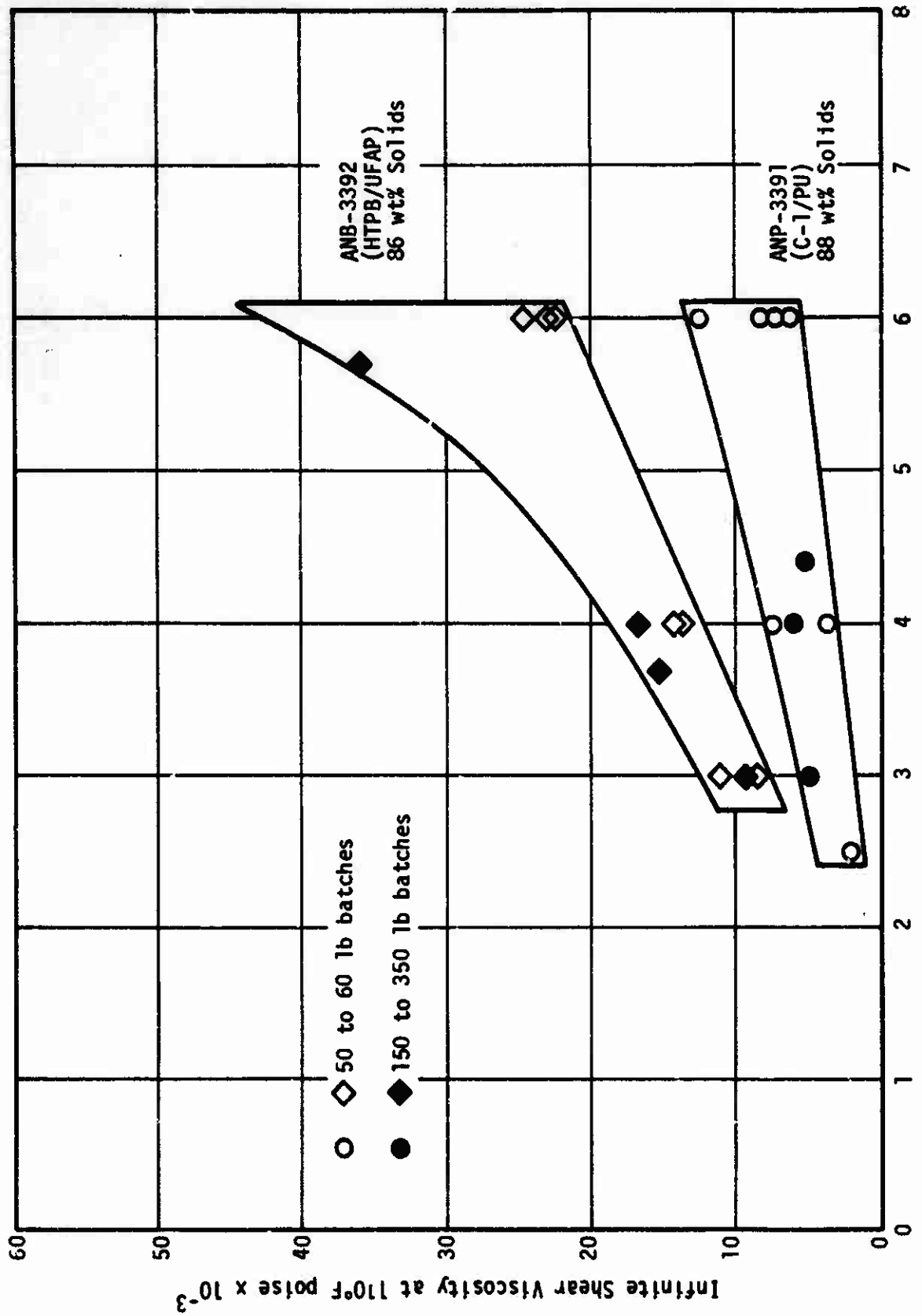

Viscosity Buildup of ANP-3391 and ANB-3392 Propellants

86

Figure 38

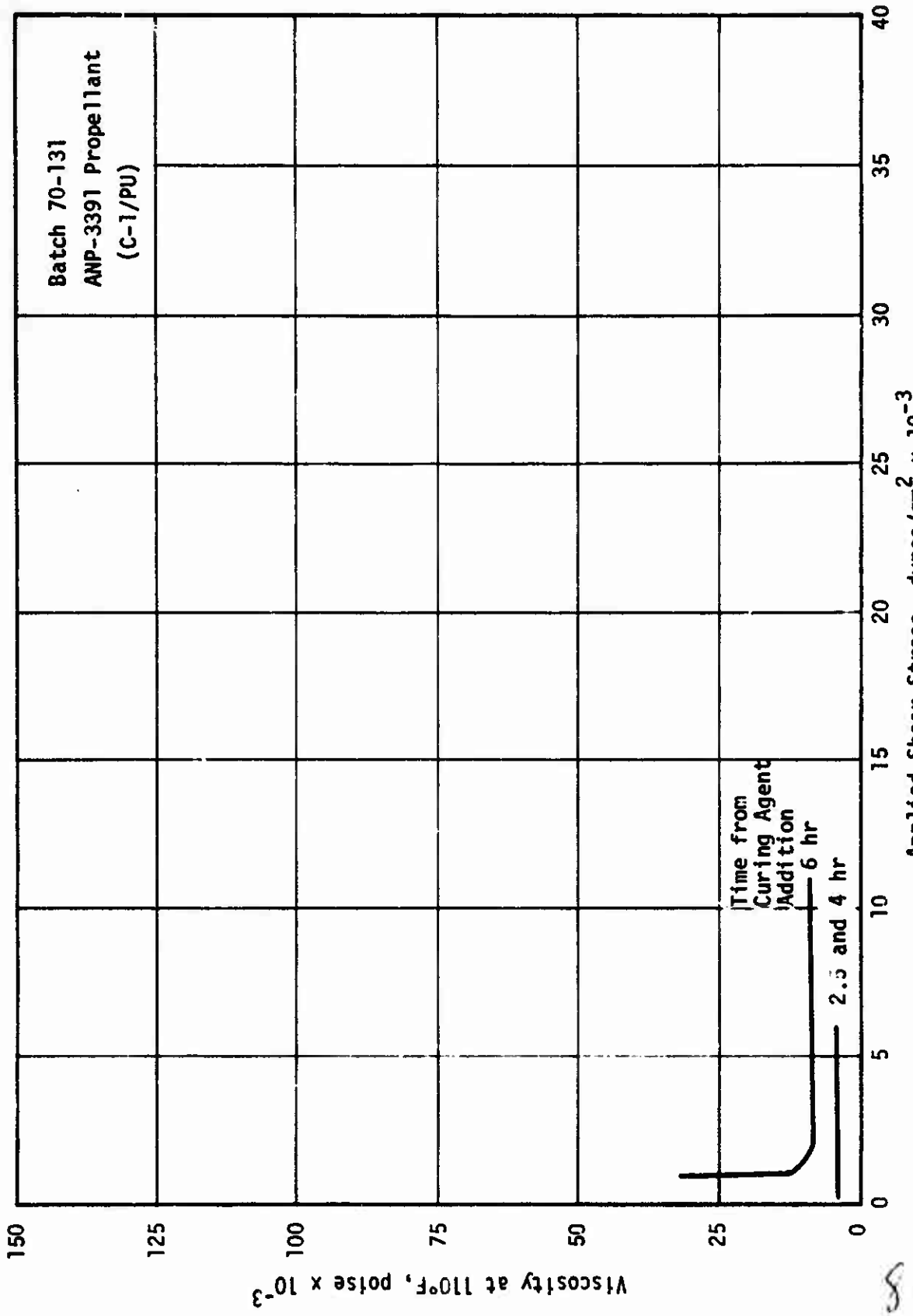

Propellant Viscosity as a Function of Shear Stress and Time From Curing Agent Addition

87

Figure 39

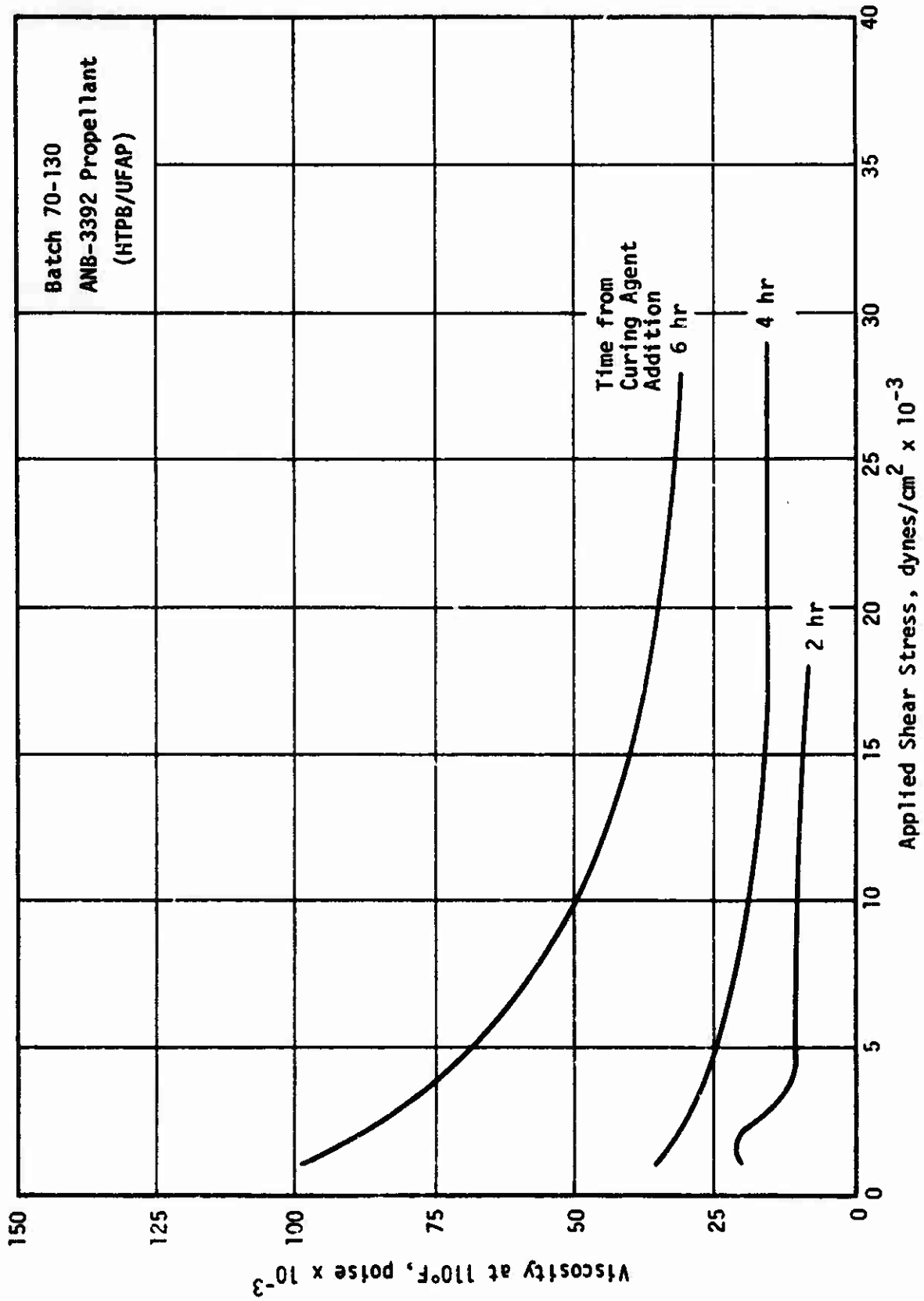

Propellant Viscosity as s Function of Shear Stress and Time From Curing Agent Addition

Figure 40

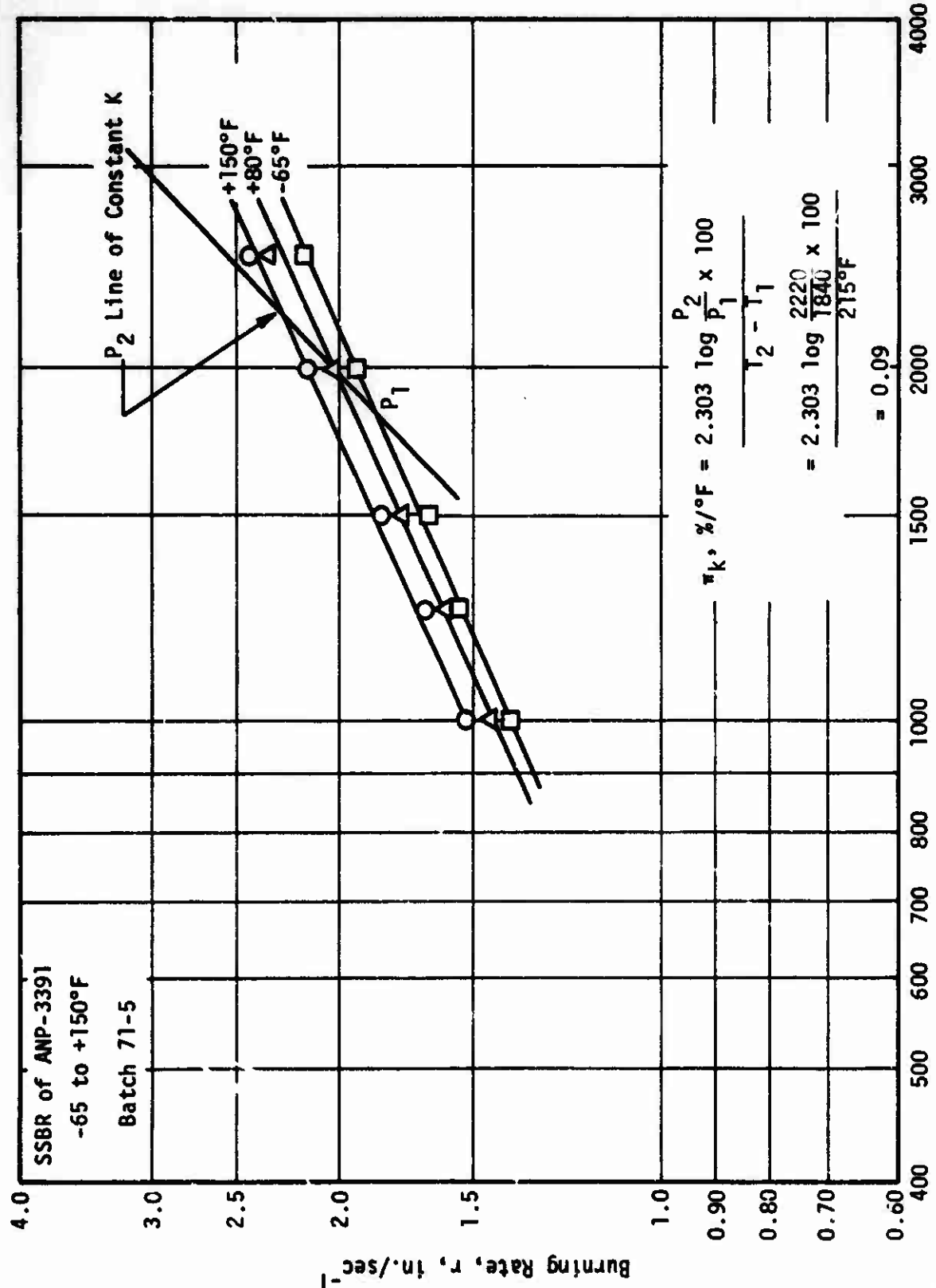

SSBR of ANP-3391

89

Figure 41

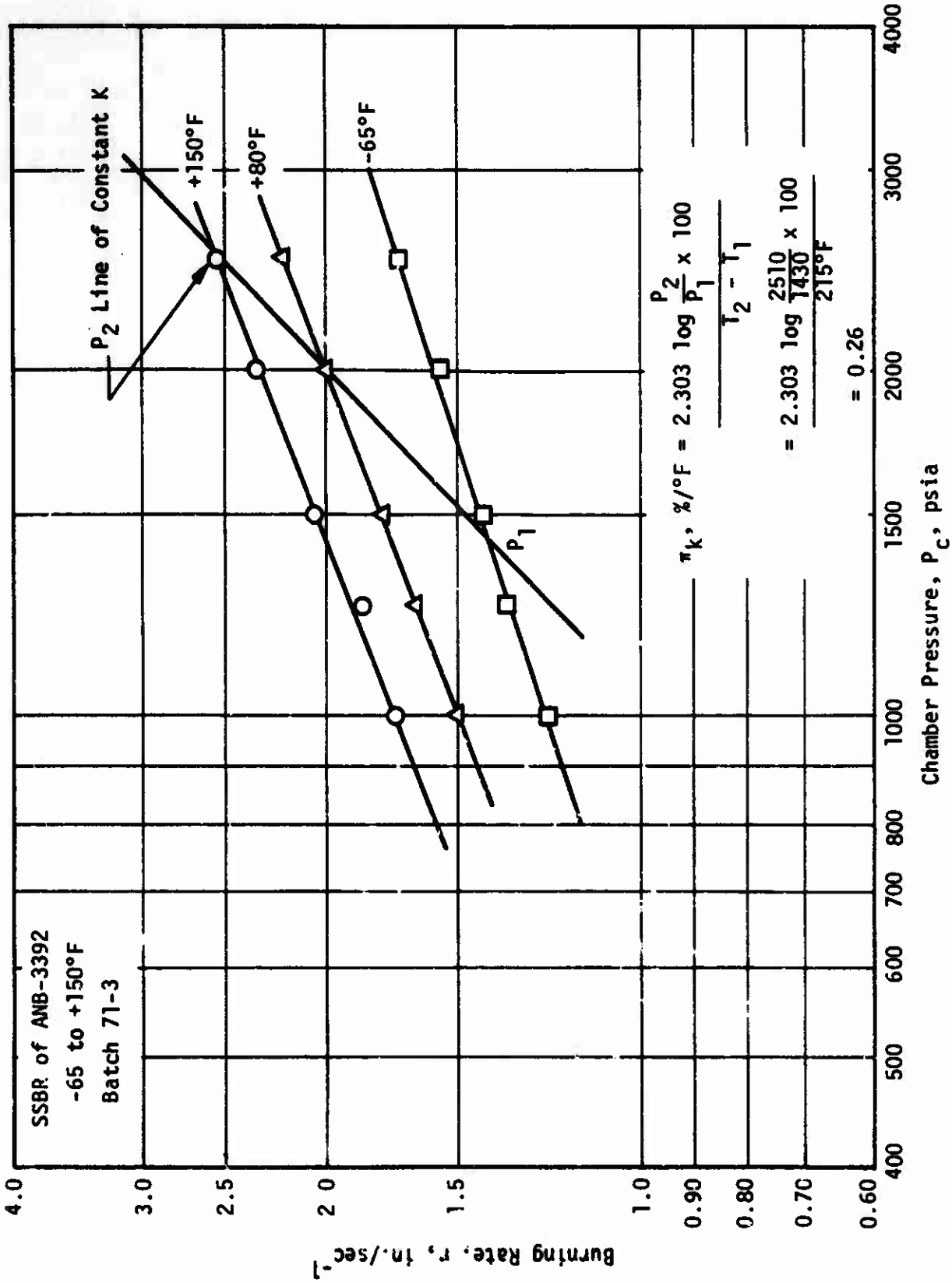

SSBR of ANB-3392

Figure 42

Batch	Batch Size, lb	UFAP Lot	UFAP Particle Size, μ (MSA 50% pt)	Burning Rate at 1000 psi in./sec	Rotovisko Viscosity, poise at 110°F Six Hours After Di-isocyanate Addition
4B-10	1	VM-25	0.57	1.54	-
4B-13	1	VM-25	0.57	1.58	23,000
10GP-1674	10	VM-25	0.57	1.52	
70-130	60	VM-71	0.55	1.53	23,000
70-141	60	VM-71	0.55	1.51	24,000
3392-60	1	VM-86	0.59	1.52	-
71-3	350	VM-86/M60-8*	(0.59/0.56)	1.52	23,000

*200-lb UFAP grind, all others are 60-lb grinds

Figure 43

Effect of Batch Size on Reproducibility of ANB-3392 (HTPB/UFAP) Propellant

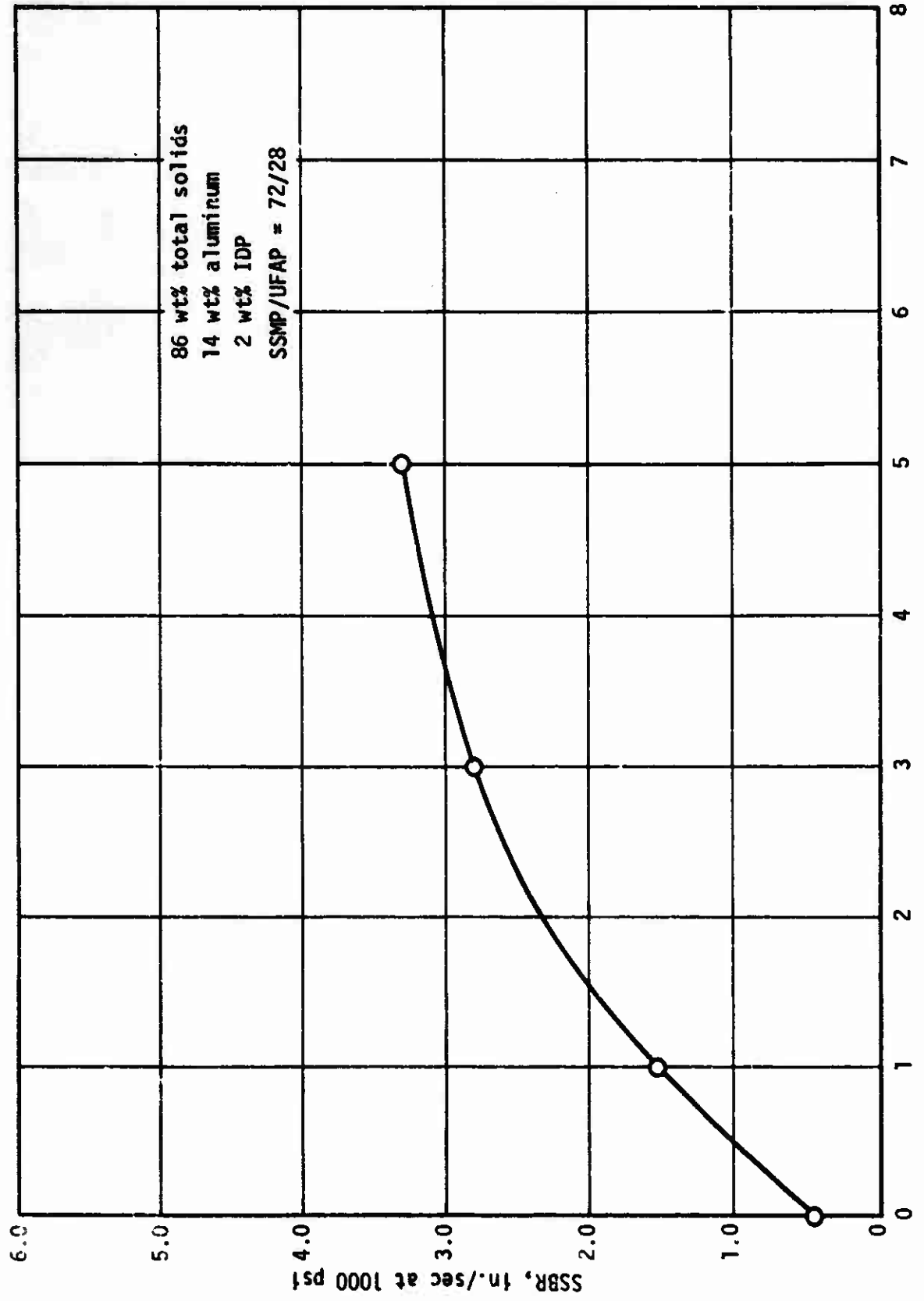

Effect of Catocene Level on Burning Rate of HTPB/UFAP Propellants

Figure 44

Pressure, psig	SSBR, in./sec		
	Initial	3 wk at 135°F	6 wk at 135°F
800	1.31	1.32	1.32
1000	1.44	1.46	1.46
1500	1.75	1.75	1.75
2000	2.04	2.04	2.00
2500	2.28	2.30	2.32
3000	2.53	2.56	2.50

Batch 71-33

Effect of 135°F Storage on Solid Strand Burning Rate of ANP-3391 Propellant

Figure 45

Pressure, psig	SSBR, in./sec			
	Initial	3 wk at 135°F	6 wk at 135°F	% Change
800	1.39	1.46	1.45	5.0
1000	1.53	1.59	1.60	4.6
1500	1.79	1.88	1.89	5.0
2000	2.04	2.14	2.12	4.9
2500	2.27	2.34	2.33	3.1
3000	2.44	2.56	2.51	3.7
				Average = 4.4

Batch 71-26

Effect of 135°F Storage on Solid Strand Burning Rate of ANB-3392 Propellant

Figure 46

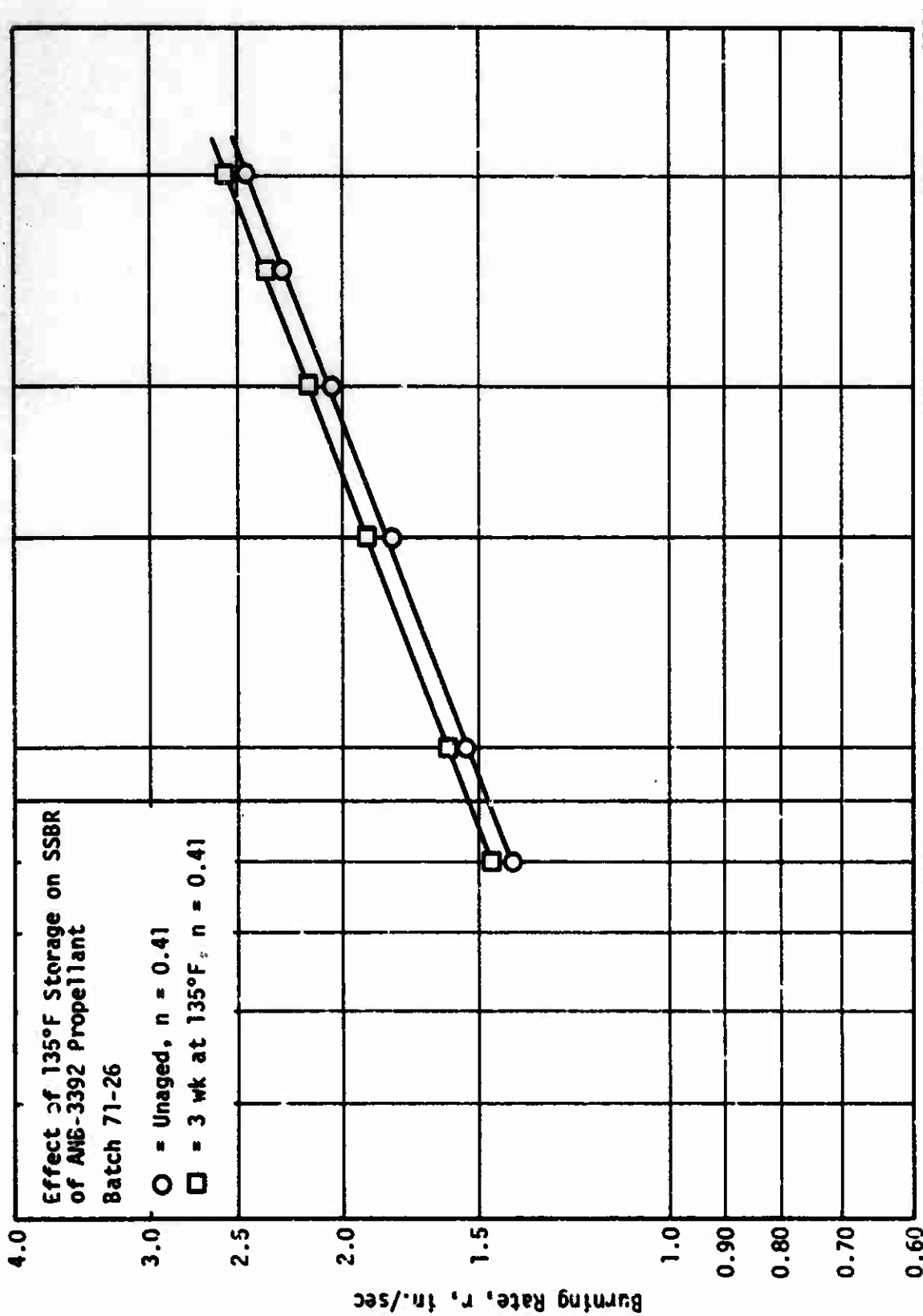

Effect of 135°F Storage on SSBR of ANB-3392 Propellant

95

Figure 47

Motor Number	1	2	3	4	5	6	7	8	9	10	11
Propellant	ANB-3392	ANB-3392	ANB-3392	ANB-3392	ANP-3391	ANB-3392	ANB-3392	ANP-3391	ANB-3392	ANP-3391	ANB-3392
Nozzle Entrence Angle, degree	45	45	20	45	45	45	45	45	45	45	45
L*, in.	224	630	630	264	600	264	600	600	172	172	172
Nozzle Throat Area, $in.^2$	0.138	0.138	0.138	0.138	0.138	0.138	0.138	0.138	0.180	0.180	0.180
K_n	91.1	89.2	91.6	92.4	93.5	90.5	83.9	84.7	60.4	59.0	60.0
Chamber Pressure, psia											
Maximum	3165	2405	3550	1740	2380	1751	2339	1817	1263	1245	-
Average	-	-	-	1716	2276	1703	2211	1773	1159	1030	-
Steady State	-	1715	1640	1740	-	1680	-	1811	1130	-	-
Net Action Time, sec	-	-	-	5.95	4.88	4.70	4.50	5.92	7.04	7.44	-
Burn Time, sec	-	6	-	6.6	6.2	5.70	5.7	7.2	8.0	7.8	-
Thrust, lbf											
Maximum	715	510	788	370	530	374	519	390	320	341	-
Average	-	-	-	362	506	360	485	379	299	280	-
Web, in.	10.90	10.84	10.94	10.97	11.97	9.05	12.04	12.04	12.10	12.04	-
Average Burn Rate, in./sec	-	-	-	1.843	2.51	1.926	2.68	2.035	1.668	1.550	-
Remarks	Case burn-through	Restriction failure at thermocouples, neutrality OK	Otto Grair 2	Neutral	Non-neutral; burn front probably increased by case bond failure	Neutral	140°F, non-neutral and progressive	Slow ignition neutral burning	Migration demonstration	Migration demonstration	Motor malfunction due to quench failure

3KS-1000 Motor Ballistic Summary (Aerojet Tests)

Figure 48, Sheet 1 of 2

Motor Number	12	13	14	15	16	17	18	19
Propellant	ANB-3392	ANB-3392	ANB-3392	ANB-3392	ANP-3391	ANP-3391	ANP-3391	ANP-3391
Nozzle Entrance Angle, degree	45	45	45	45	45	45	45	45
L^*, in.	600	600	600	600	600	600	600	600
Nozzle Throat Areas, $in.^2$	0.138	0.138	0.138	0.138	0.138	0.138	0.138	0.138
K_n	85.9	86.0	85.5	85.9	85.0	86.1	86.0	85.4
Chamber Pressure, psia								
Maximum	1780	1620	1780	1830	1930	2080	1910	1910
Average	1544	1441	1566	1581	1663	1749	1693	1631
Burn time, sec	6.86	7.14	6.77	6.75	6.42	6.16	6.41	6.56
Thrust, lbf								
Maximum	360.0	346.7	373.3	376.6	426.7	450.0	416.7	416.7
Average	322.0	306.6	324.9	328.8	356.0	379.4	363.2	352.2
Web, in.	12.00	12.00	12.04	12.03	12.02	12.00	12.00	12.00

Note: All NWC test showed excellent neutrality

3KS-1000 Motor Ballistic Summary (NWC Tests)

Figure 48, Sheet 2 of 2

ANB-3392

TIER, cal/cm^2	Exposure Time, millisec	Pressure, atm
2.2	28 ± 3	1
1.4	17 ± 2	2
1.0	13 ± 1	3

P* = 4.8 ± 0.3 psia

ANB-3391

2.6	32 ± 3	1
1.3	16 ± 2	2
1.0	14 ± 2	3

P* = 3.8 ± 0.3 psia

Arc-Image Furnace Data
($\dot{Q}$ = 80 cal/cm^2-sec)

Figure 49

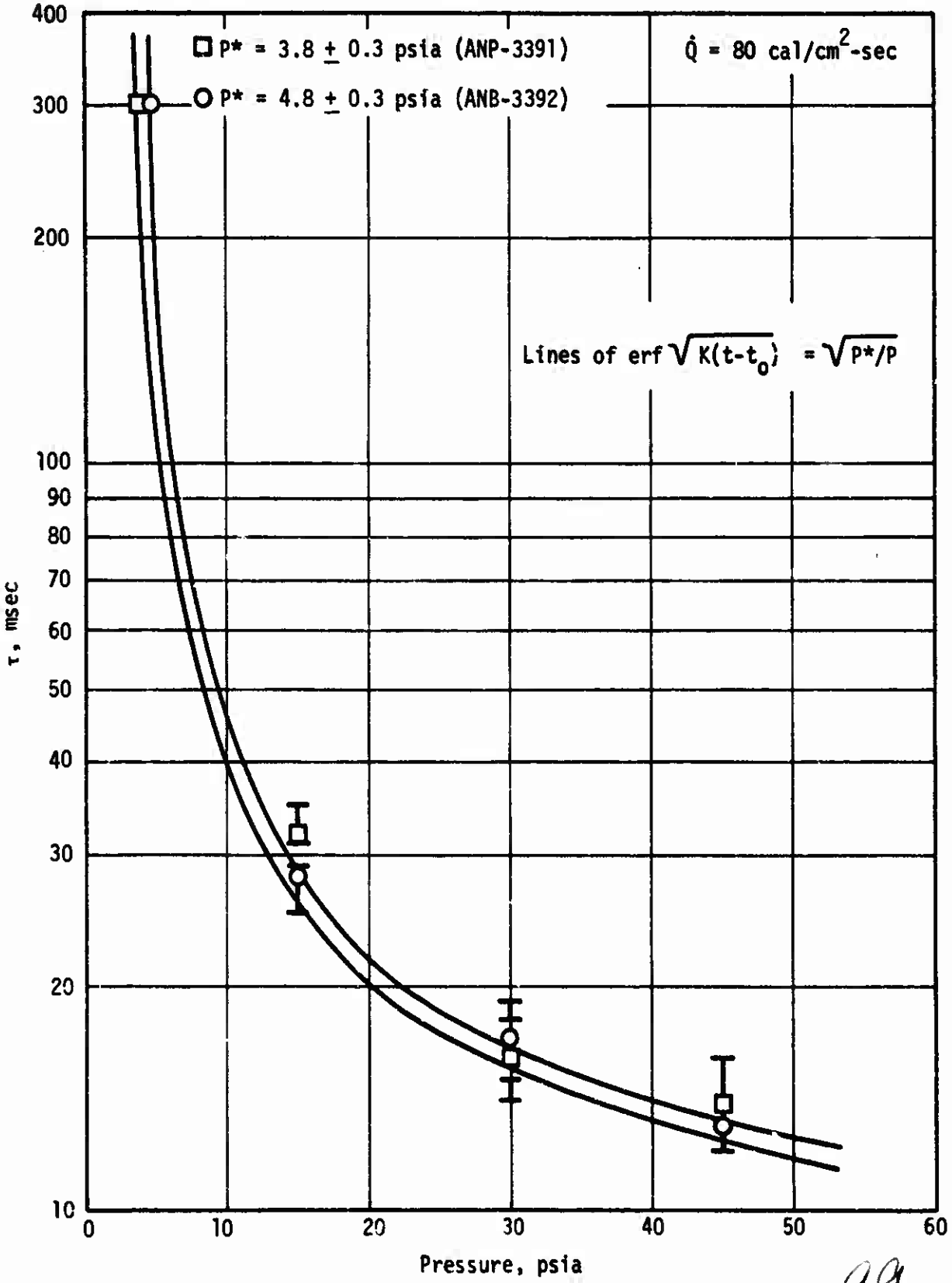

99

Arc-Image Furnace Ignitability Data,
ANB-3392 and ANP-3391 Propellants

Figure 50

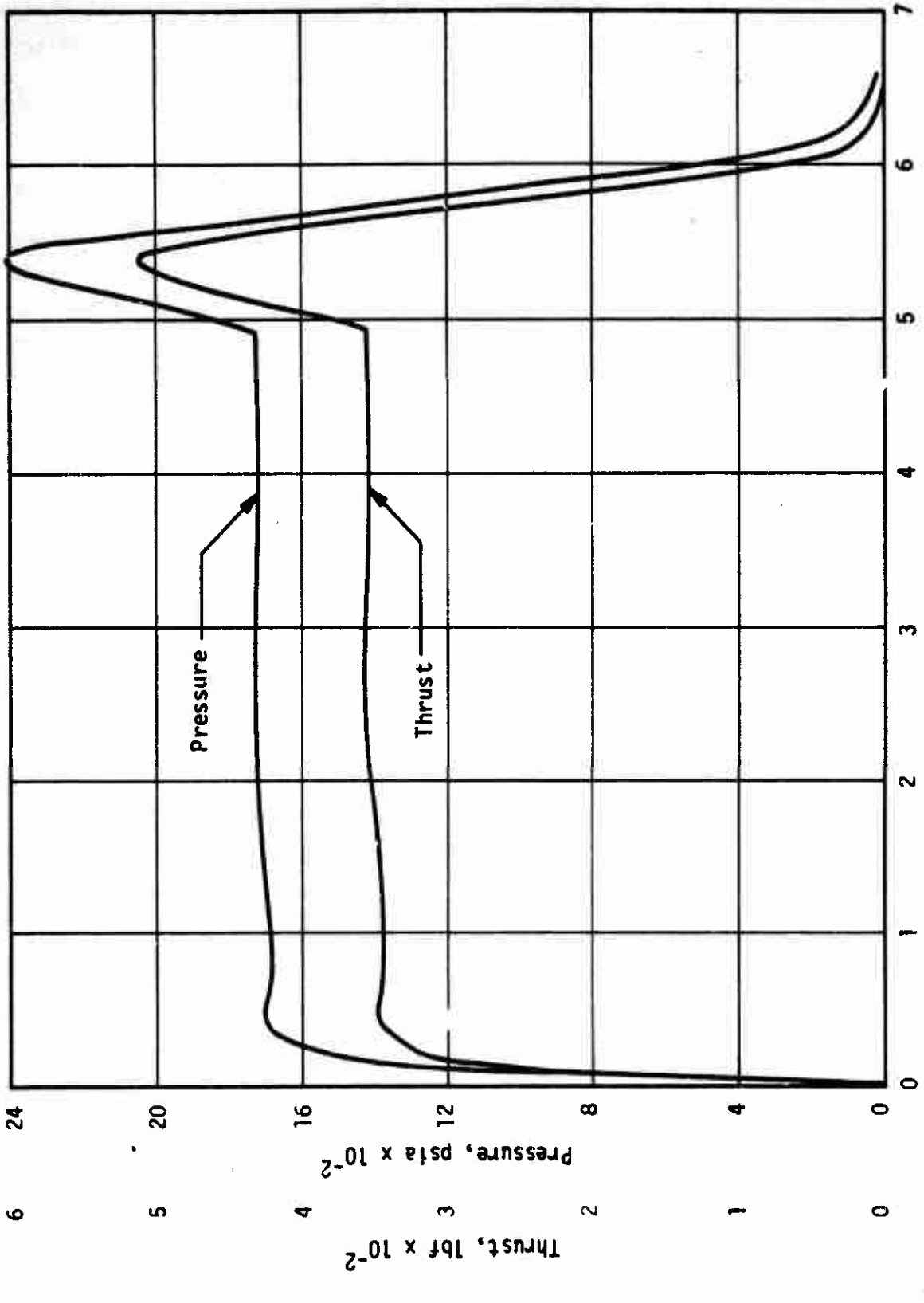

Pressure and Thrust vs Time Curves, 3KS-1000 Motor No. 2 (ANB-3392)

Figure 51

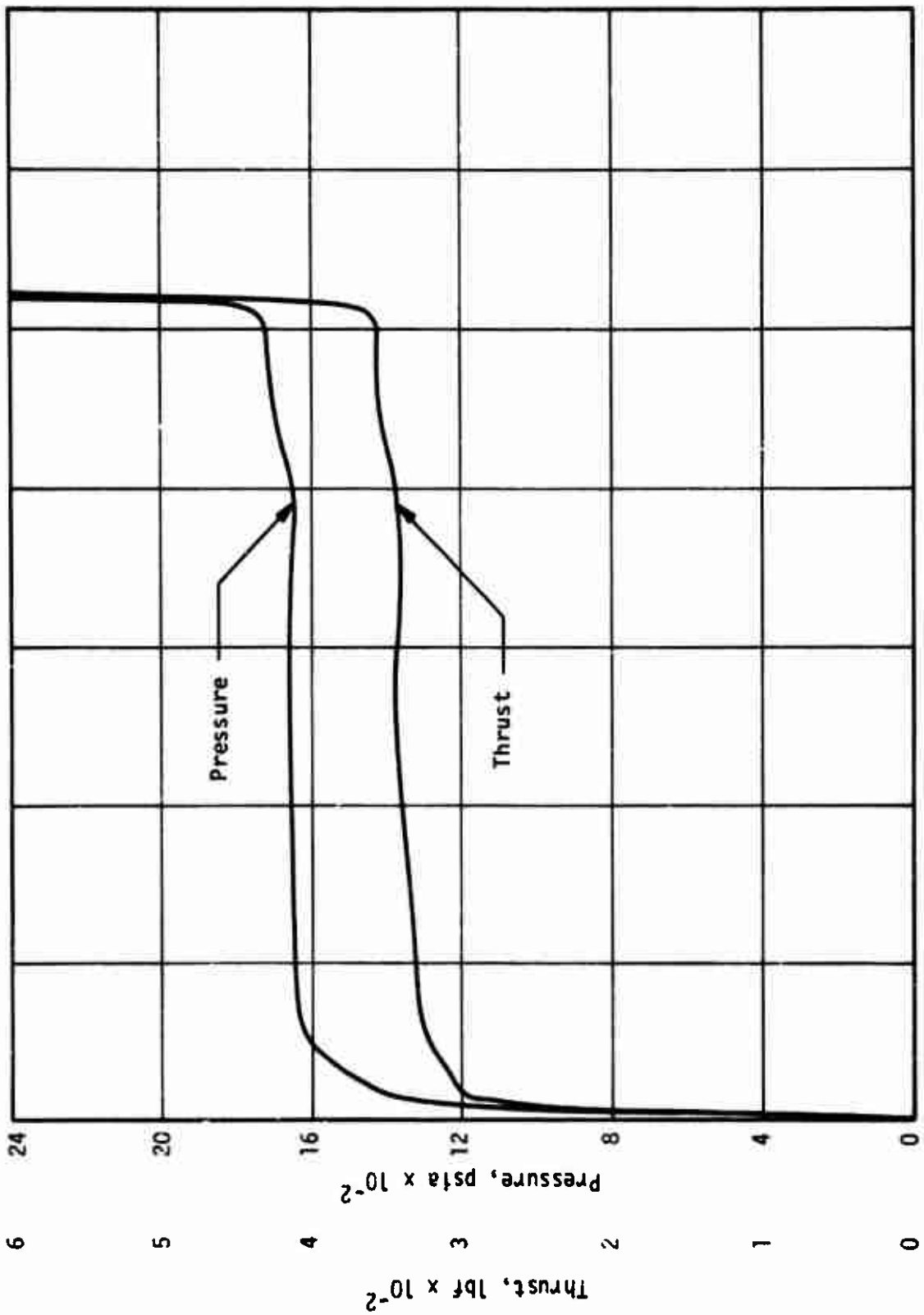

Pressure and Thrust vs Time Curves, 3KS-1000 Motor No. 3 (ANB-3392)

Figure 52

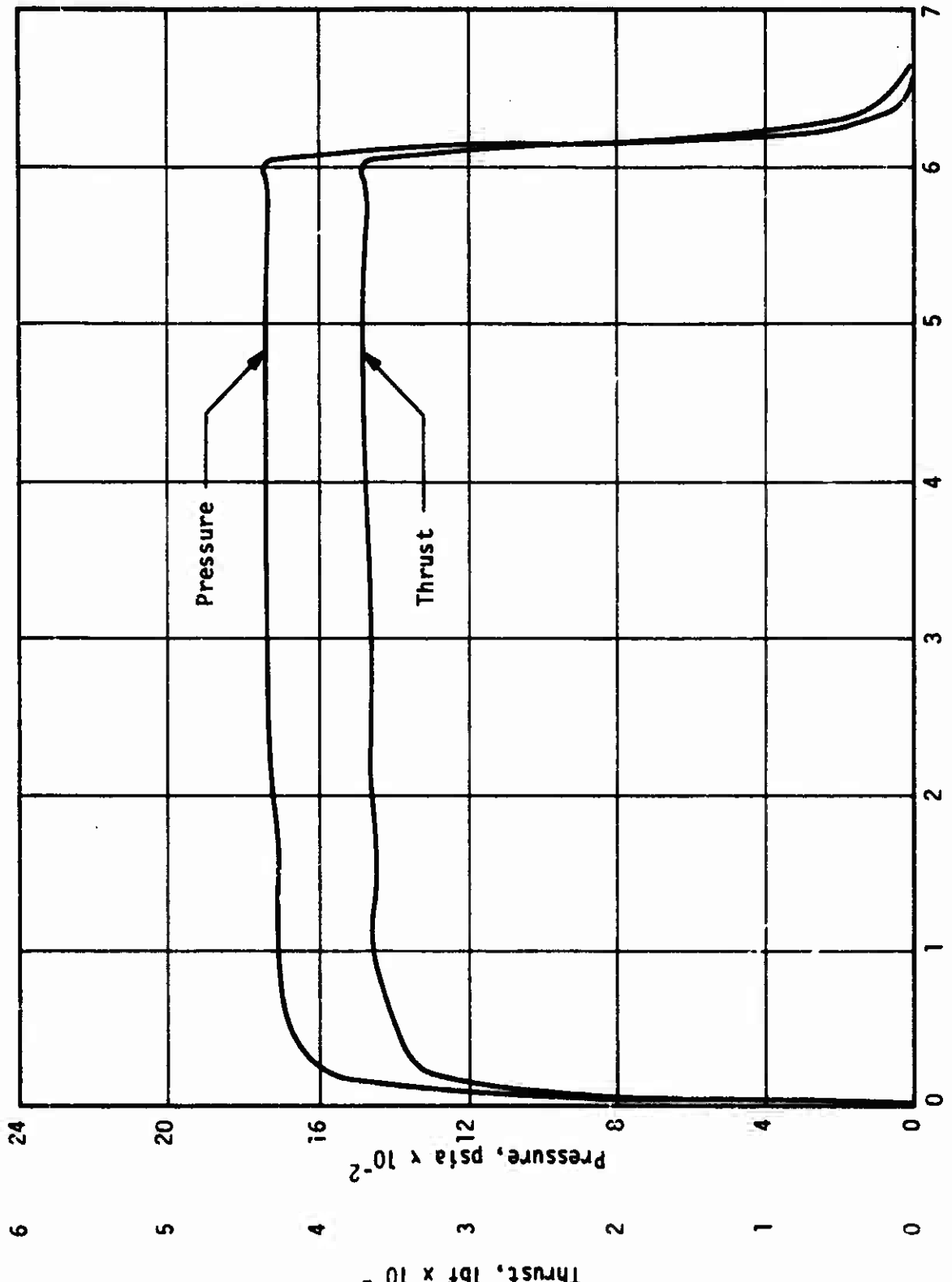

Pressure and Thrust vs Time Curves, 3KS-1000 Motor No. 4 (ANB-3392)

Figure 53

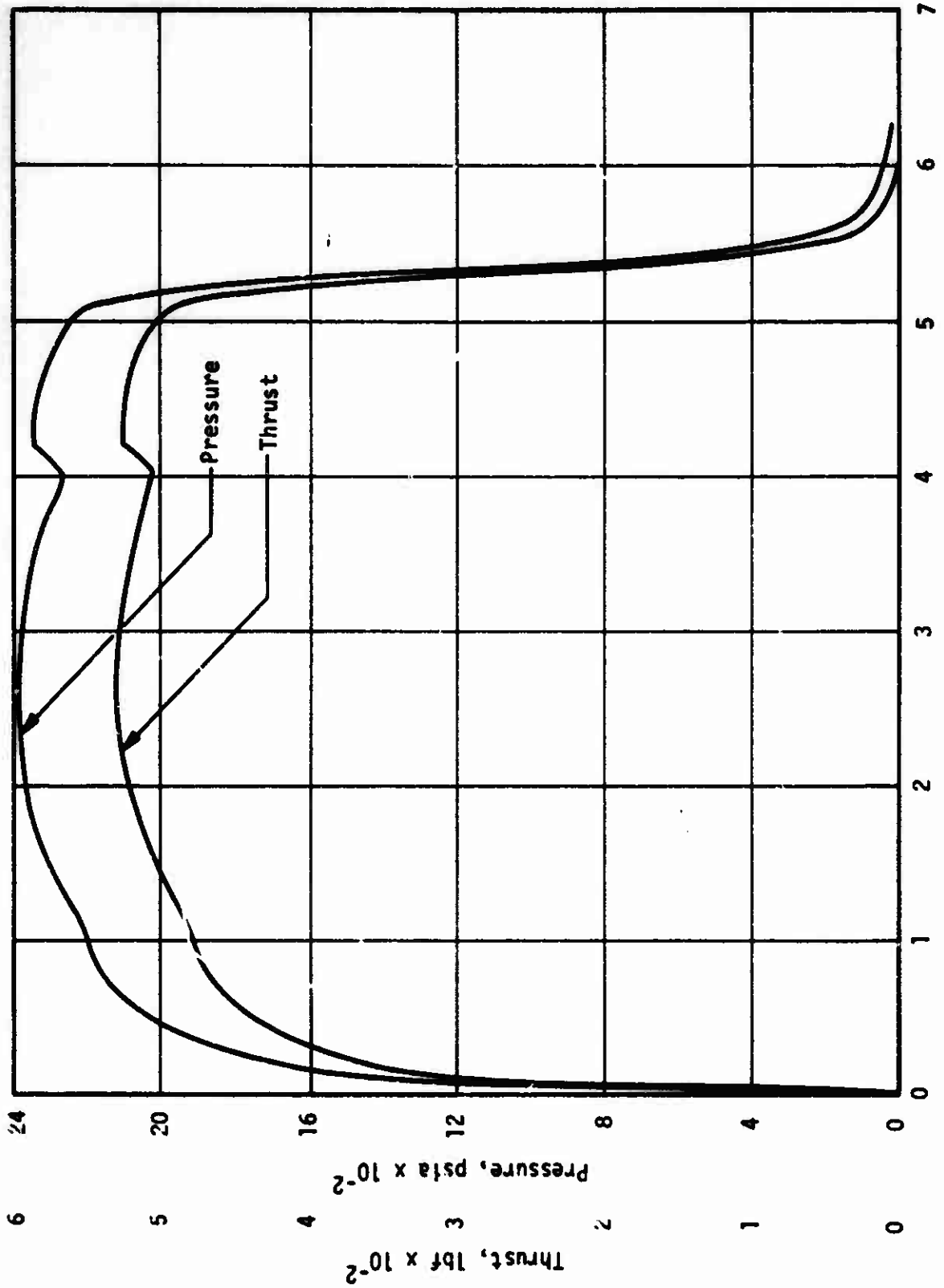

Pressure and Thrust vs Time Curves, 3KS-1000 Motor No. 5 (ANP-3391)

Figure 54

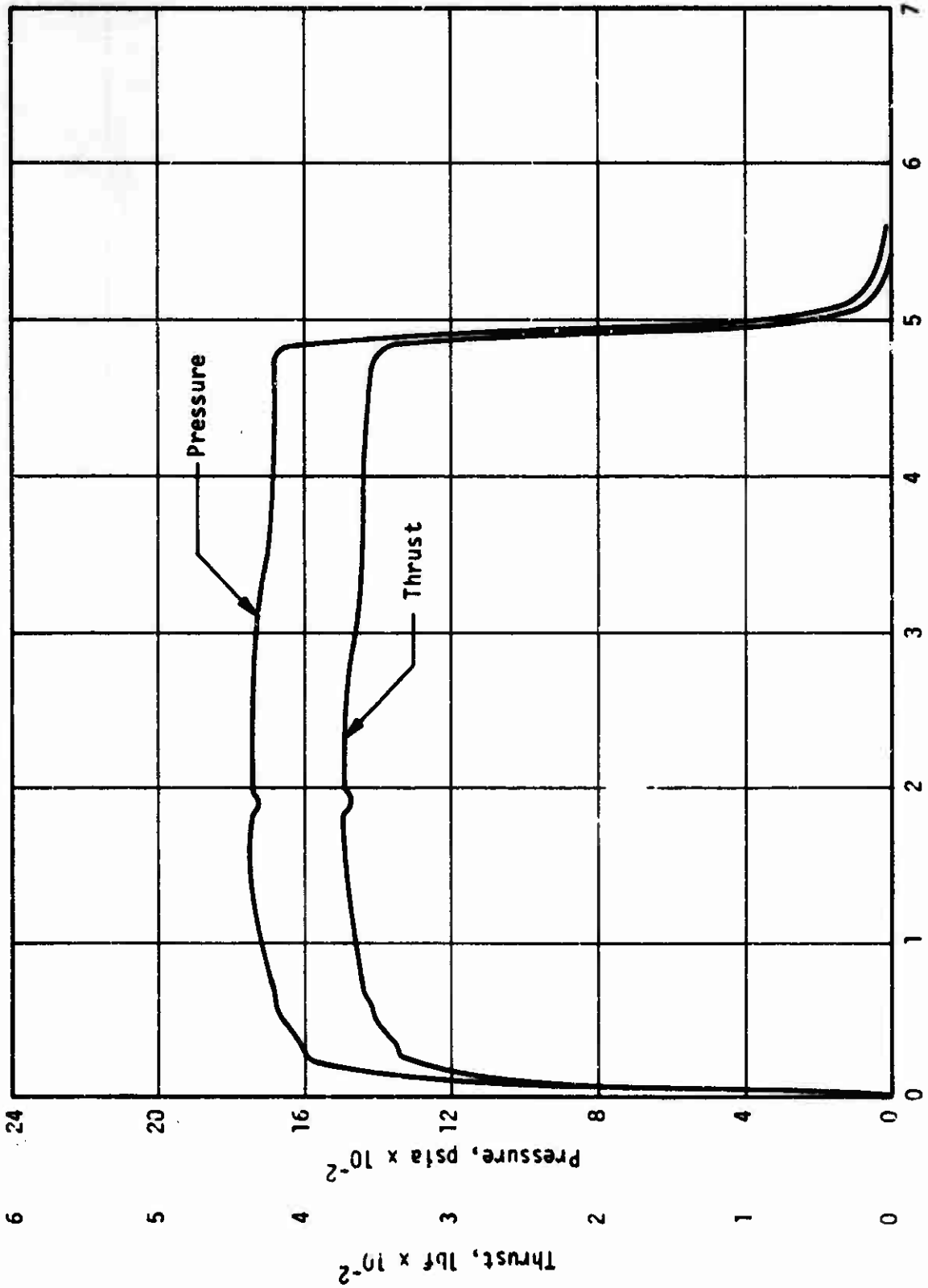

Pressure and Thrust vs Time Curves, 3KS-1000 Motor No. 6 (ANP-3392)

Figure 55

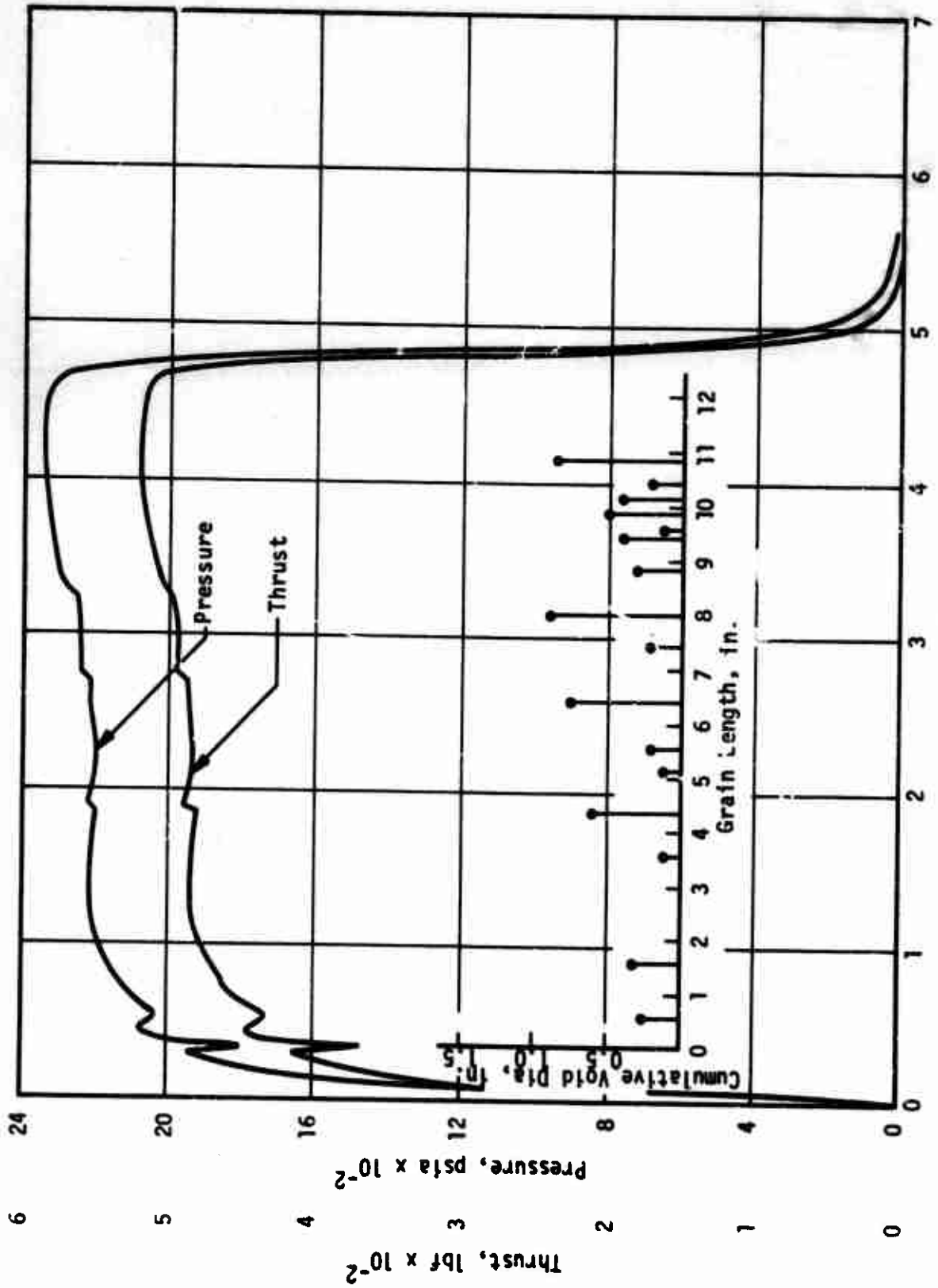

Pressure and Thrust vs Time Curves, 3KS-1000 Motor No. 7 (ANB-3392, 140°F)

Figure 56

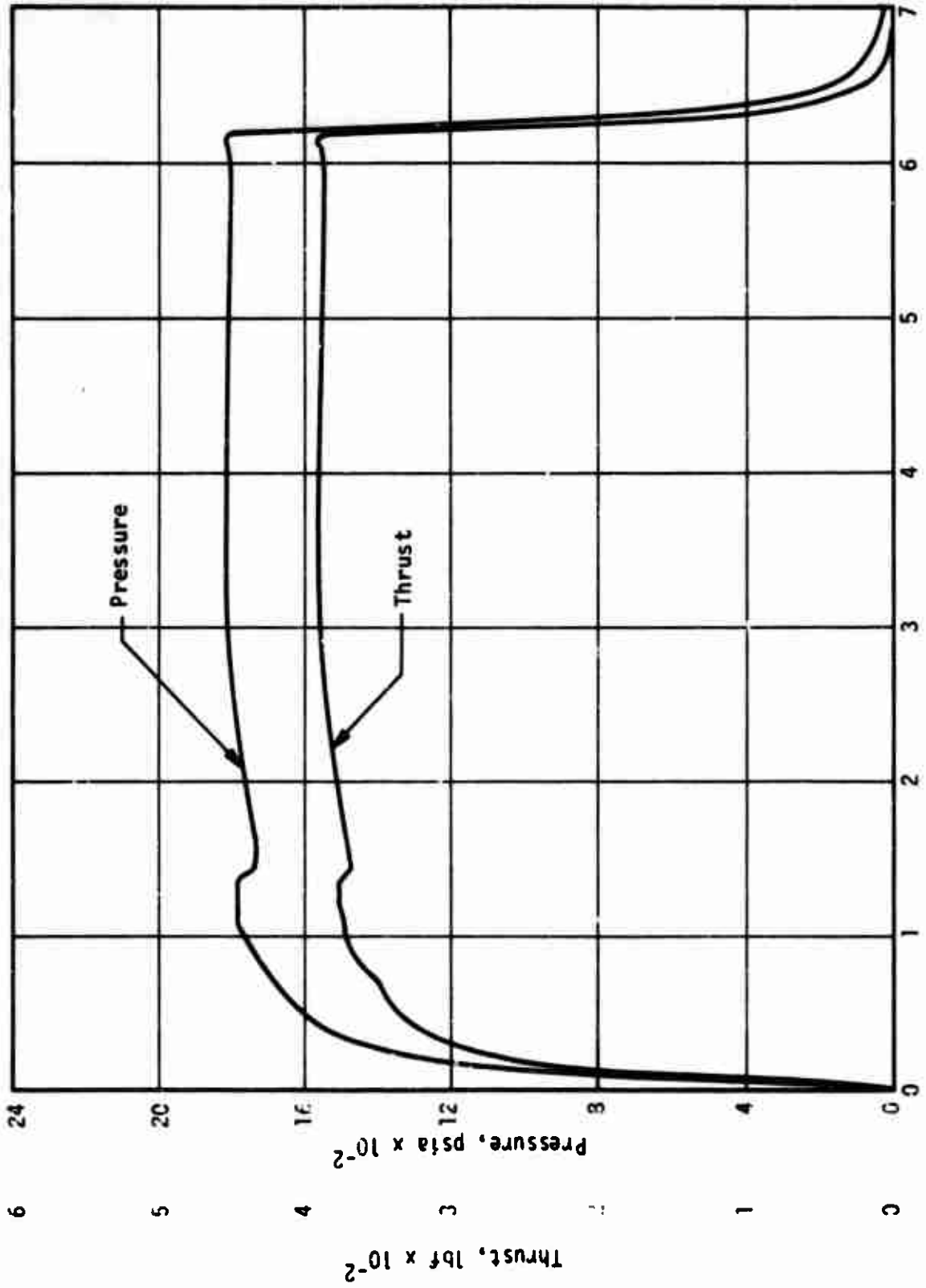

Pressure and Thrust vs Time Curves, 3KS-1000 Motor No. 8 (ANP-3391)

Figure 57

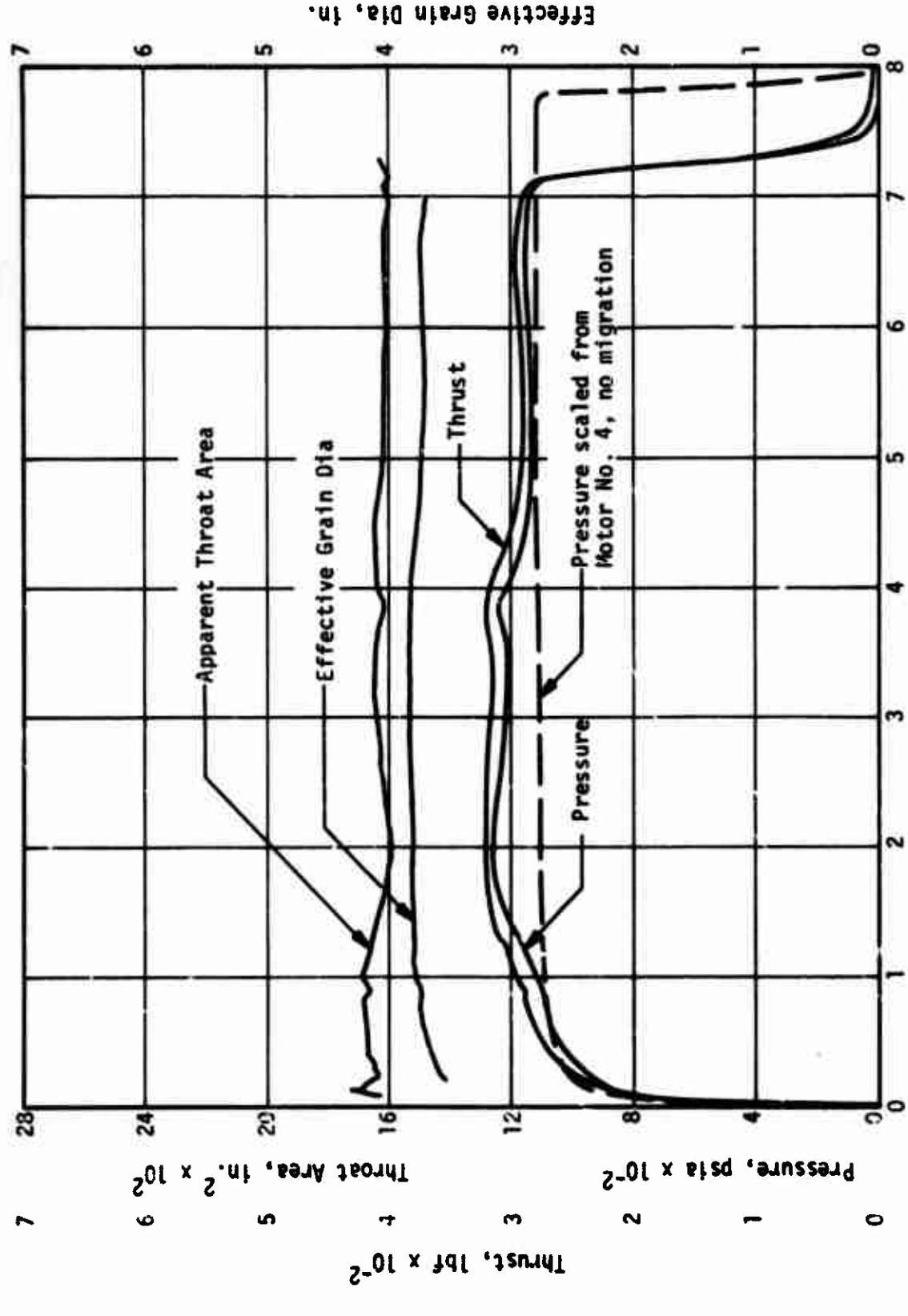

Pressure and Thrust vs Time Curves, 3KS-1000 Motor No. 9 (ANB-3392)

Figure 58

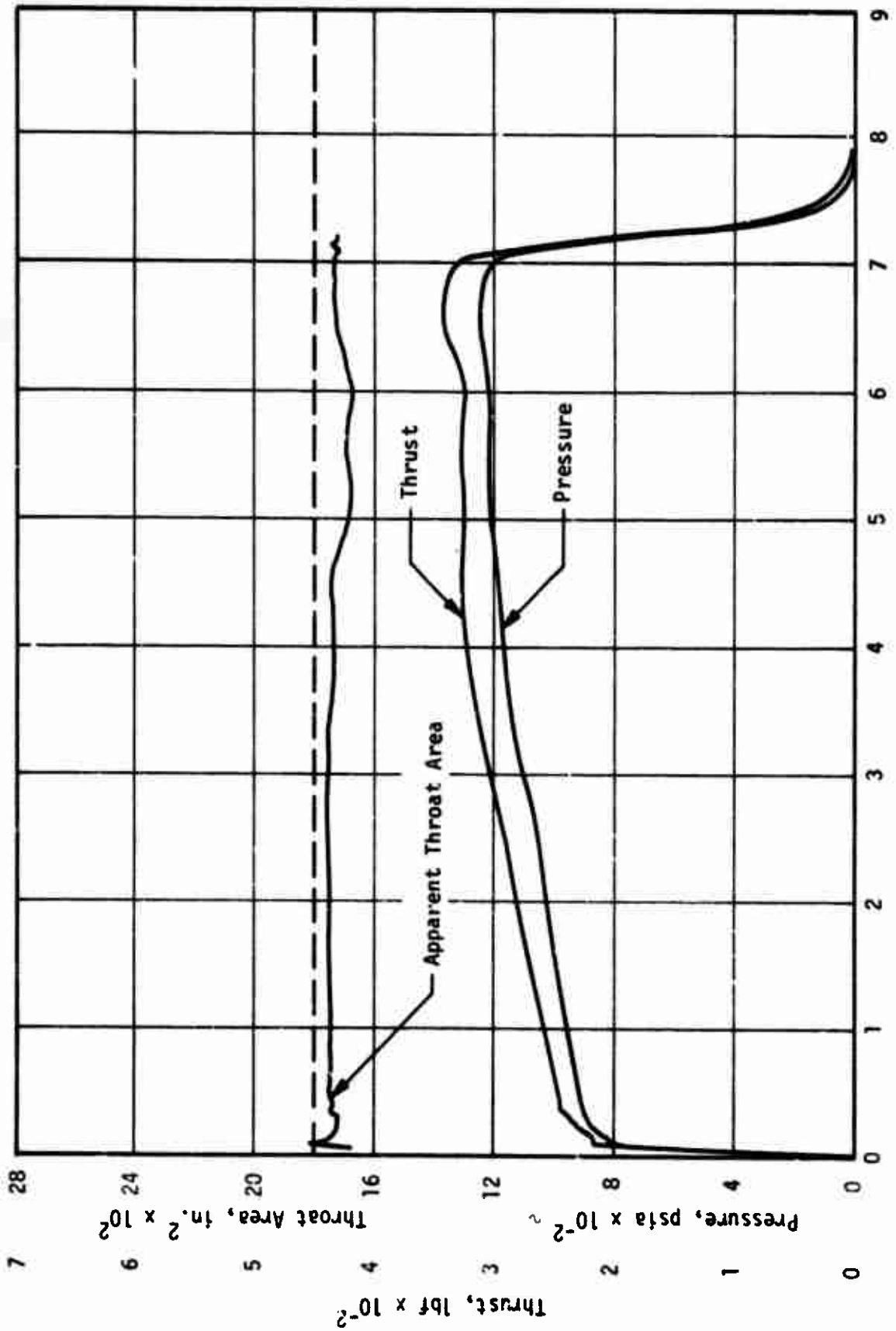

Pressure and Thrust vs Time Curves, 3KS-1000 Motor No. 10 (ANP-3391)

Figure 59

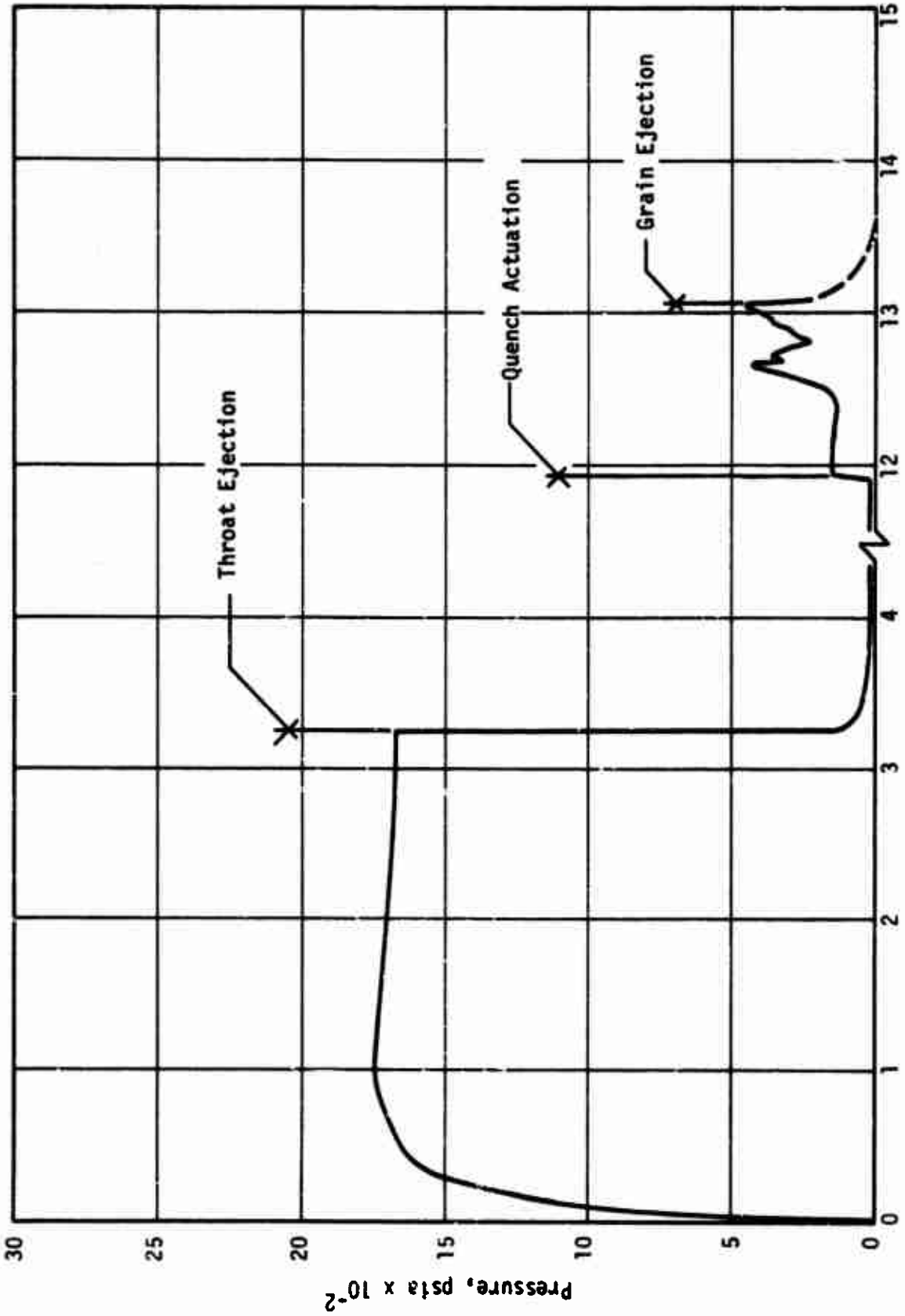

Pressure vs Time Curve 3KS-1000 Motor Stop-Fire Test (ANB-3392)

Figure 60

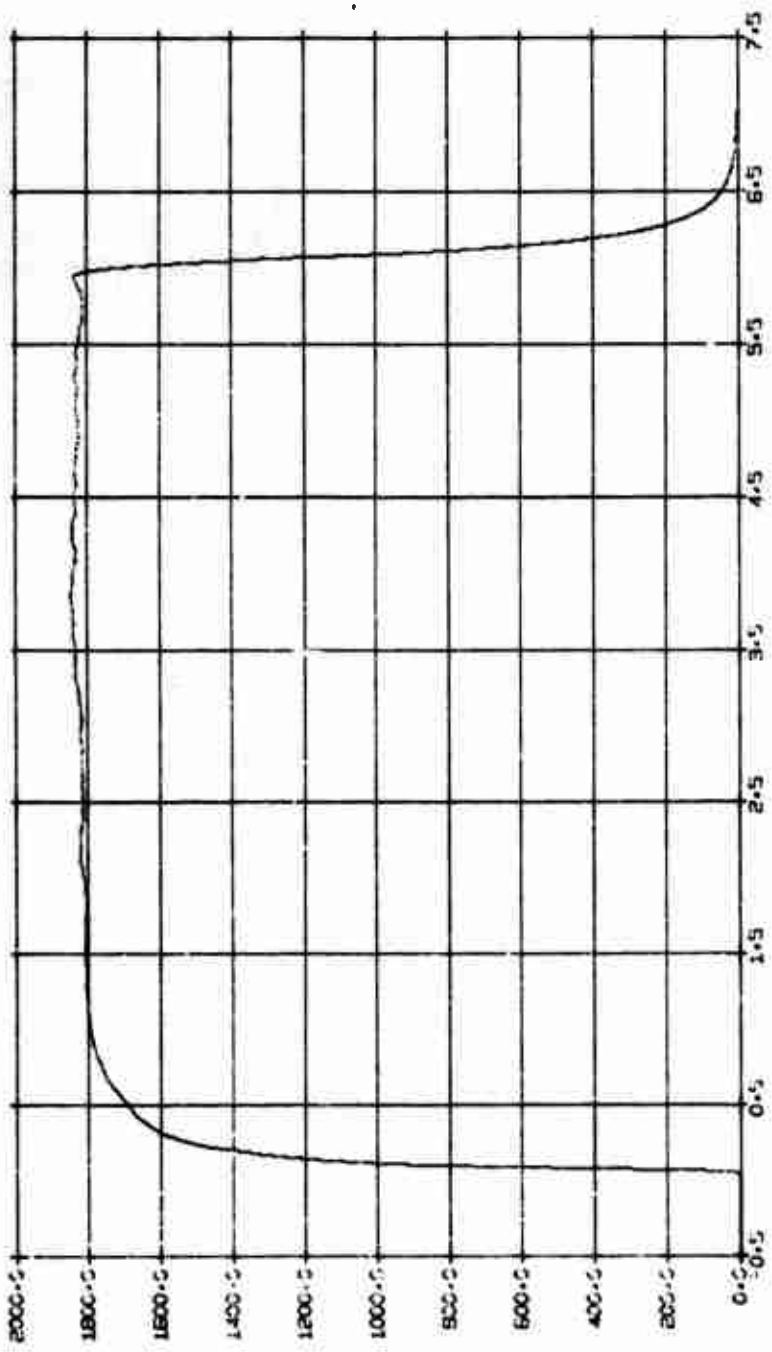

Batch 7133, Grain 4, Pressure vs Time, ANP-3391

Figure 61

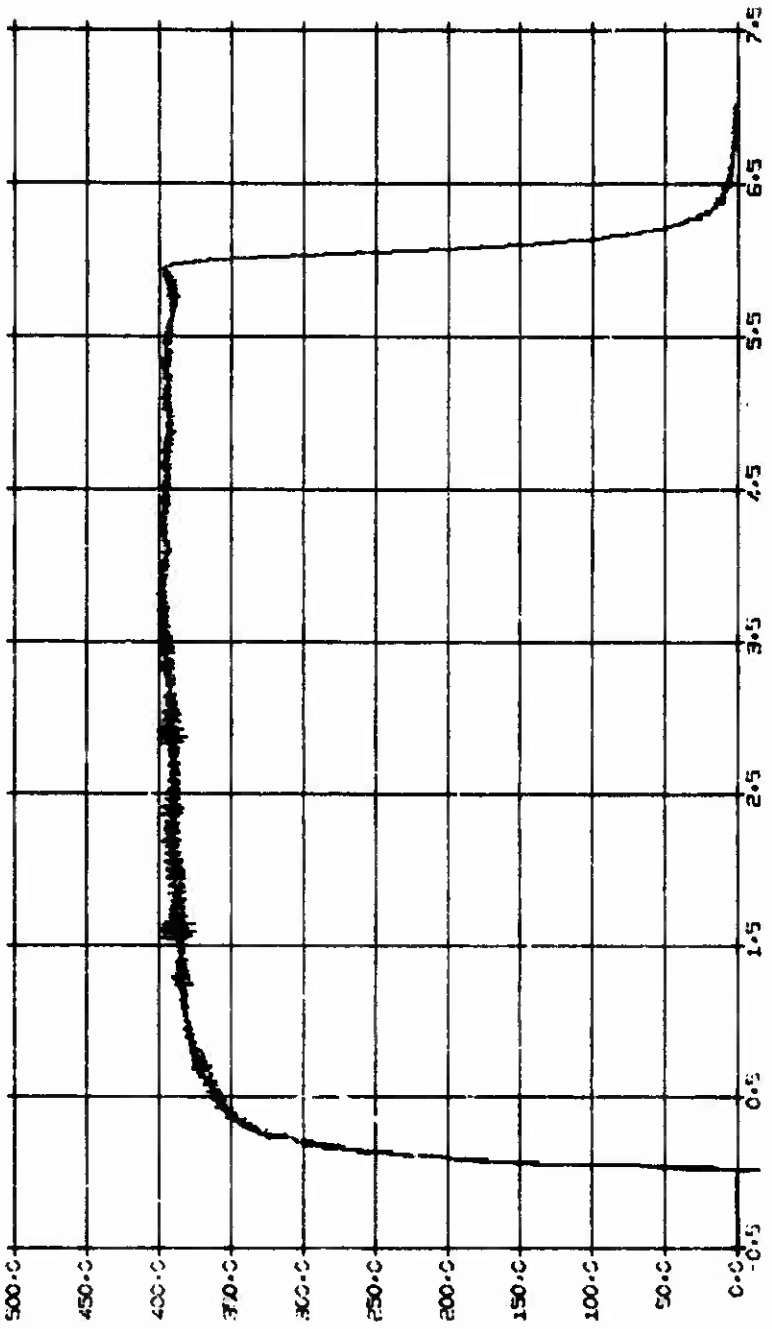

Batch 7133, Grain 4, Thrust vs Time, ANP-3391

Figure 62

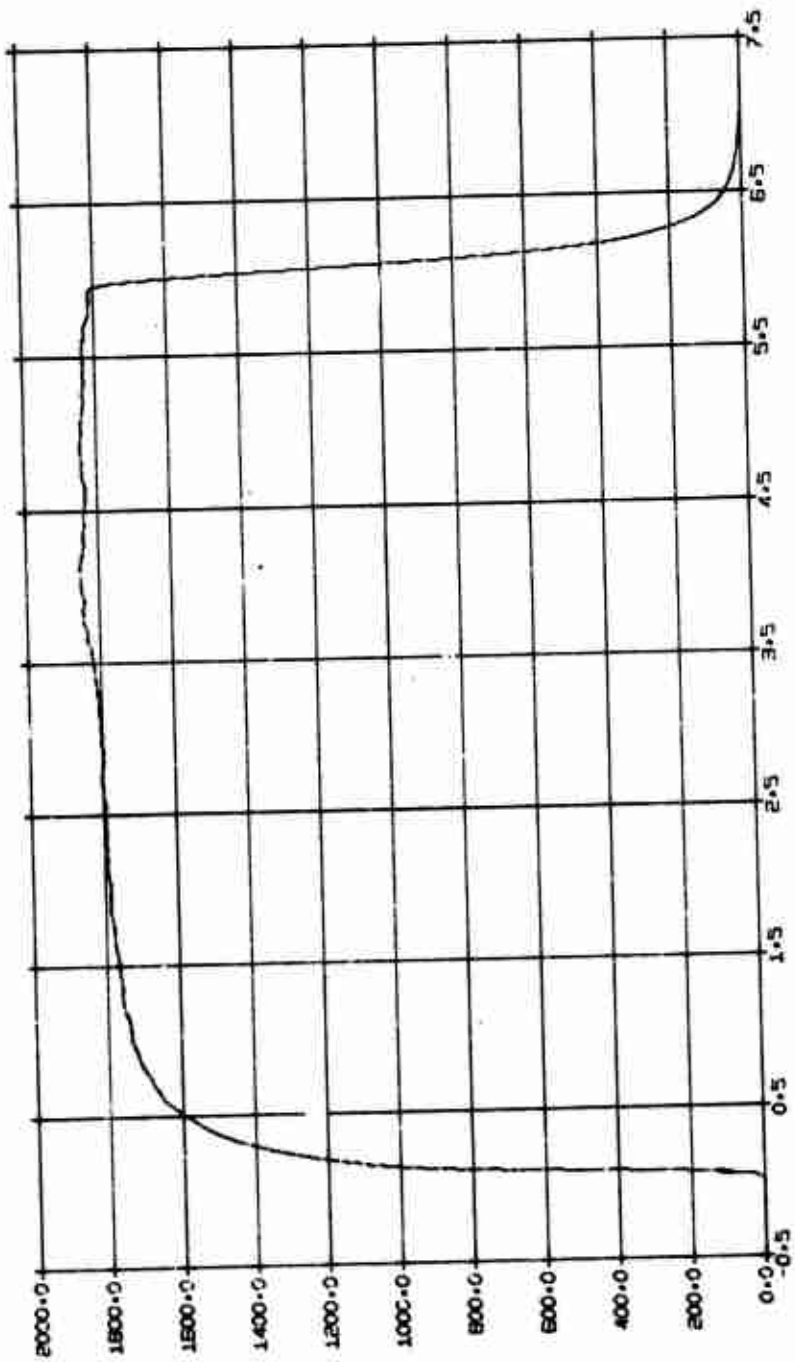

Batch 7133, Grain 5, Pressure vs Time, ANP-3391

Figure 63

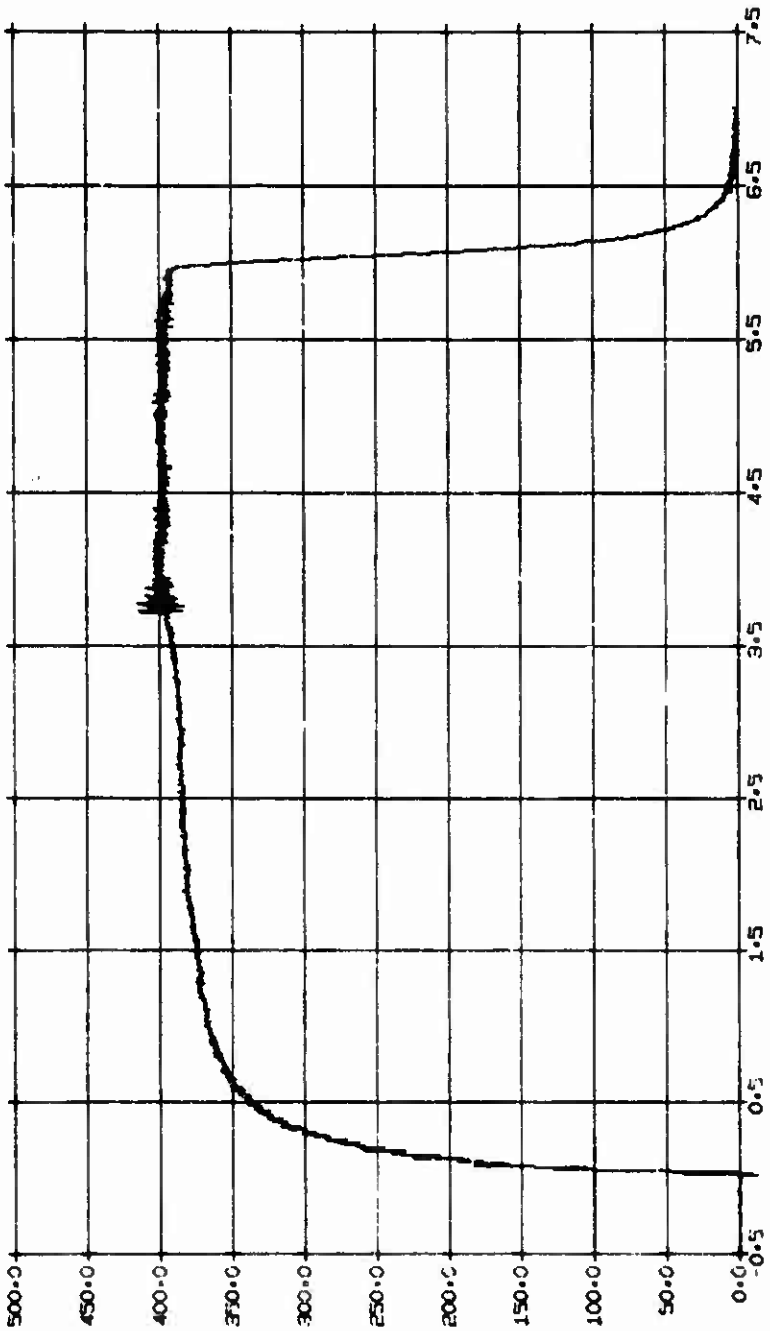

Batch 7133, Grain 5, Thrust vs Time, ANP-3391

Figure 64

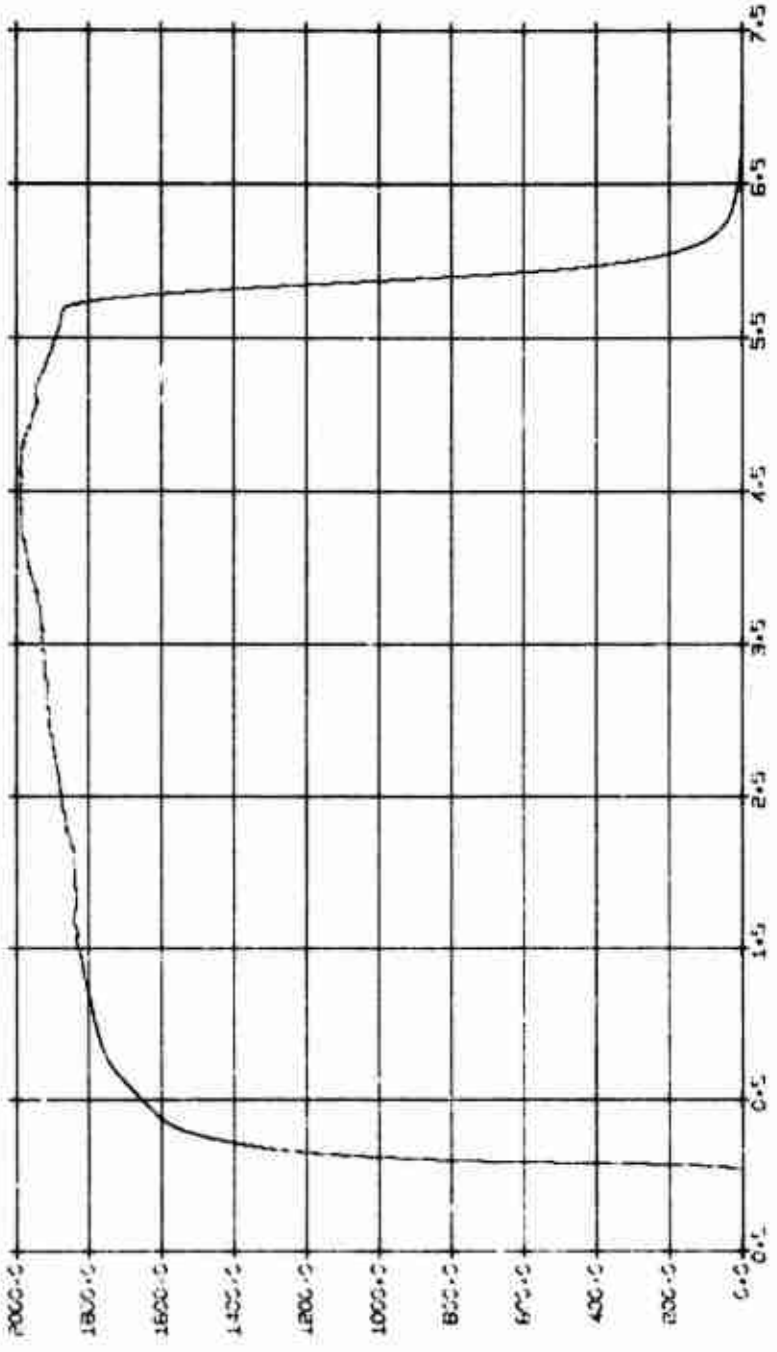

Batch 7133, Grain 6, Pressure vs Time, ANP-3391

Figure 65

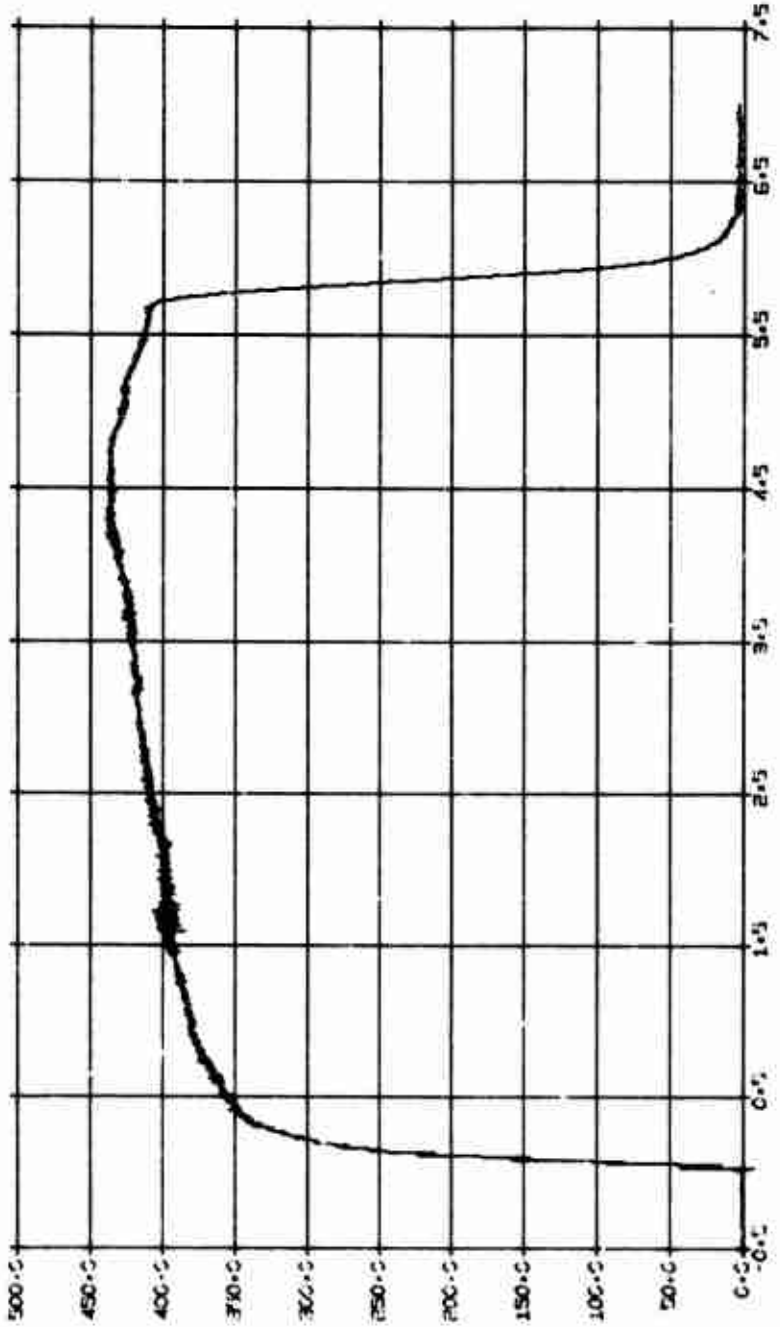

Batch 7133, Grain 6, Thrust vs Time, ANP-3391

Figure 66

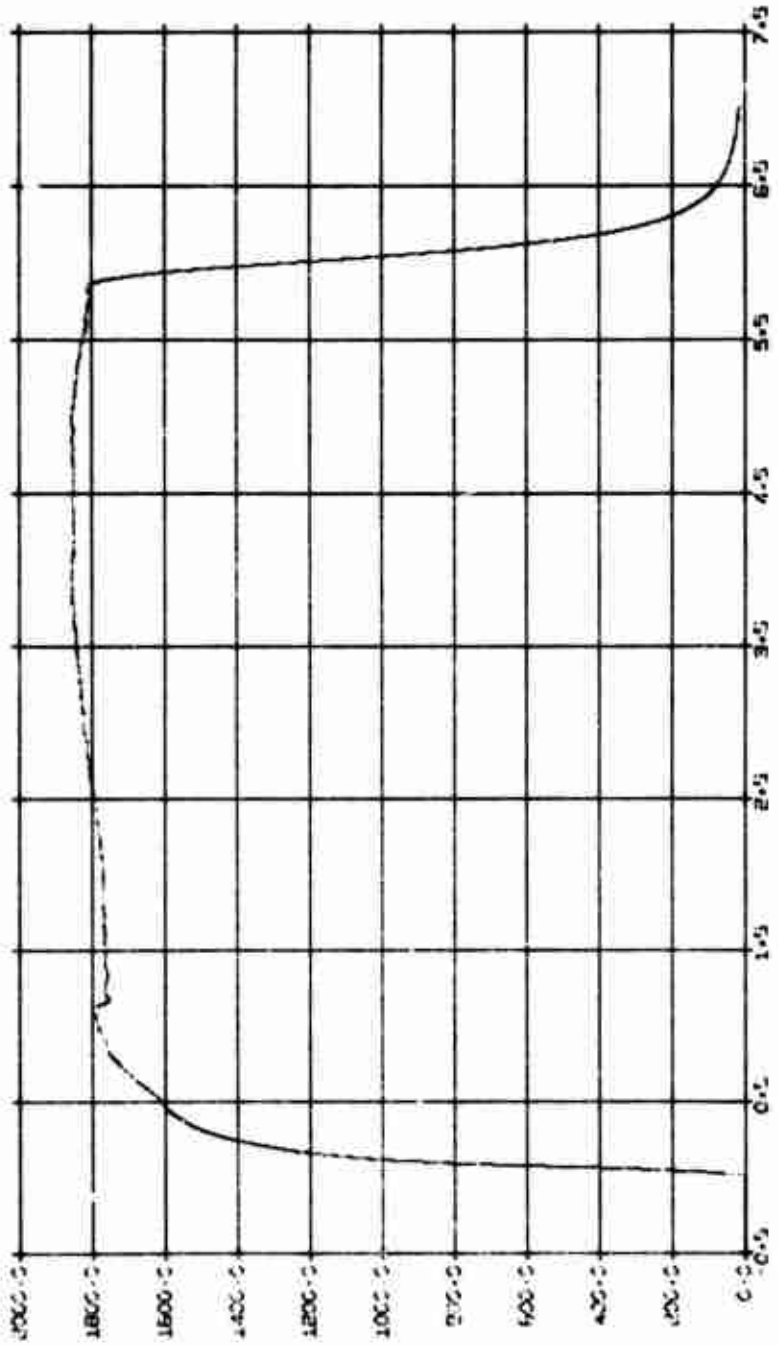

Batch 7133, Grain 7, Pressure vs Time, ANP-3391

Time, sec

Pressure, psi

Figure 67

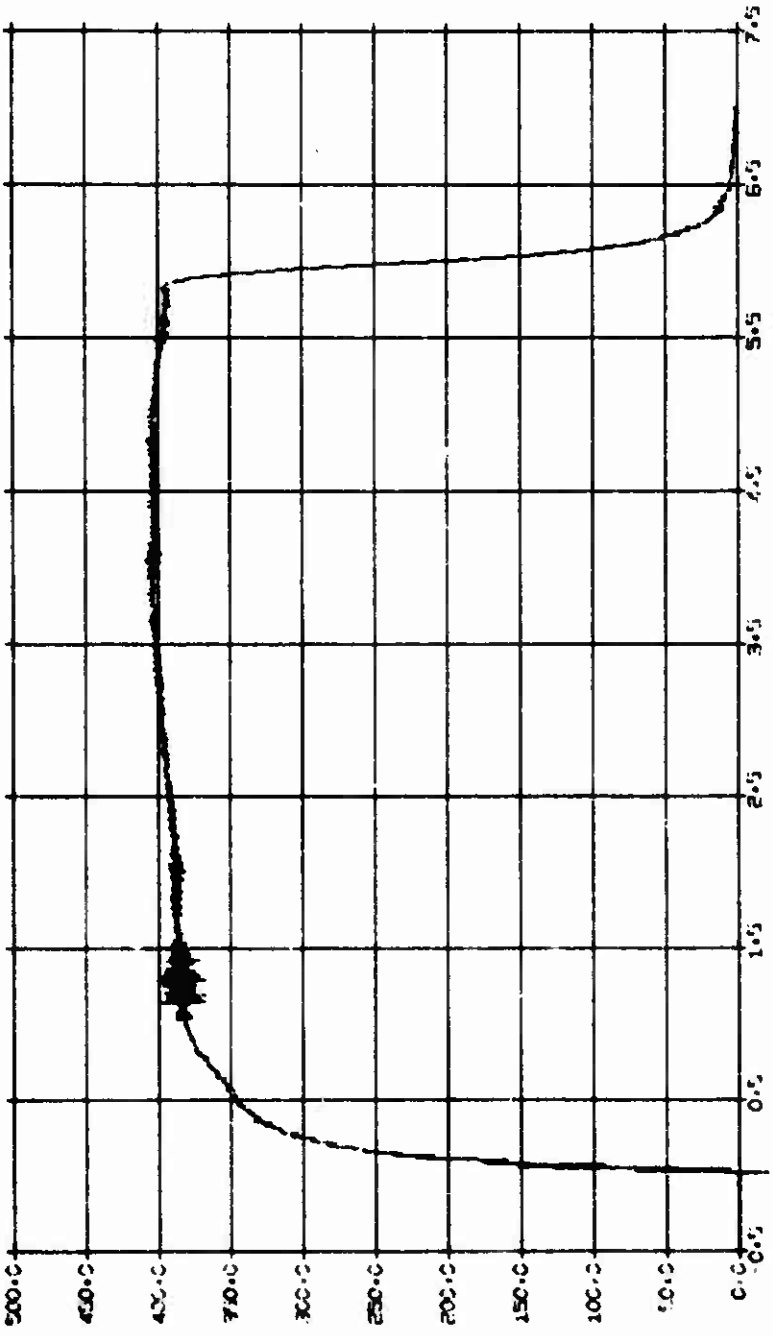

Batch 7133, Grain 7, Thrust vs Time, ANP-3391

Figure 68

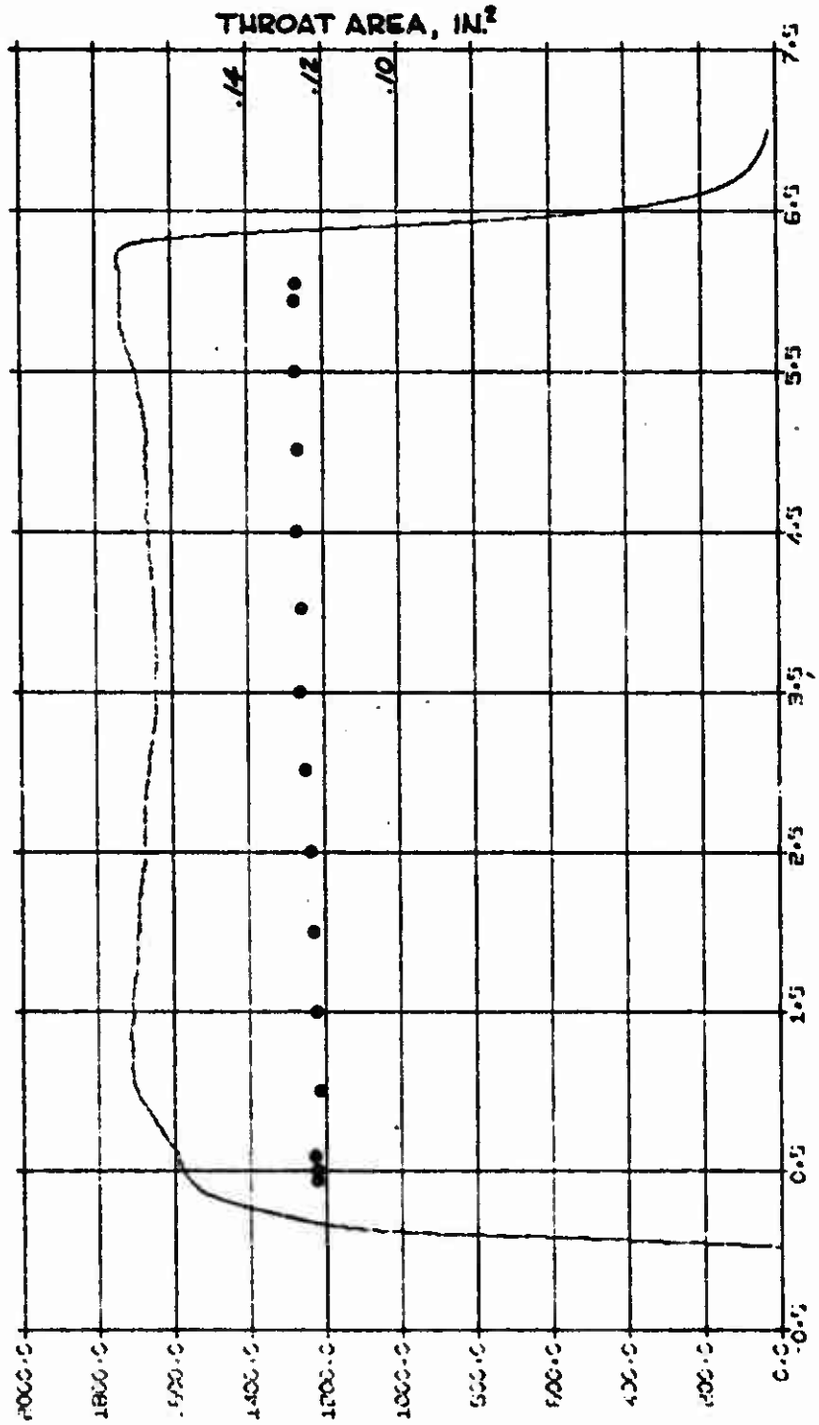

Batch 7126, Grain 5, Pressure vs Time, ANB-3392

Figure 69

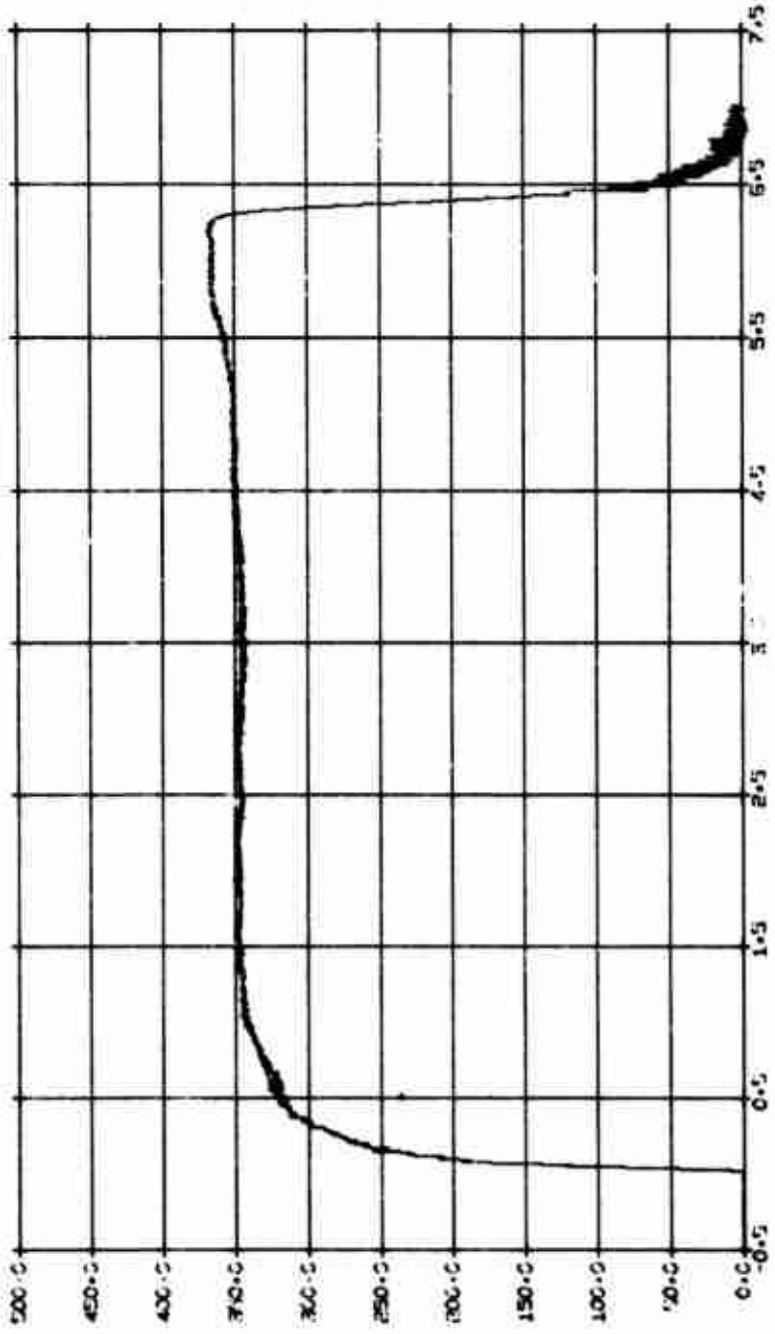

Batch 7126, Grain 5, Thrust vs Time, ANB-3392

Figure 70

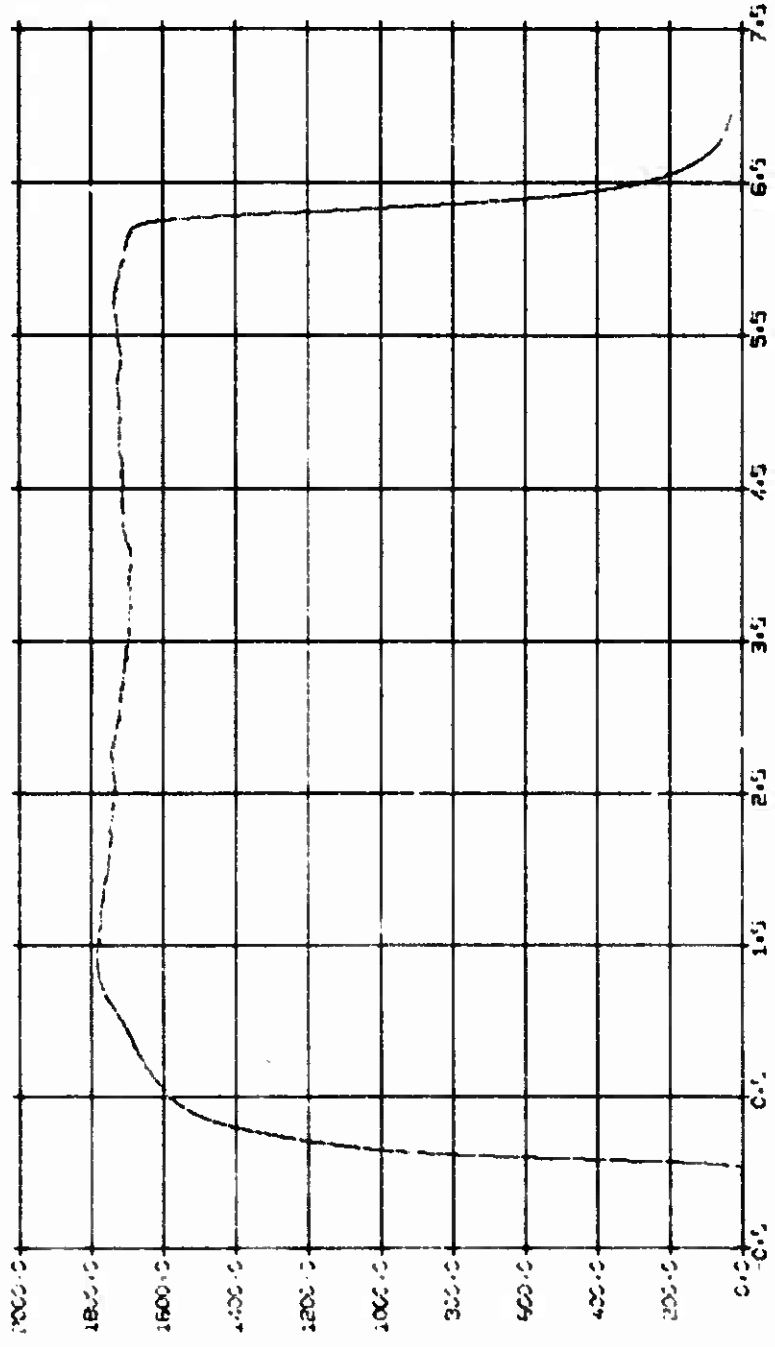

Batch 7126, Grain 6, Pressure vs Time, ANB-3392

Figure 71

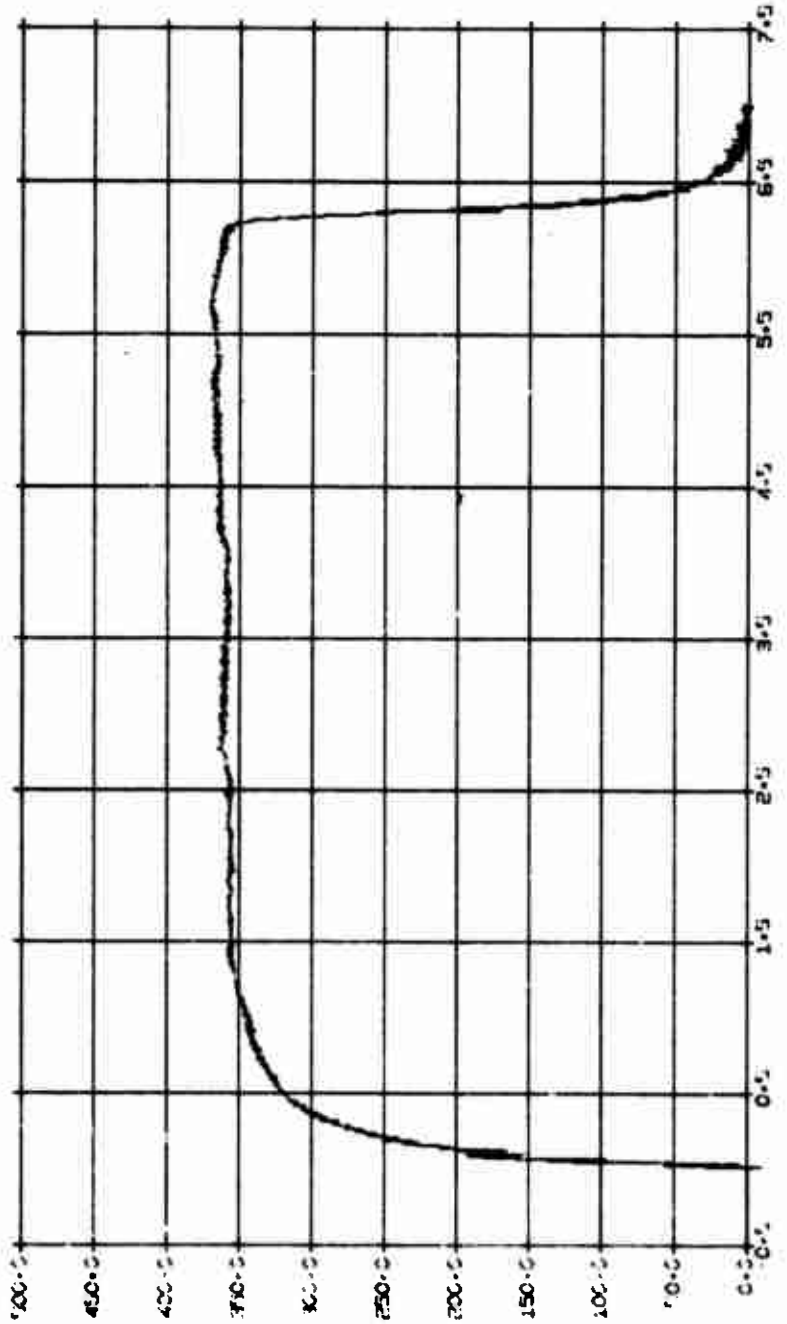

Batch 7126, Grain 6, Thrust vs Time, ANB-3392

Figure 72

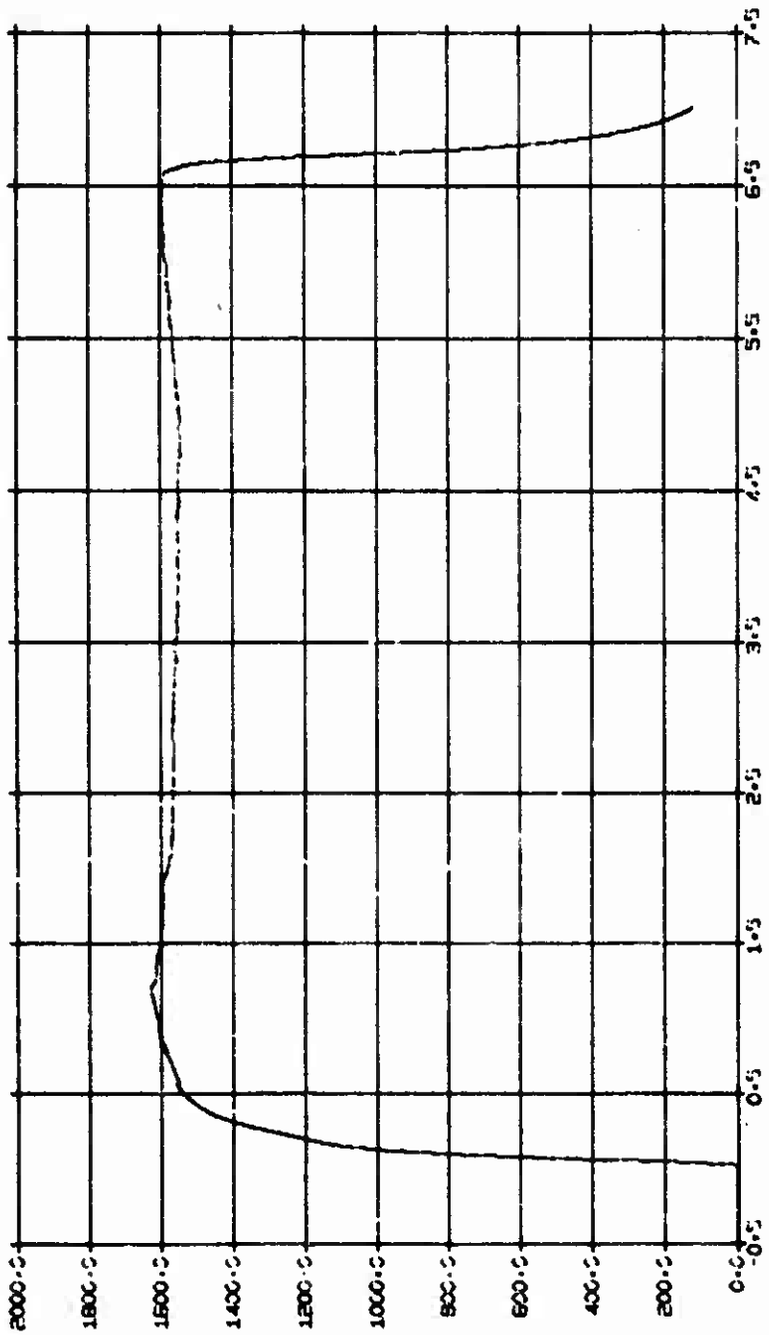

Batch 7126, Grain 7, Thrust vs Time, ANB-3392

Figure 73

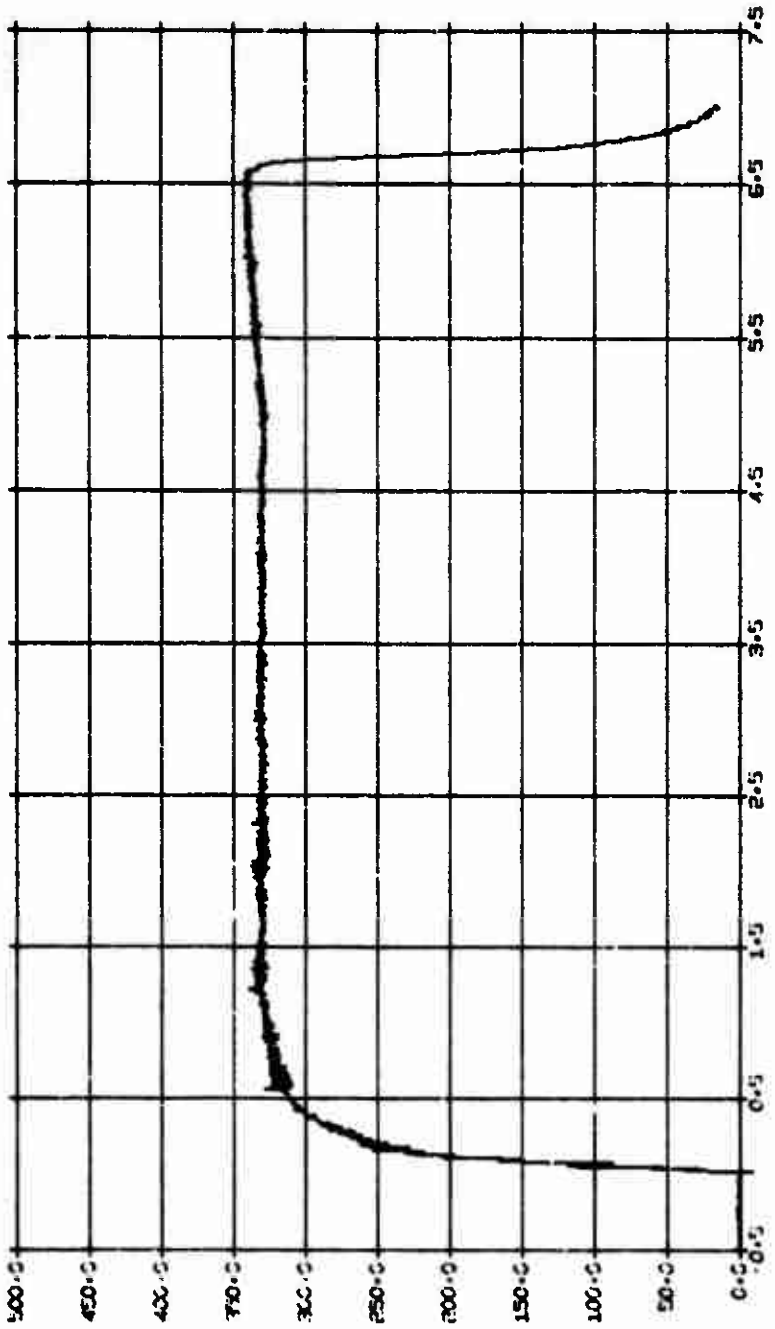

Batch 7126, Grain 7, Thrust vs Time, ANB-3392

Figure 74

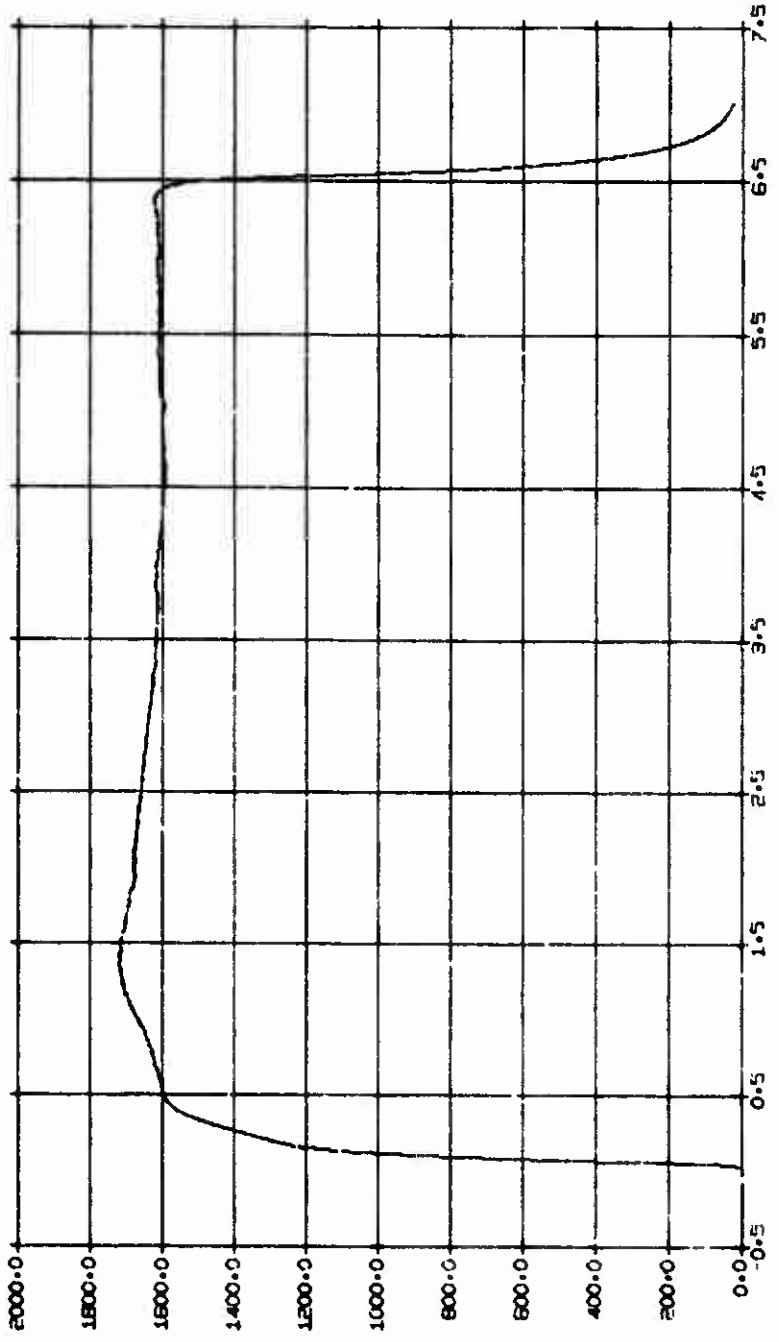

Batch 7126, Grain 8, Pressure vs Time, ANB-3392

Figure 75

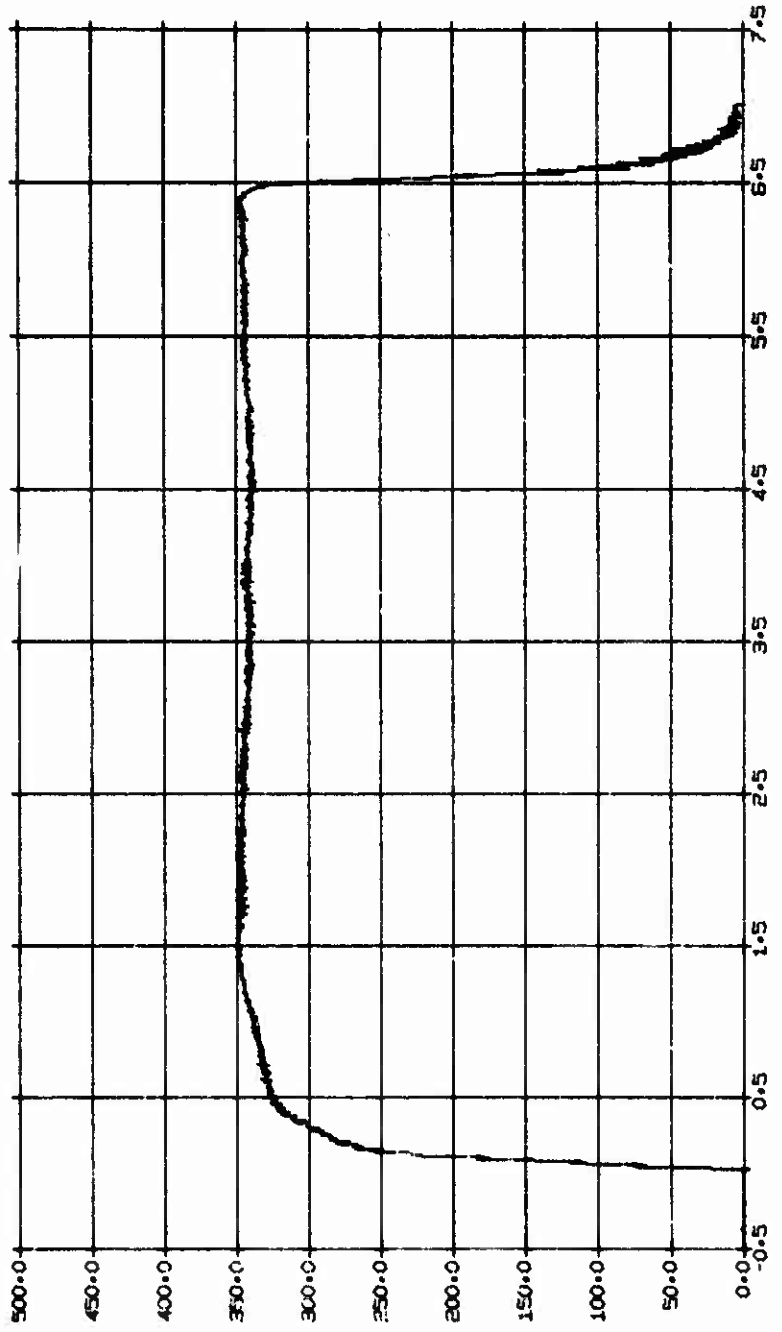

Batch 7126, Grain 8, Thrust vs Time, ANB-3392

Figure 76

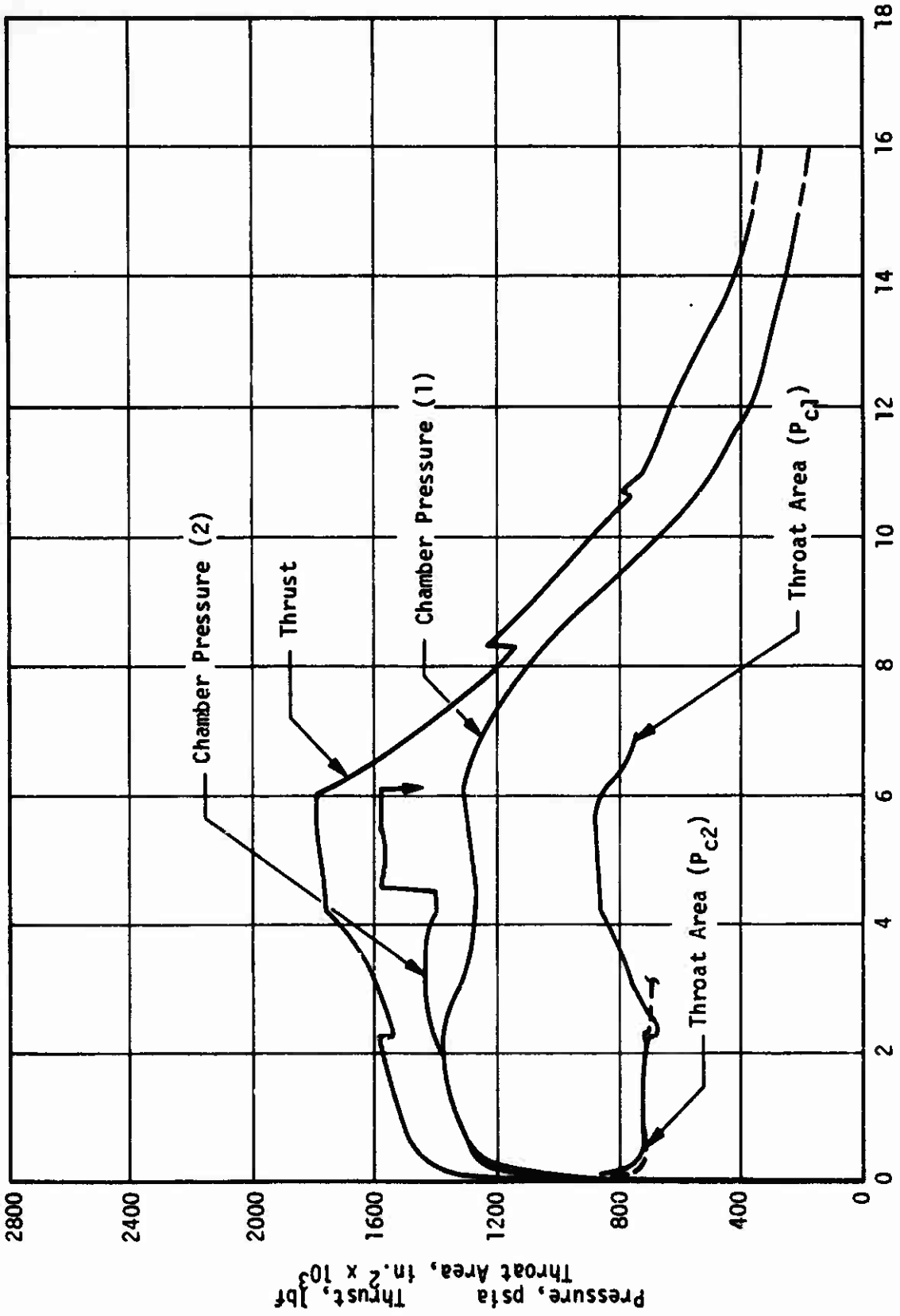

Pressure and Thrust vs Time Curves, 10KS-2500 Motor No. 1 (ANP-3391)

Figure 77

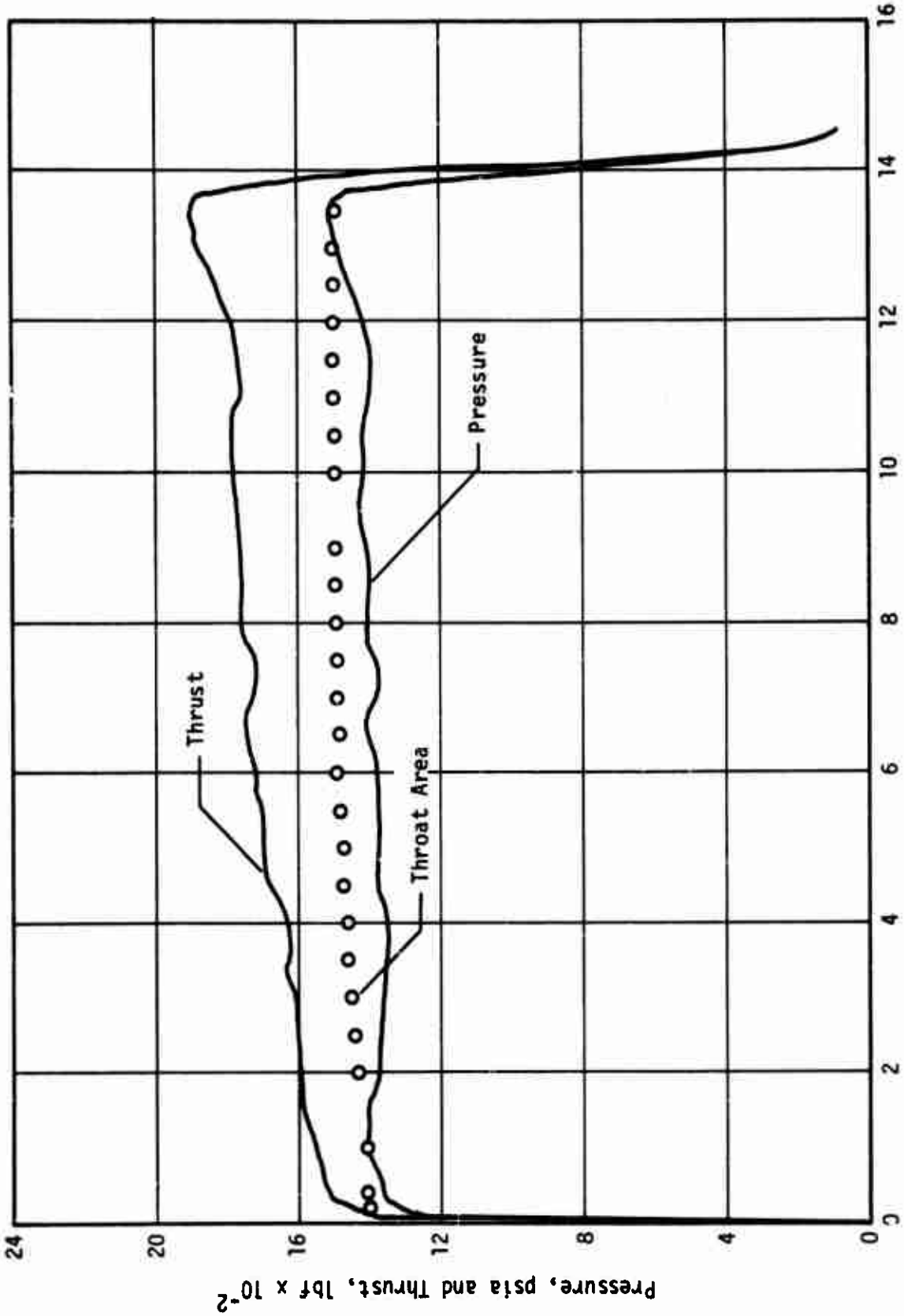

HBR Motor Firing, ANB-3392 Propellant

Figure 78

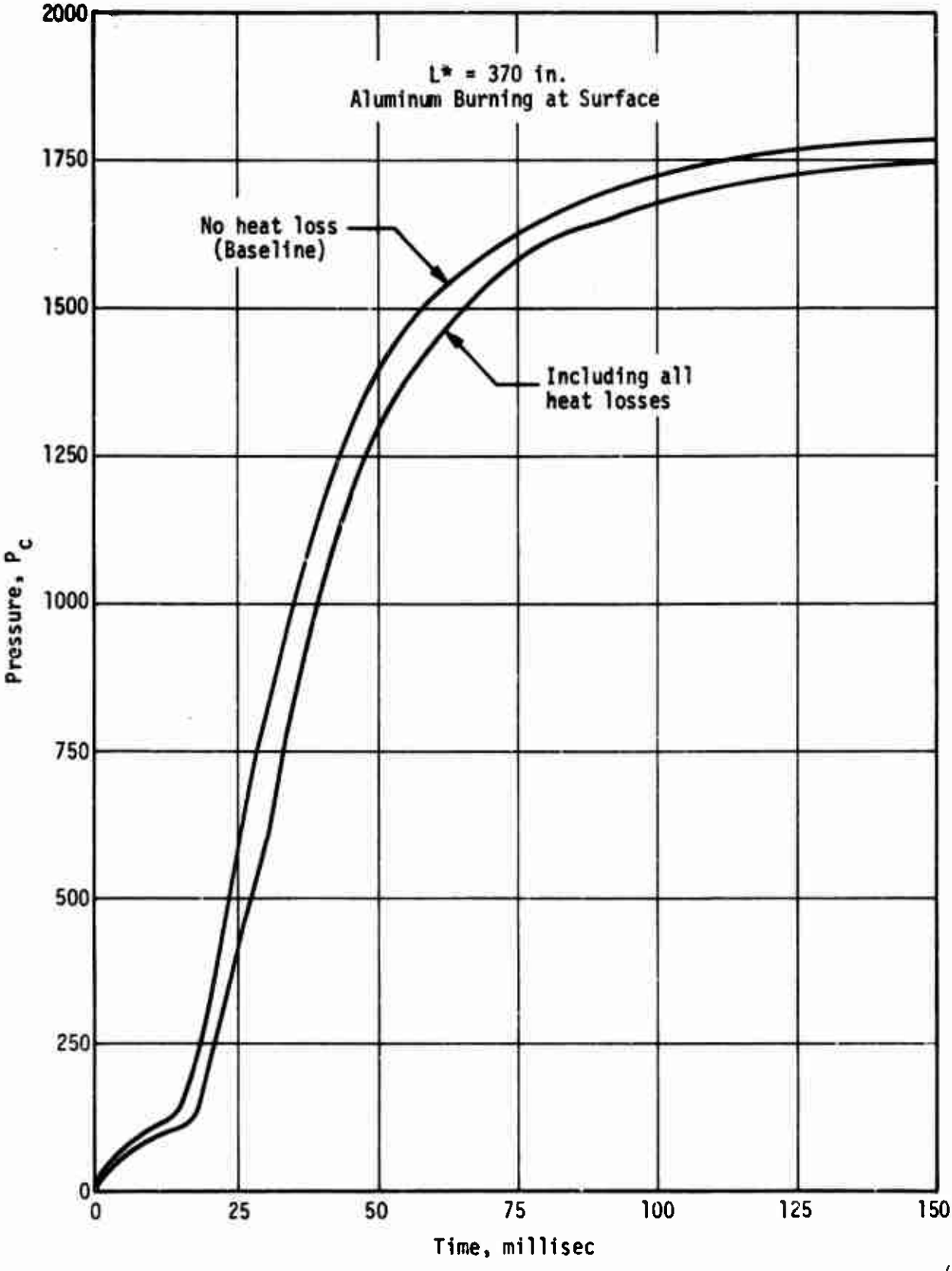

Effect of Heat Loss During Ignition Assuming Instantaneous Burning of Aluminum

Figure 79

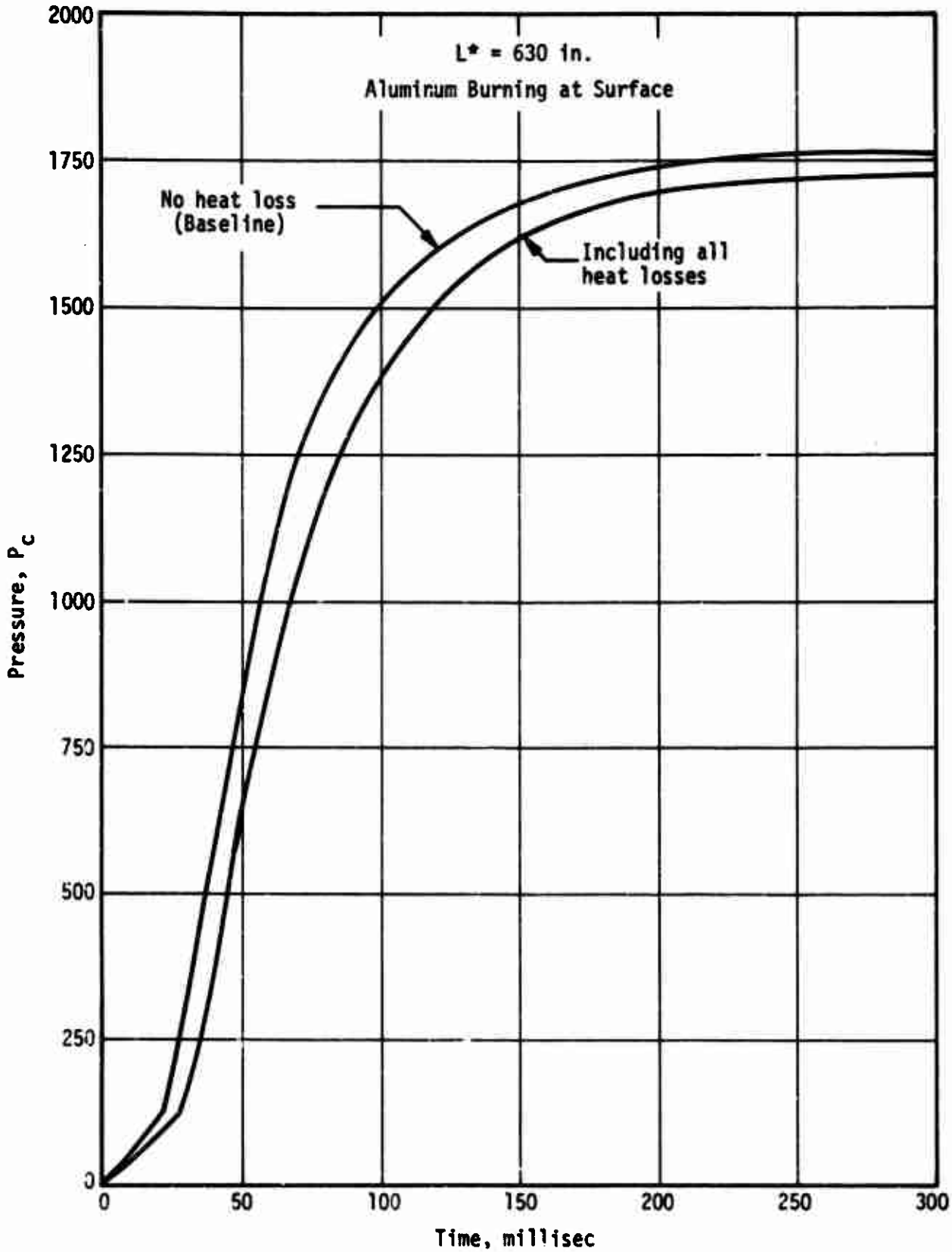

Effect of Heat Loss During Ignition Assuming Instantaneous Burning of Aluminum

Figure 80

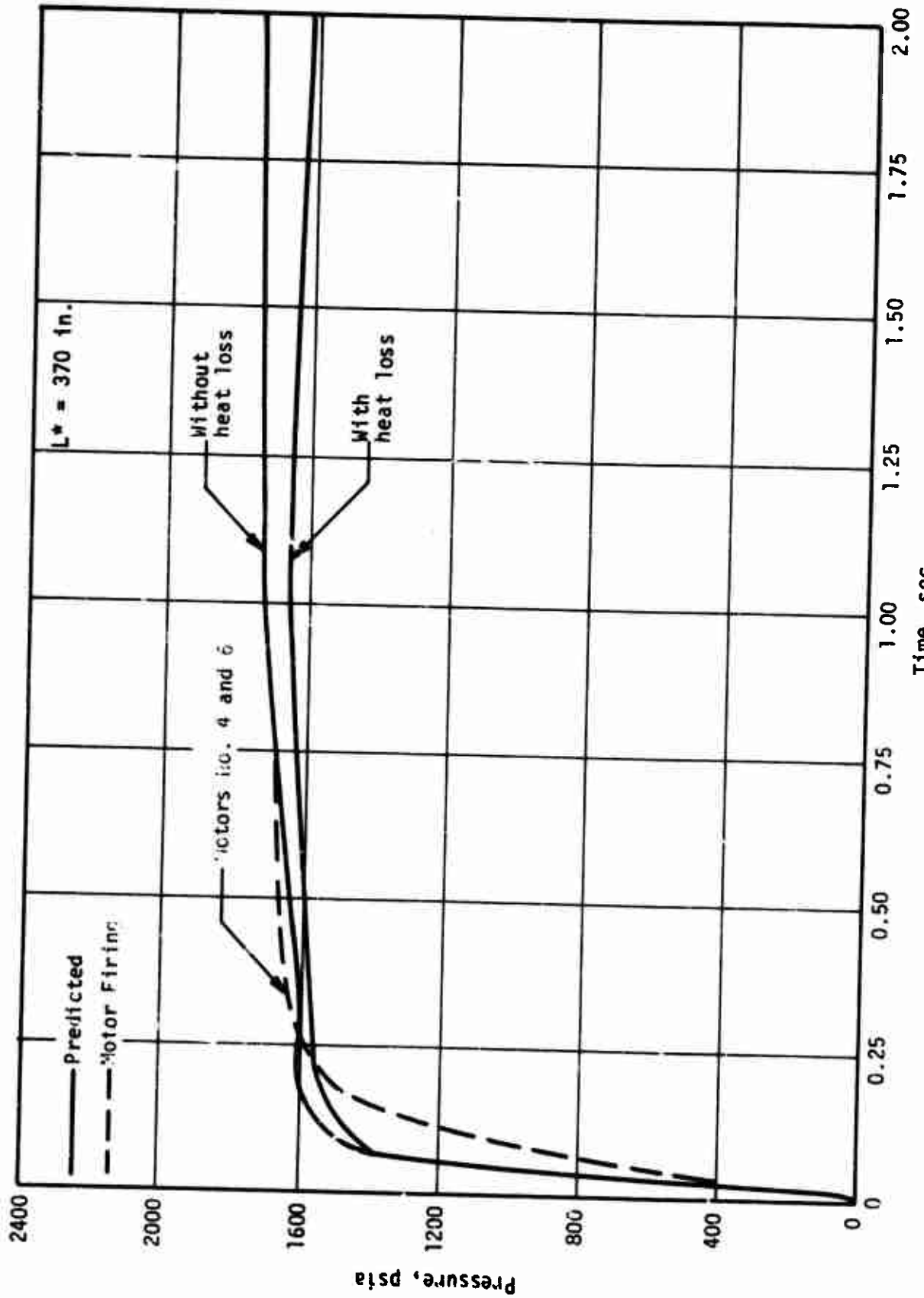

Performance Prediction Showing Effect of Aluminum Combustion and Heat Losses

130

Figure 81

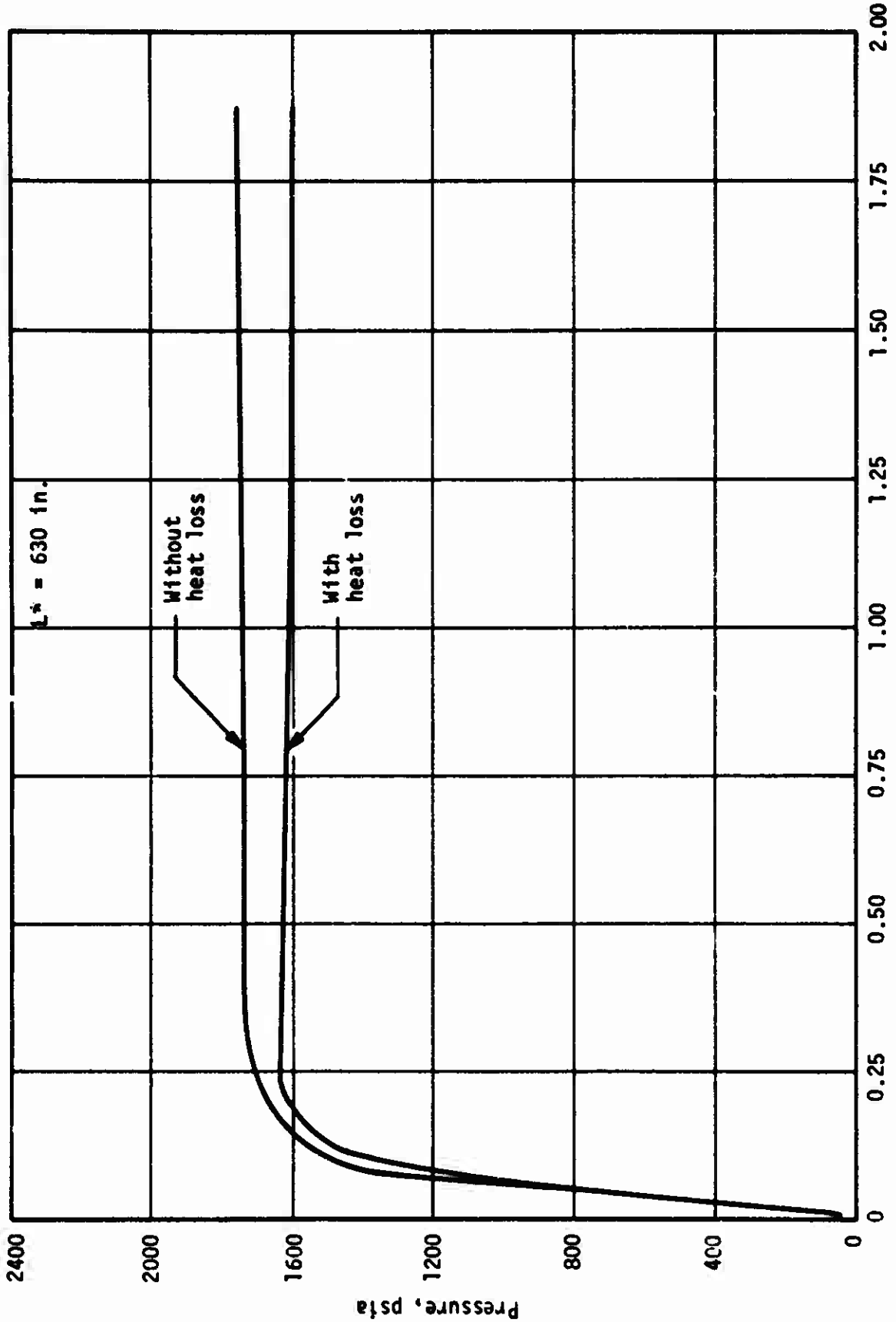

Performance Prediction Showing Effect of Aluminum Combustion and Heat Losses

Figure 82

APPENDIX

MECHANICAL PROPERTY ANALYSIS

APPENDIX

A series of tests were conducted for the purpose of characterizing the mechanical responses and failure behaviors of the ANP-3391 and ANB-3392 formulations. Resulting data that have been summarized in tabular form and plotted in a manner found to be most applicable for use in stress analyses and structural integrity evaluations are shown in Figures 1a through 17a. A brief description of the types of tests performed and the significance of the data are presented below.

The propellant's coefficient of thermal expansion determines the magnitude of the strains developed in the grain upon cooling from the cure temperature. It is determined experimentally from measurements of density at various temperatures by means of a buoyancy technique. The volumetric coefficient is obtained directly from the slope of a density-temperature plot and the linear coefficient is taken as one-third of the volumetric value.

Various types of modulus data are required for an analysis. For calculating stresses produced during long-term storage the appropriate relaxation modulus, taken from a "master relaxation curve" is used (Figures 5a and 13a). This curve is generated from the results of relaxation tests conducted at various temperatures. The test involves applying a small, fixed strain to a specimen and measuring the decay of the stress with time. The "master curve" is constructed by empirically shifting the individual log modulus vs log time curves along the time axis until they superimpose at a selected reference temperature, usually 77°F. The amount of shift required for each curve determines the shift factor, a_T (Figures 4a and 12a).

For determination of the bond shear stresses produced by motor firing the pertinent modulus values are obtained from uniaxial tensile tests performed at various rates and temperatures. The data, plotted in the form modulus vs log reduced strain rate, $\dot{\varepsilon}a_T$, (Figures 7a and 15a) can be used to obtain the appropriate modulus for any desired firing conditions.

133

APPENDIX (cont)

The uniaxial tensile data can also provide an indication of the propellant strain bearing capabilities for storage and firing at various temperatures by constructing plots of elongation vs log reducted strain, $\dot{\varepsilon}a_T$, (Figures 6a, 8a, 14a, and 16a). The applicable rates can be determined by dividing the expected strain for cooling or pressurization by the time required to reach thermal equilibrium or the time to reach maximum pressure.

The propellant's capability to withstand long-term stress can be assessed from uniaxial tensile data through use of plots of log maximum true stress vs log reduced time to maximum true stress. This plot also provides the parameters required for cumulative damage analysis.

134

	ANP-3391	ANB-3392
Cure Temperature, °F	110	110
Cured Density (25°C) g/cc (lb/in.^{3})	1.825 (0.0658)	1.756 (0.0634)
Volumetric Cure Shrinkage, %		
Liquid - Solid	0.55	0.57
After gel	0.25 (est)	0.25 (est)
Glass Temperature, °F	-135	-131
Coefficient of Thermal Expansion, in./in./°F		
-100 to +32°F	5.4 by 10^{-5}	5.7 by 10^{-5}
+30 to 150°F	5.9 by 10^{-5}	5.9 by 10^{-5}
Heat Capacity, Cp, Btu/°F/lb	0.288	0.296
Thermal Conductivity* Btu . $ft^{-2}.hr^{-1}.(°F/ft)^{-1}$	0.171	0.175

* $\lambda = K \rho C$

where λ = thermal conductivity

K = thermal diffusivity in $ft^2.hr^{-1}$

ρ = density, in $lb.ft^{-3}$

C = heat capacity in $Btu.°F^{-1}.lb^{-1}$

Propellant Properties Summary

Figure 1a

The following data are presented:

Effect of Test Temperature and Strain Rate on Uniaxial Tensile properties

a_T vs Temperature

Master Relaxation Curve

ε_m vs $\dot{\varepsilon} a_T$

ε_b vs $\dot{\varepsilon} a_T$

E_o vs $\dot{\varepsilon} a_T$

σ_m / E_o vs $\dot{\varepsilon} a_T$

True Stress vs t_m / a_T

Mechanical Property Summary Sheets for ANP-3391 Propellant

Figure 2a

Test Temp, °F	Strain Rate, Min^{-1}	σ_m, psi	ε_m, %	ε_b, %	E_o, psi
150	0.0074	104	12.0	12.8	1056
	0.74	129	14.2	21.0	1414
110	0.0074	113	16.0	17.8	920
	0.074	150	17.4	20.8	1150
	0.74	193	18.9	20.4	1446
77	0.0074	194	18.4	19.0	1339
	0.074	210	15.6	16.0	1631
	0.74	285	19.3	19.8	2067
40	0.74	350	17.5	17.7	2633
0	0.74	461	21.0	22.0	3441
-25	0.74	523	22.9	25.7	4040
-40	0.74	572	26.3	27.4	4584
-65	0.74	620	21.0	21.8	5760

*Each value is the average of two specimens.

Effect of Test Temperature and Strain Rate on Uniaxial Tensile Properties*
ANP-3391 Propellant (Batch 70-131)

Figure 3a

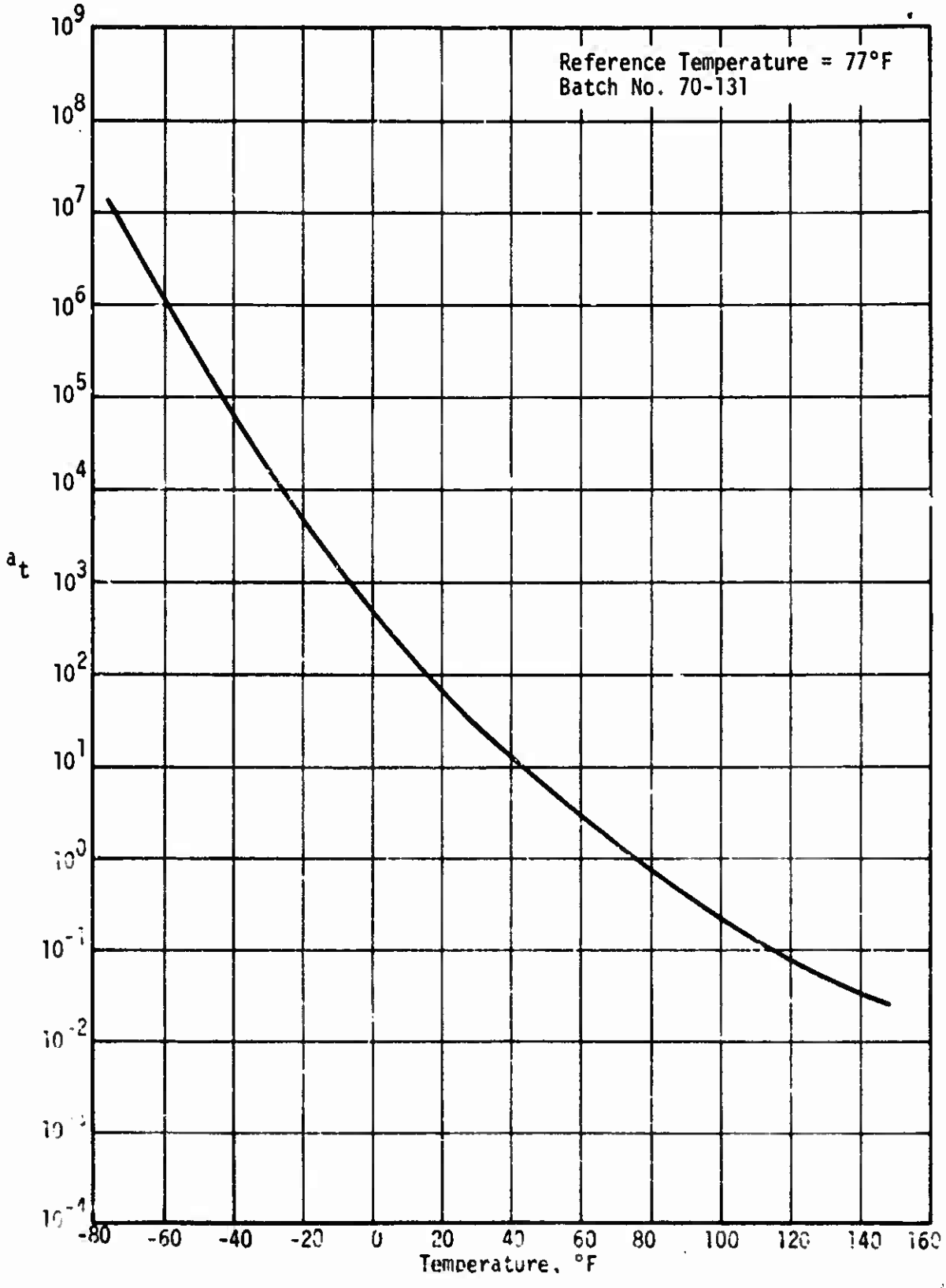

138

Plot of Log a_t vs Temperature for ANP-3391

Figure 4a

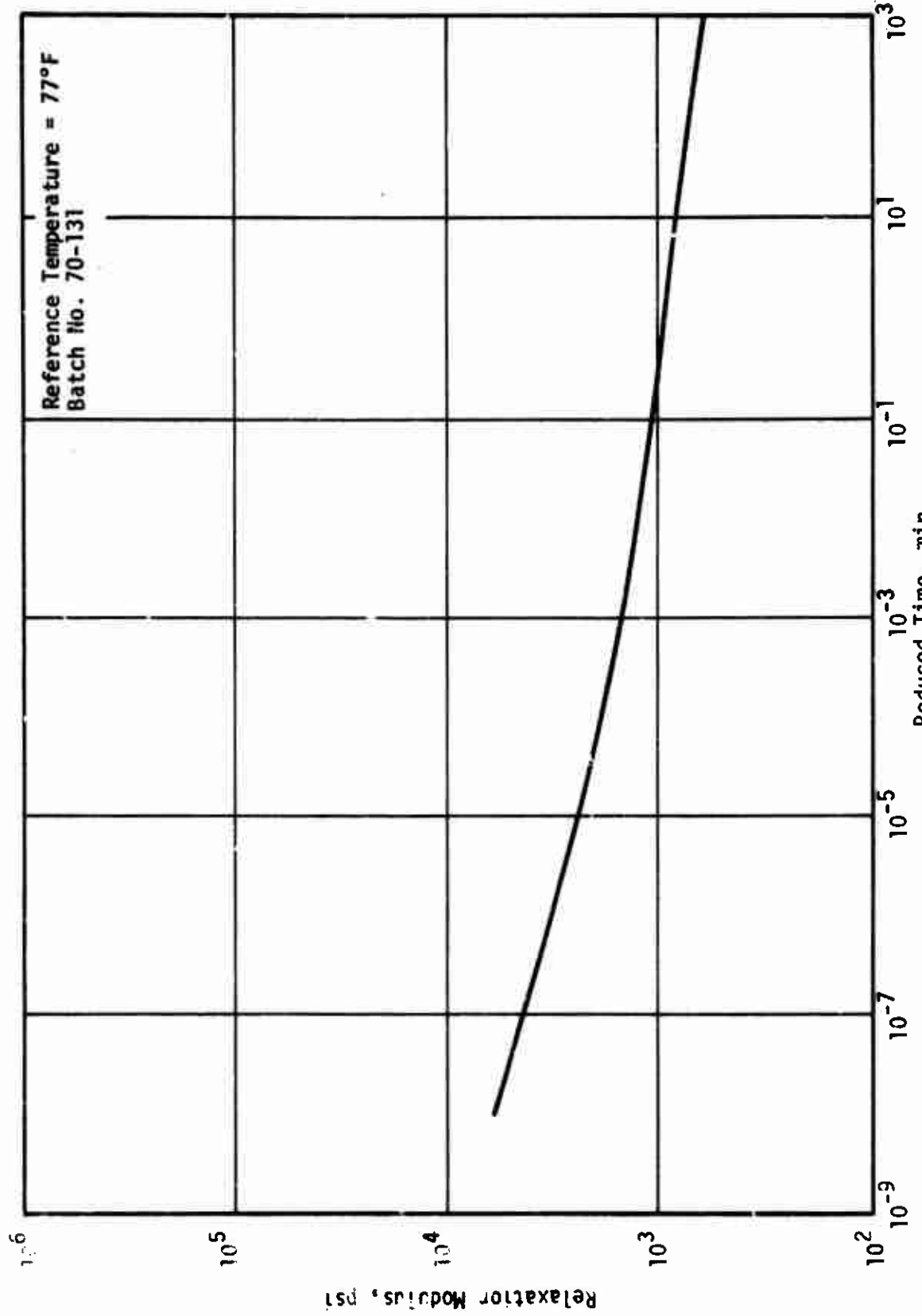

Master Relaxation Curve for ANP-3391 Propellant

139

Figure 5a

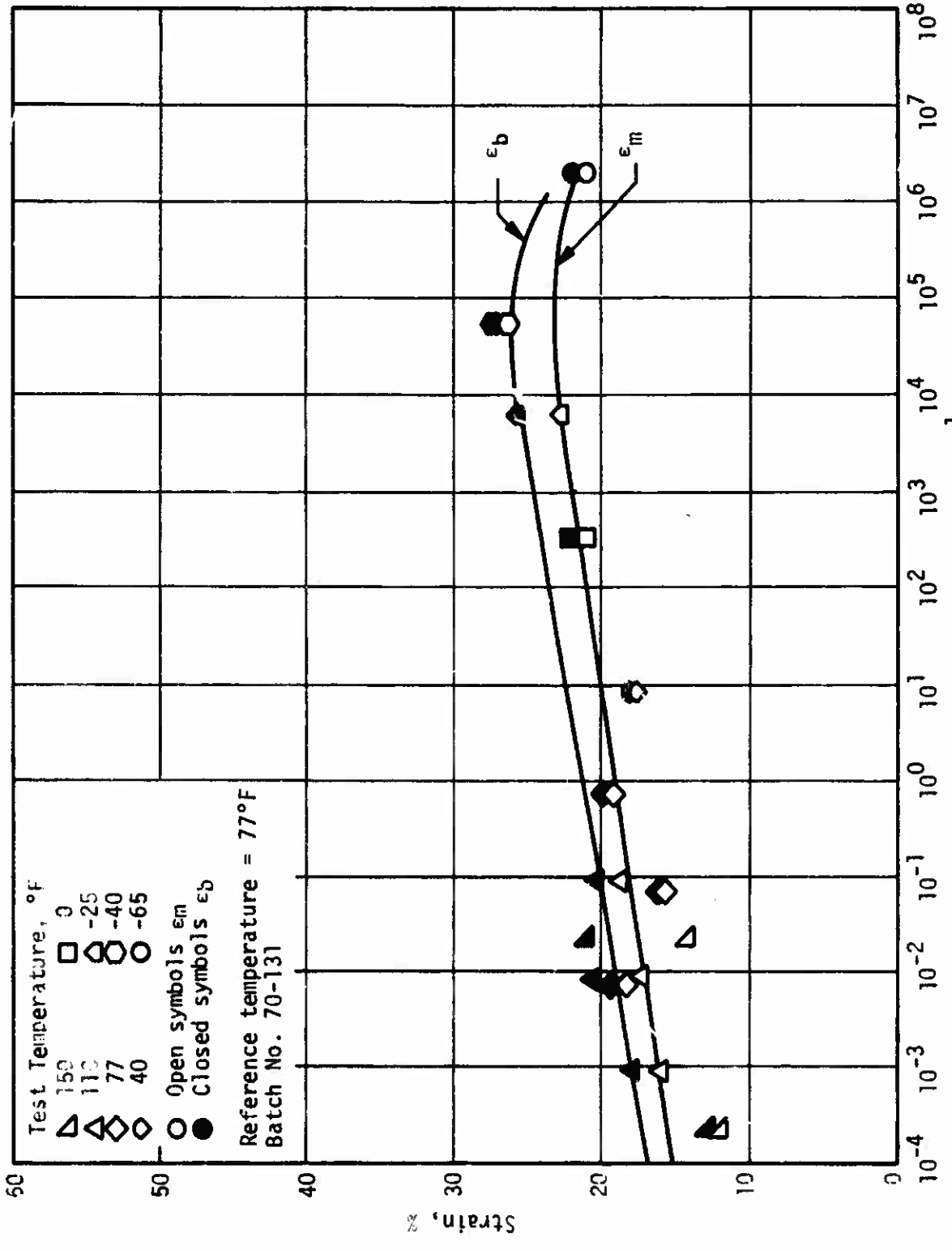

Plot of Strain vs Reduced Strain Rate for ANP-3391

140

Figure 6a

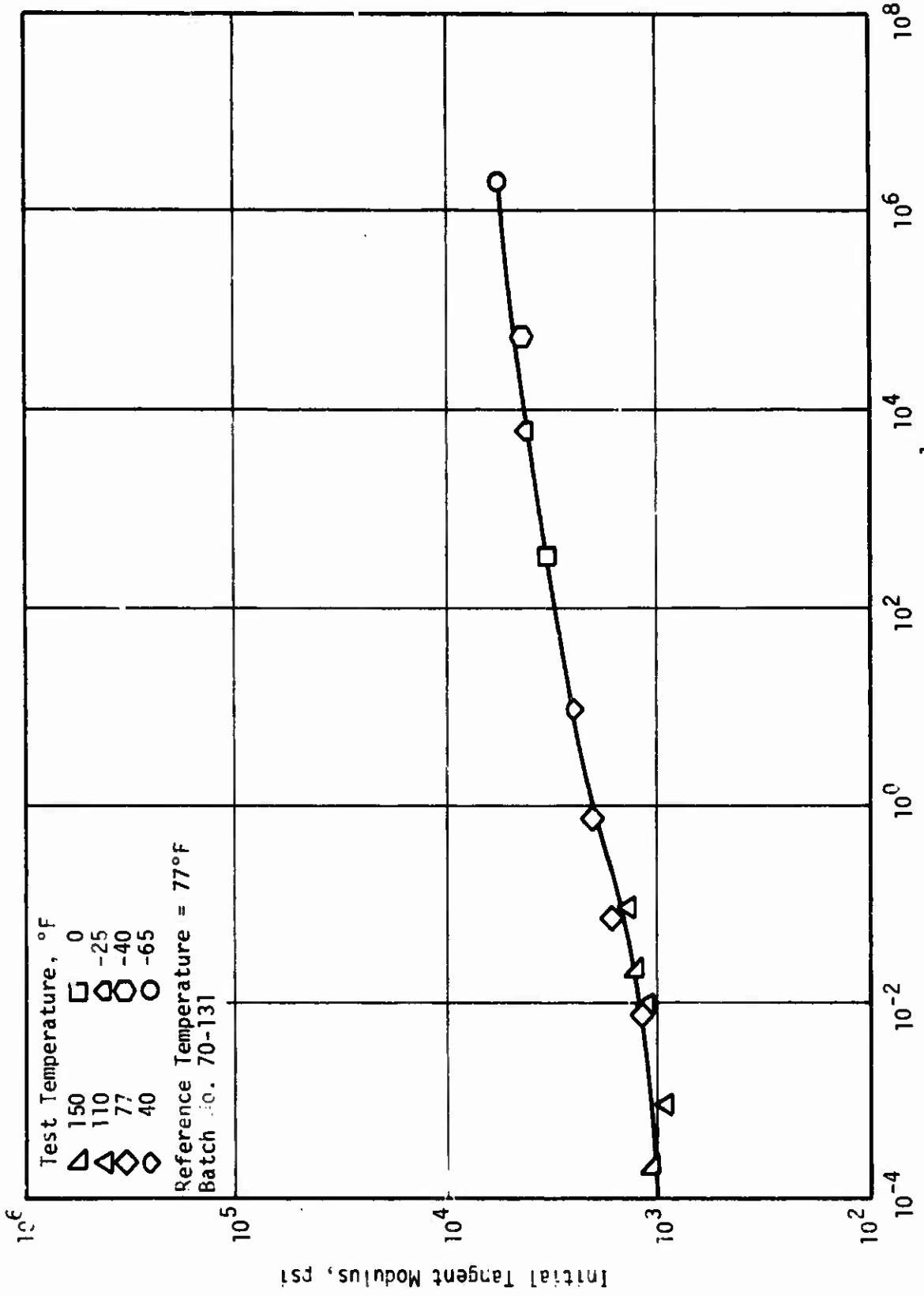

Initial Tangent Modulus vs Reduced Strain Rate for ANP-3391 Propellant

Figure 7a

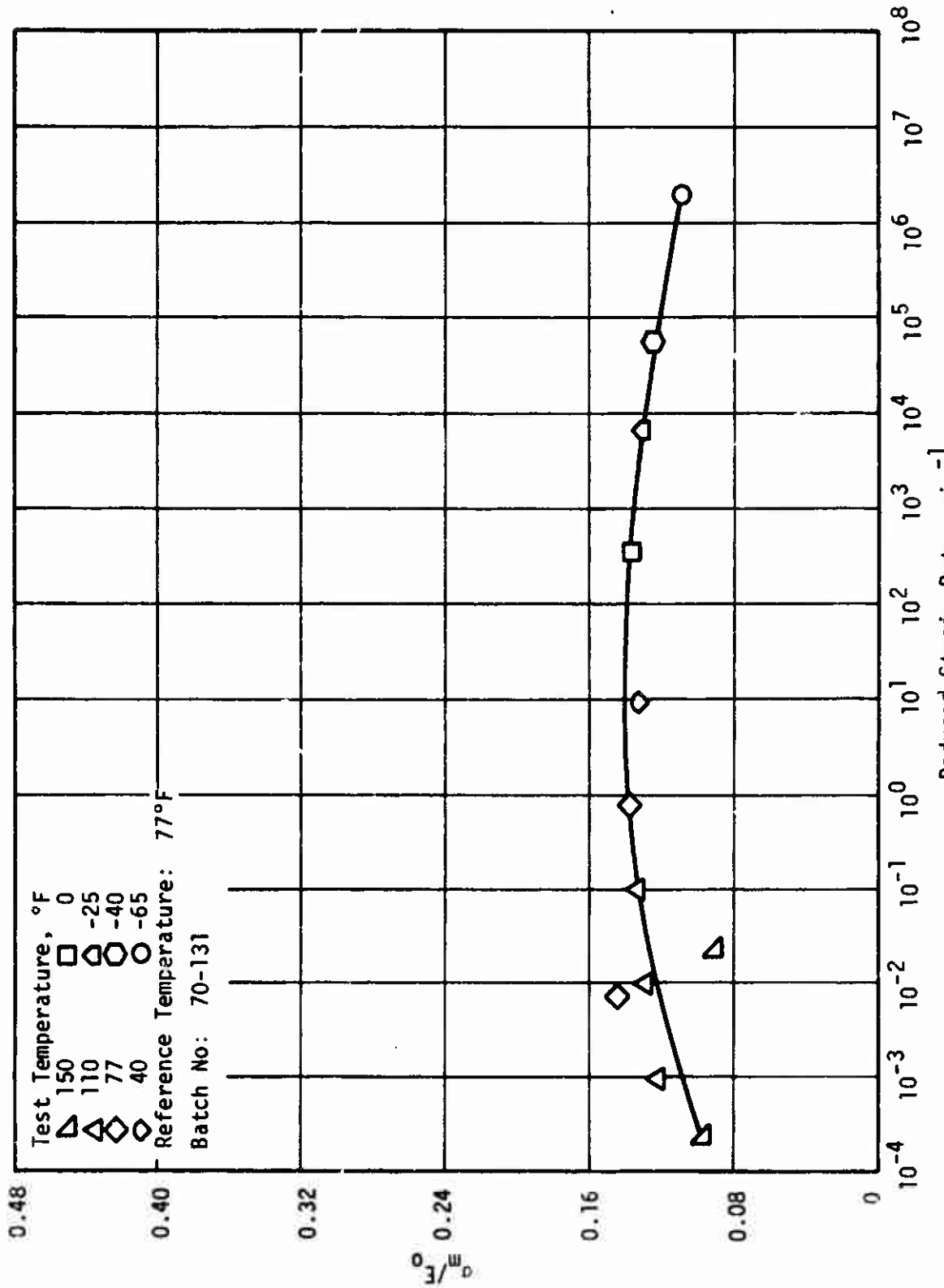

Ratio of Maximum Nominal Stress to Initial Modulus vs Reduced Strain Rate for ANP-3391 Propellant

142

Figure 8a

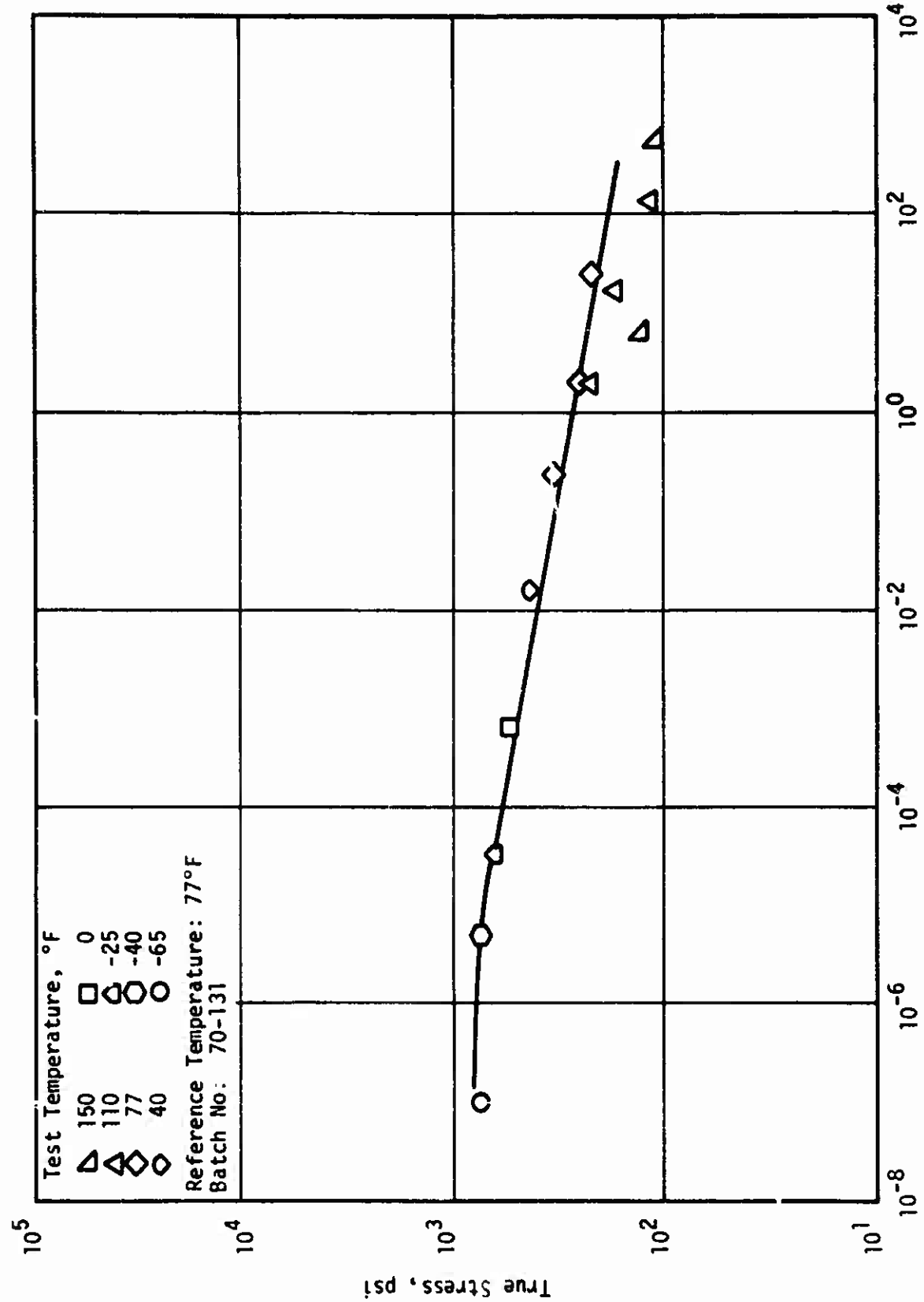

True Stress vs Reduced Time to Maximum Stress for ANP-3391 Propellant

143

Figure 9a

The following data are presented:

Effect of Test Temperature and Strain Rate on Uniaxial Tensile Properties

a_T vs Temperature

Master Relaxation Curve

ε_m vs $\dot{\varepsilon} a_T$

ε_b vs $\dot{\varepsilon} a_T$

E_o vs $\dot{\varepsilon} a_T$

σ_m/E_o vs $\dot{\varepsilon} a_T$

True Stress vs t_m/a_T

Mechanical Property Summary Sheets for ANB-3392 Propellant

Figure 10a

Test Temp, °F	Strain Rate, Min^{-1}	σ_m, psi	ϵ_m, %	ϵ_b, %	E_o, psi
150	0.0074	70	15.4	17.6	675
	0.74	127	16.0	19.1	1132
110	0.0074	112	14.6	15.2	920
	0.074	116	13.2	14.0	1088
	0.74	137	15.6	23.0	1363
77	0.0074**	123	15.0	16.8	1085
	0.074	136	14.8	19.8	1326
	0.74**	162	17.1	25.1	1539
40	0.74	214	16.0	22.0	2243
0	0.74	289	18.5	27.6	297
-25	0.74**	360	17.5	30.0	4672
-40	0.74**	463	15.8	28.8	6376
-65	0.74	682	11.1	14.8	10949

* Each value is the average of two specimens except as noted.
**One specimen (bubble breaks in second specimen)

Figure 11a

Effect of Test Temperature and Strain Rate on Uniaxial Tensile Properties*
ANB-3392 Propellant (Batch 70-130)

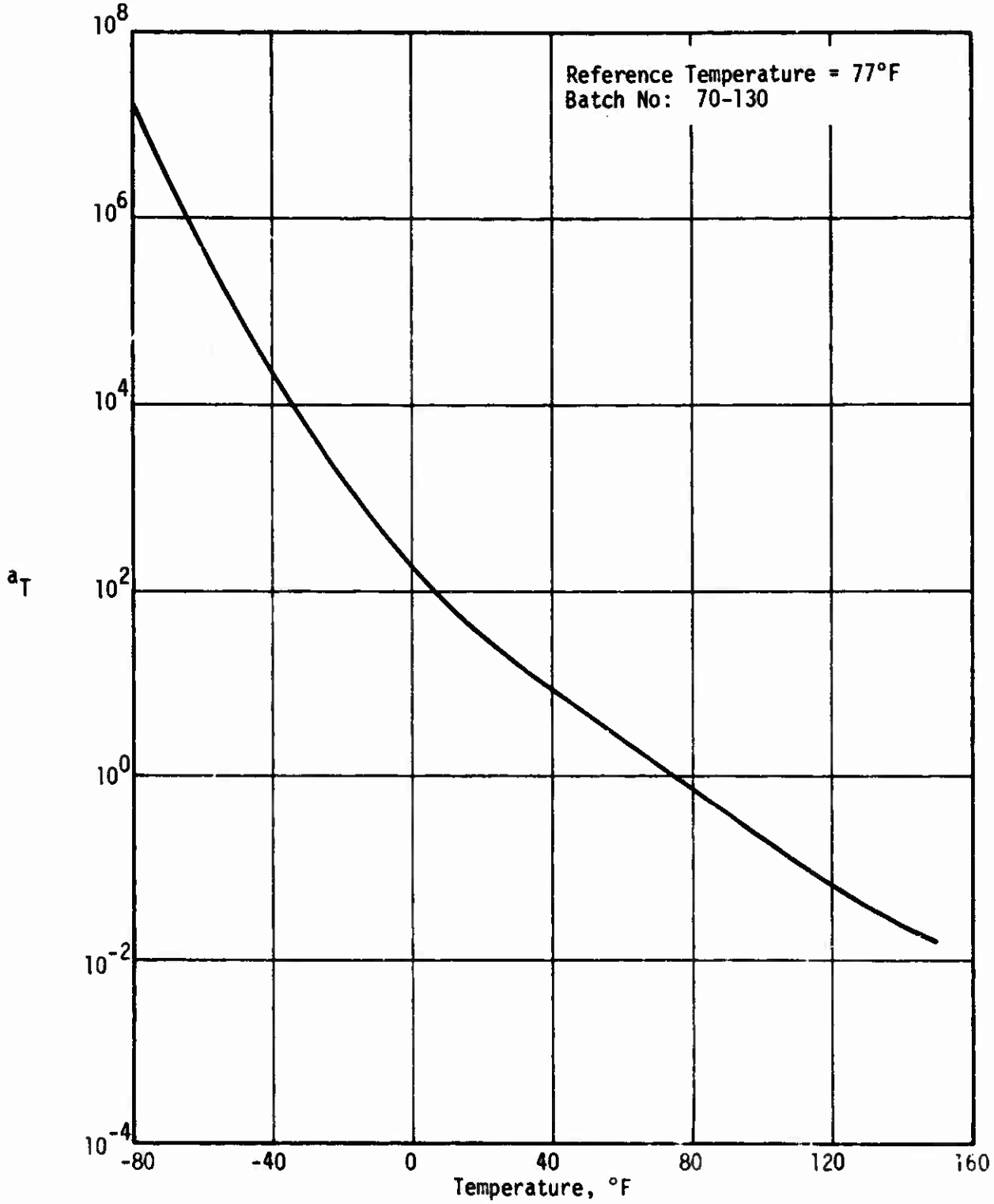

Plot of Log a_t vs Temperature for ANB-3392 Propellant

146

Figure 12a

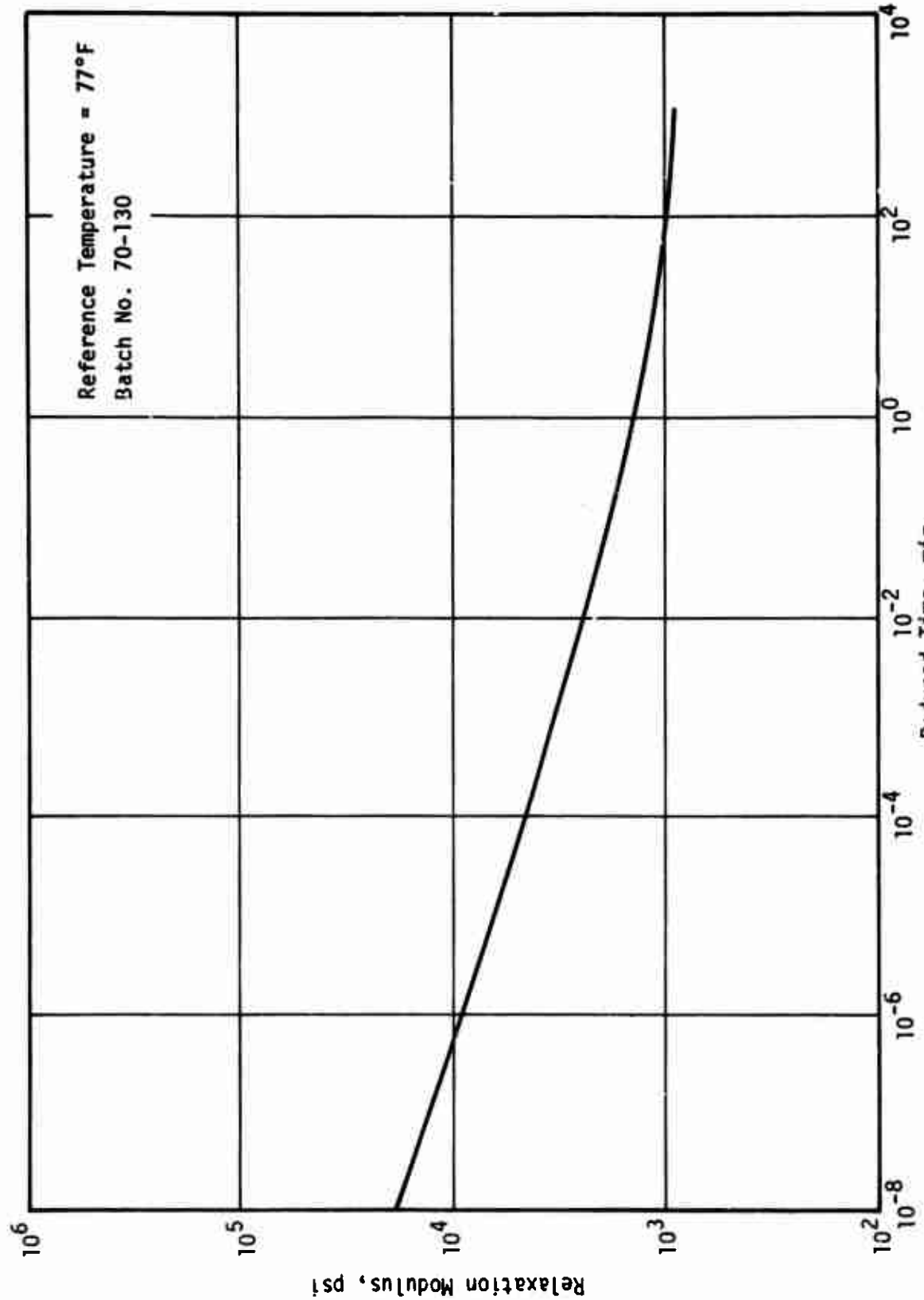

Master Relaxation Curve for ANB-3392 Propellant

147

Figure 13 a

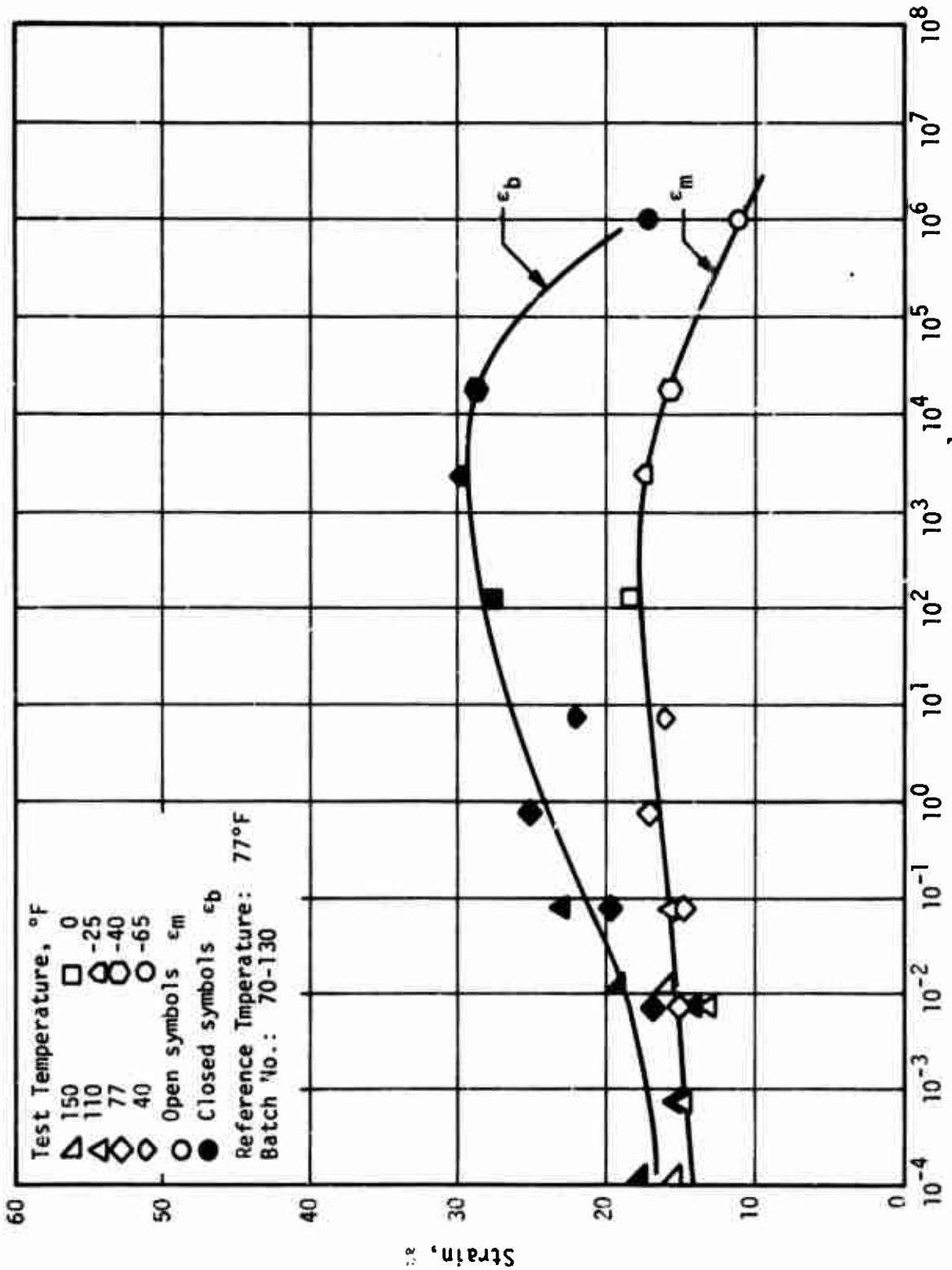

Plot of Strain vs Reduced Strain Rate for ANB-3392 Propellant

148

Figure 14a

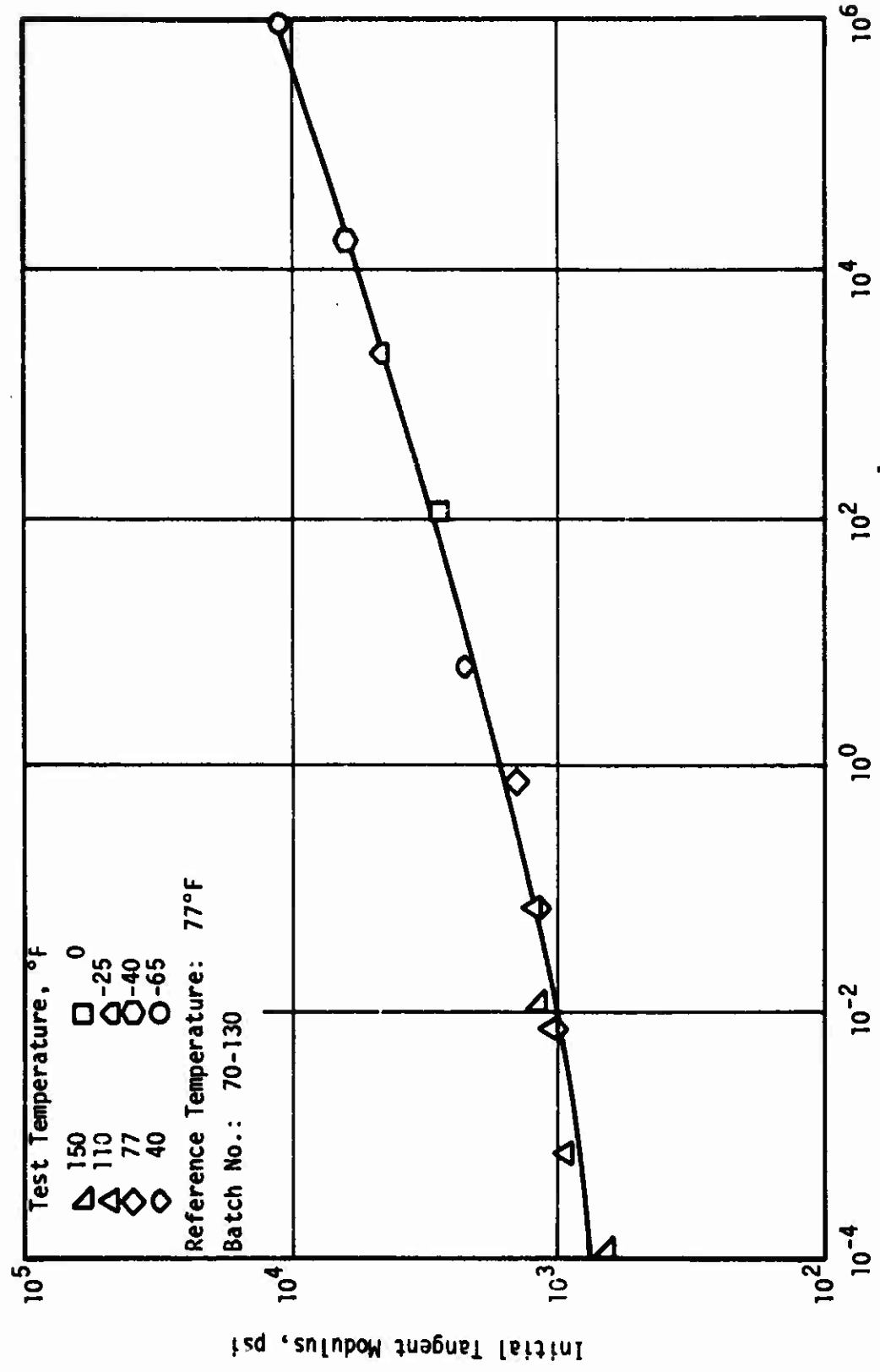

Initial Tangent Modulus vs Reduced Strain Rate for ANB-3392 Propellant

49

Figure 15a

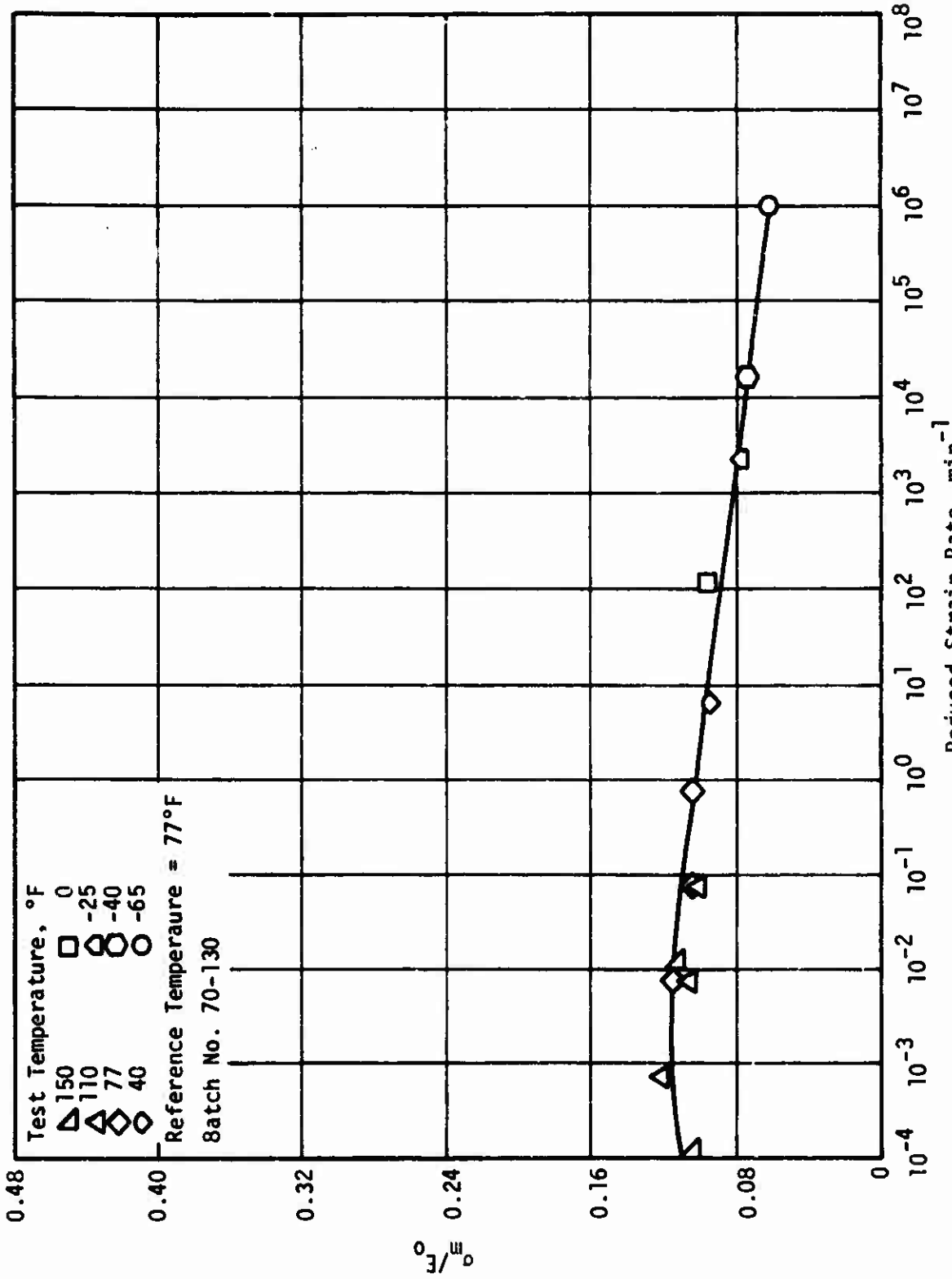

Ratio of Maximum Nominal Stress to Initial Modulus vs Reduced Strain Rate for ANB-3392 Propellant

150

Figure 16a

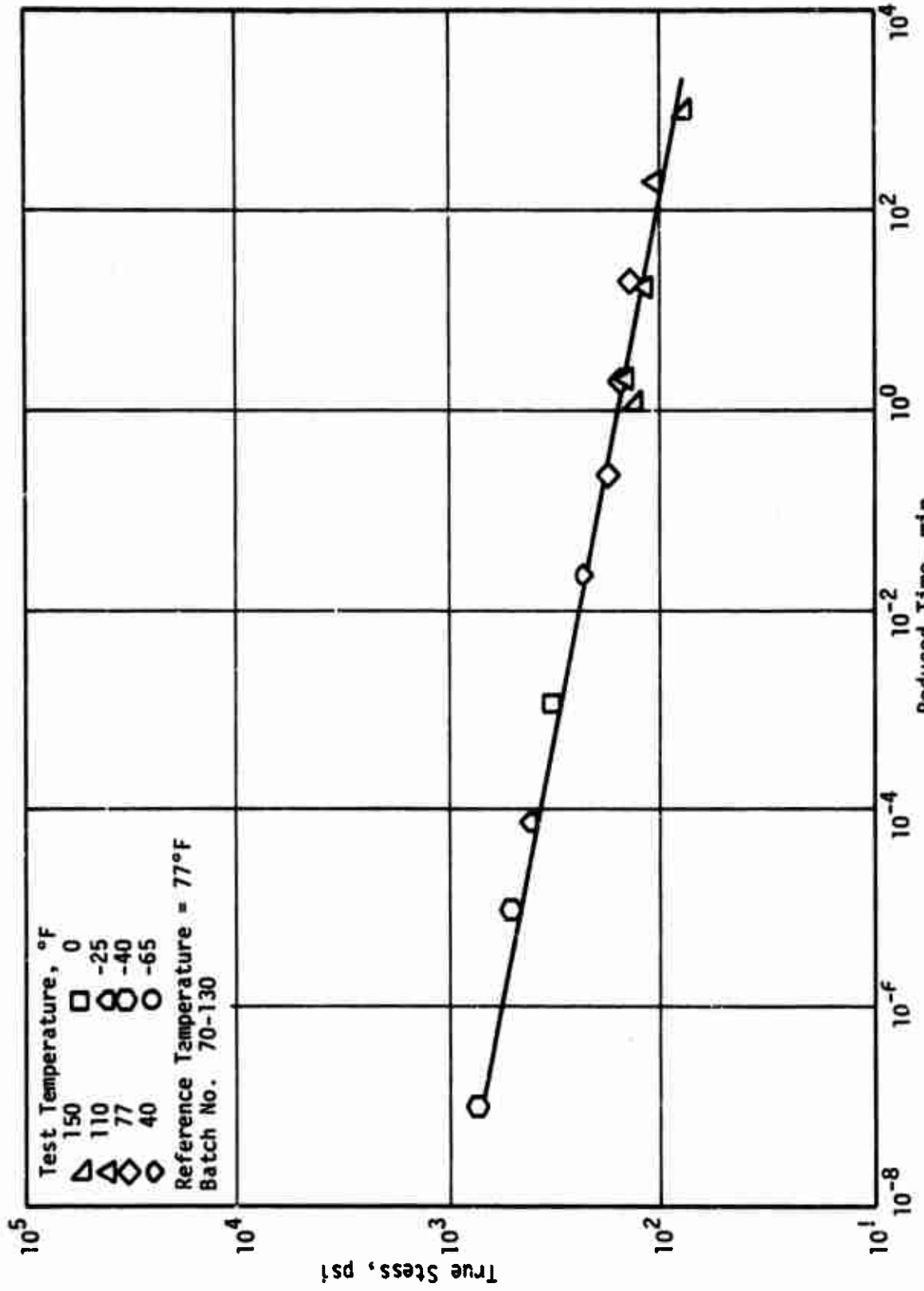

True Stress vs Reduced Time to Maximum Stress for ANB-3392 Propellant

151

Figure 17a